

2013-09-16

Plant Mechanics, Optimization and Remodeling

Gholamirad, Maryam

Gholamirad, M. (2013). Plant Mechanics, Optimization and Remodeling (Doctoral thesis, University of Calgary, Calgary, Canada). Retrieved from <https://prism.ucalgary.ca>. doi:10.11575/PRISM/27366
<http://hdl.handle.net/11023/982>

Downloaded from PRISM Repository, University of Calgary

UNIVERSITY OF CALGARY

Plant Mechanics, Optimization and Remodeling

by

Maryam Gholamirad

A THESIS

SUBMITTED TO THE FACULTY OF GRADUATE STUDIES IN PARTIAL FULFILLMENT
OF THE REQUIREMENTS FOR THE DEGREE OF DOCTOR OF PHILOSOPHY

DEPARTMENT OF MECHANICAL AND MANUFACTURING ENGINEERING

CALGARY, ALBERTA

SEPTEMBER 2013

© Maryam Gholamirad 2013

Abstract

The thesis presented here is focused on plant mechanics and structural optimization; the major finding of the work is that the micro-structure of the Arabidopsis root does sense and show reactions to external mechanical stresses; such reactions involve re-orientation of the microtubule (MT) cytoskeleton closer to the maximum principal tensile stress direction after a significant bending moment is applied. If the root is free of external mechanical stresses (only having internal turgor pressure) then there are two scenarios: in the first scenario, within the cell division zone, the microtubules direction is perpendicular to the main axis of the cell (along maximum principal tensile stress direction and aligned with hoop stress). In the second scenario, within the cell elongation zone, microtubules make a 45 degree angle with the main axis of the cell (possibly due to maximum shear stress).

Another focus of the work presented here is to draw inspiration from nature and apply the “self-optimizing” rules found in natural tissues to engineering frame structural design. This was achieved by simulating frame structures based on two different theories: Wolff’s theory (for natural tissues) and Michell’s theory (for engineering comparative analysis). The performance of the two frame structures studied was evaluated against each other, and it was shown that, for an example of a cantilever beam, structures created based on Wolff’s theory are easier to generate under dimensional restrictions and have greater strength than analogous frame structures modeled based on Michell’s theory.

In order to observe microtubule re-orientation, Arabidopsis root cells were observed by means of a confocal microscope, and the data were analyzed using image

processing to find the dominant pattern of microtubules. The influence of gravity on microtubules direction was also studied by rotating control samples in different directions; gravity was found to have negligible impact on microtubule orientation. The root cell was then simulated numerically to study the direction of principal stresses, and confirm the re-orientation of the microtubules closer to the maximum principal tensile stress direction.

For the strength comparison of the frame structures based on the two theories (Wolff and Michell), a cantilever domain was defined, and the curves were then generated for a computer programming environment, and results were later exported for finite element analysis.

Acknowledgements

First and foremost, I'd like to thank my husband, Wesley Teskey, for his exceptional support during the course of my PhD work. I'd also like to thank my family and friends whose love and support truly helped me to conduct my doctoral research work.

I'd like to thank my supervisor, Dr. Marcelo Epstein, who was instrumental for the thesis work. He provided me with a great deal of encouragement and support which offered me a great opportunity to carry out this research.

I also would like to greatly appreciate Dr. Arezki Boudaoud, my co-supervisor, whose guidance and assistance to my research work was extremely valuable. He generously provided me with his full laboratory resources, and I had the honor to work with his friendly and knowledgeable team members who also helped me a lot when I was doing my experimental tests at ENS de Lyon facilities. Some of these most influential team members were Agata Burian, Olivier Hamant, Annick Dedieu, Pascale Milani and Claire Lionnet.

Lastly I'd like to thank my committee Dr. Les Sudak, Dr. Simon Park, Dr. Marcus Samuel and Dr. Samer Adeeb for their time, insights and suggestions.

To all the family gatherings and warm summer breezes that passed me by...

Table of Contents

Abstract.....	ii
Acknowledgements.....	iv
Dedication.....	v
Table of Contents.....	vi
List of Tables.....	viii
List of Figures.....	ix
Abbreviations.....	xiii
Symbols.....	xiv
Chapter 1: Introduction.....	1
1.1 Main thesis objectives.....	2
1.2 Novel thesis contribution.....	3
1.3 Chapter overview.....	4
Chapter 2: Introduction and Literature Review.....	7
2.1 “Wolff’s law” and a brief history.....	8
2.1.1 Principal (maximum-minimum) stress trajectories.....	11
2.1.2 Wolff’s hypothesis was more investigated afterwards.....	12
2.2 Structural design from mathematical (non-biological) point of view: Michell theory.....	14
2.2.1 Shape optimization.....	15
2.2.2 Topology optimization.....	15
2.2.3 A brief history of Michell theory highlighting its restriction.....	16
2.3 Extending Wolff’s theory from bone to plant tissue.....	19
2.3.1 The role of mechanical forces in botany.....	20
2.3.2 The rationale behind selecting plants.....	20
2.3.3 Central role of mechanical stresses versus other cues.....	20
2.3.4 Microtubules.....	21
2.3.5 History of plants micro-structural adaptation to mechanical forces.....	22
2.4 Chapter conclusion.....	35
Chapter Three: Engineering Frame Structures and Principal Stresses.....	36
3.1 What is Wolff’s premise known as “Wolff’s law?”.....	37
3.2 Principal stress trajectories.....	42
3.2.1 Principal stresses.....	42
3.2.2 Principal stress curves known as stress “trajectories”.....	46
3.2.3 Building stress trajectories in Matlab.....	50
3.2.4 Role of stress concentration.....	53
3.2.4.1 Isoparametric interpolation.....	54
3.2.4.2 Generating stress trajectories in Matlab via Ansys output.....	58
3.3 Michell theory.....	62
3.3.1 Michell’s theory formulation.....	63
3.3.1.1 Virtual deformation.....	64
3.3.1.2 Developing Michell curves.....	66

3.4 Strength assessment of frame structures modeled based on Michell and Wolff theories.....	76
3.5 Some notes about how Thesis Chapter 3 is associated to Chapter 4 and 5...	79
Chapter Four: Biological Preliminaries and Experimental Tests.....	82
4.1 Microtubules.....	85
4.1.1 Why Microtubule and why orientation of Microtubule?.....	87
4.2 Arabidopsis plant.....	91
4.2.1 Why Arabidopsis and why Arabidopsis root?.....	93
4.2.2 More about Arabidopsis in this research.....	95
4.3 Materials and methods.....	102
4.3.1 Visualizing preparation.....	103
4.3.2 Applying mechanical bending stress.....	104
4.3.3 Some details of imaging process.....	109
4.3.4 Measuring radius of curvature for each cell.....	111
4.3.5 Effect of gravity on the Cortical Microtubules orientation.....	112
4.4 Observation results.....	115
4.4.1 Sample controls with no external mechanical loading.....	115
4.4.2 Effect of mechanical bending force on MT orientation.....	119
4.5 Experimental Sources of Error.....	134
4.6 Chapter conclusion.....	135
Chapter Five: Microtubules Orientation and Principal Stress Directions.....	136
5.1 Some bio-science replication challenges for engineering software.....	136
5.1.1 Modulus of elasticity of the cell wall.....	137
5.2 Arabidopsis root cell deformation simulation in Ansys under the mechanical bending load.....	146
5.2.1 Principal directions in the simulated Arabidopsis root cell.....	151
5.3 Chapter conclusion.....	158
Chapter Six: Conclusions and Recommendations.....	161
6.1 Objectives achieved.....	162
6.2 Assumptions and limitations.....	164
6.3 Future work and recommendations.....	165
References.....	168
Appendix A: Matlab Program Details.....	177
Matlab program set #1.....	177
Matlab program #2.....	181
Matlab program #3.....	184
Matlab program #4.....	189
Appendix B: Confocal Microscopy Images from the Arabidopsis Root Cells.....	194

List of Tables

Table 5-1: Force-Displacement values obtained from a finite element analysis simulating an AFM experiment on a cell wall.....	143
Table 5-2: Material properties of the cell wall for each simulation shown in Figure 5-5..	145
Table 5-3: Nodal stress values along with principal stress direction in three different cross sections of the root cell.....	154
Table 5-4: Principal stress directions of the average value of stress.....	155
Table 5-5: Stress components and principal stress value and direction in three different cross sections of the root cell for two different models with two different displacements.....	157
Table 5-6: Principal stress directions of the average value of stress evaluated in three different cross sections of the root cell for two different models with two different displacements.....	158

List of Figures

Figure 2-1: A vector field indicating the directions of the principal stresses at nodal points.....	12
Figure 2-2: A model indicating steps of shape optimization.....	15
Figure 2-3: An illustration of material optimization.....	16
Figure 2-4: A 3D reconstruction of Michell topology.....	17
Figure 2-5: A Michell structure and a similar structure when made simpler.....	19
Figure 2-6: A picture demonstrating the cell wall (W), Microtubules (MT), Microfibrils (MF) and Plasma Membrane (PM).....	24
Figure 2-7: Arabidopsis Hypocotyl cells with cellulose synthase complexes.....	25
Figure 2-8: Different λ angles in neighboring cells.....	26
Figure 2-9: Mechanical buckling deformations influence on the plant tissue.....	28
Figure 2-10: Hypocotyl of sunflower under rotational torque examine.....	29
Figure 2-11: Cortical microtubules orientation in a sunflower hypocotyls being (A) transverse and (B-C) oblique.....	30
Figure 2-12: Proposed stress patterns for the meristem.....	31
Figure 2-13: A shoot apical meristem (SAM) showing the directions of cell expansion, principal stresses, and microtubules.....	32
Figure 2-14: Schematic picture showing apparatus employed to apply force to the pea roots.....	34
Figure 3-1: A frontally sectioned view of a femur bone.....	37
Figure 3-2: A human femur bone frontally sectioned.....	38
Figure 3-3: Culmann and von Meyer's drawings illustrating trabecular patterns for different specimens of human bones.....	39
Figure 3-4: Wolff's drawings comparing femur bone trabecular arrangement with an arched beam based on Culmann's original work.....	40
Figure 3-5: Koch's mathematical analysis illustrating the stress trajectories.....	42
Figure 3-6: State of stress in a selected point of a continuum body under a system of external forces.....	43
Figure 3-7: Mohr's circle for a given stress condition at a point.....	45
Figure 3-8: Normal and shear stresses being transformed from a given coordinate system to the principal directions.....	46
Figure 3-9: Stress trajectories illustrated in a continuum cantilever beam having a concentrated load at the free end.....	47
Figure 3-10: An arbitrary element in the XY plane of a cantilever beam under a concentrated transverse force.....	47
Figure 3-11: Top-Principal stresses distribution for section A and B of the beam.....	49
Figure 3-12: Tensile and compressive stress trajectories for a cantilever beam with	

single transverse force at the free end of the beam.....	52
Figure 3-13: Generating stress trajectories in SolidWorks software in 2D and 3D by means of Matlab program producing the curve points.....	53
Figure 3-14: A linear square element shown in natural coordinates system.....	56
Figure 3-15: A square element mapped into quadrilateral in the curvilinear coordinate system.....	57
Figure 3-16: A cantilever beam in global coordinate system.....	58
Figure 3-17: Stress trajectories illustrated by means of Matlab program for a sample beam analyzed in Ansys software.....	60
Figure 3-18: Stress trajectories generated in Ansys by means of Matlab and SolidWorks software.....	60
Figure 3-19: Principal stress trajectories of a cantilever with a rectangular opening in the middle of the beam, rigid support and a concentrated force at the free end of the beam.....	62
Figure 3-20: Cartesian and curvilinear coordinate system.....	64
Figure 3-21: Angles between compressive and tensile strain curves could lead to four different arrangements of Michell curves.....	67
Figure 3-22: An arbitrary point S in the curvilinear coordinate system.....	69
Figure 3-23: Family of α lines intersecting family of β lines at a constant angle.....	70
Figure 3-24: An arbitrary point in the curvilinear coordinate system.....	71
Figure 3-25: Producing Michell curves step by step.....	72
Figure 3-26: First step used to create Michell layouts by means of the Matlab program #4.....	73
Figure 3-27: Michell layout generated in Matlab programming environment by means of graphical method.....	74
Figure 3-28: Michell layout generated in Matlab programming environment by means of graphical method.....	75
Figure 3-29: An example of a cantilever beam generated based on the Wolff's premise and an example of a model of a cantilever obtained based on Michell's theorem having identical aspect ratio, total mass and fairly the same mass distribution.....	77
Figure 3-30: Changing the five independent parameters $\Delta\phi, OM, ON, m$ and n , will result in multiple cantilever models with unpredictable aspect ratios.....	78
Figure 4-1: A tree trunk deformed under the strong wind condition.....	83
Figure 4-2: Microtubule schematic structure- each Microtubule is made of protein called tubulin.....	85
Figure 4-3: Microtubule polymerization and de-polymerization process.....	86
Figure 4-4: Cellulose Synthase and Microfibrils, along with Microtubules in a newly born and mature cell.....	87
Figure 4-5: Positional location of Microtubules with respect to Plasma Membrane.....	89
Figure 4-6: A general outline of a typical plant cell.....	90
Figure 4-7: Microtubules positions versus Cortical Microtubules.....	91
Figure 4-8: Arabidopsis Thaliana plant.....	92
Figure 4-9: Microtubule bundles in Arabidopsis cell.....	93
Figure 4-10: Cross-sectional view of an Arabidopsis root.....	94
Figure 4-11: Root Apical Meristem (RAM) versus Shoot Apical Meristem (SAM) position in a plant.....	95

Figure 4-12: A typical Arabidopsis root and a close-up view of the root.....	98
Figure 4-13: Typical expected Microtubules arrangement in region B or C.....	99
Figure 4-14: Dominant Microtubules pattern observed in different sections of a root.....	100
Figure 4-15: Images of an Arabdopsis plant.....	101
Figure 4-16: Air bubbles trapped between the cover slip surface and agar media.....	104
Figure 4 17: A sample Arabidopsis root under mechanical bending stress applied by three surrounding needles.....	106
Figure 4-18: Tracking Arabidopsis root appearance after applying the bending load.....	107
Figure 4-19: Arabidopsis root destroyed under the excessive bending load applied.....	108
Figure 4-20: Basics of how a confocal microscope works.....	109
Figure 4-21: ImageJ software utilized in measuring the dominant orientation of Microtubules in the area of interest.....	110
Figure 4-22: Measuring the radius of curvature in each individual cell by means of SolidWorks software.....	111
Figure 4-23: Gravity direction alteration of 90 degrees and 180 degrees for a period of six to seven hours.....	113
Figure 4-24: Gravity direction changed 90 degrees and 180 degrees to the original direction.....	114
Figure 4-25: Some selected samples indicating transverse arrangement of Microtubules in the root tip and cell division zone.....	116
Figure 4-26: Observations in cell elongation zone confirm the existence of a dominant arrangement of Microtubules angled about 45 degrees relative to the cell main axis....	117
Figure 4-27: An individual cell shows different orientation of Microtubules while transitioning from division to elongation zone and three neighboring cells having different orientation of Microtubules.....	118
Figure 4-28: Microtubules orientation along the root cell visualized after 6 to 7 hours after the bending moment was applied to the root.....	120
Figure 4-29: Another sample showing Microtubules orientation along the root cell visualized after 6 to 7 hours after the bending moment was applied to the root.....	123
Figure 4-30: Microtubules have lost their arrangement in one of the cells (right) after being under the bending load for 7 hours.....	126
Figure 4-31: Two important sections in tracking Microtubules orientation are Middle part of an individual cell (M) and Tail end sides of the cell (T).....	128
Figure 4-32: Microtubule orientations with respect to the cell's main axis are compared for control samples and bent samples for the overall length of an individual cell.....	129
Figure 4-33: Microtubules orientations with respect to the cell's main axis are compared for control samples and bent samples for Middle "M" and Tail-end "T" portion of an individual cell.....	130
Figure 4-34: Microtubules average angle relative to the main axis of the cell versus the radius of curvature of the same portion of the cell are compared for each individual cell.....	132
Figure 4-35: The influence of cell's positional location in a bent root.....	134
Figure 5-1: Function of Atomic Force Microscopy.....	138
Figure 5-2: Force-displacement curve obtained from the AFM performed on the SAM of an Arabidopsis plant.....	139

Figure 5-3: Left- TARGE170 and CONTA175 right- SOLID45 geometry and coordinate system.....	140
Figure 5-4: One quarter model of the AFM cantilever beam touching the cell wall.....	141
Figure 5-5: Force-displacement outcome of Ansys simulation for the AFM experiment on the plant cell wall with diverse material properties.....	144
Figure 5-6: Arabidopsis root cell simulated with Ansys software.....	147
Figure 5-7: Mesh style of the cell walls.....	149
Figure 5-8: Solution convergence tracking in Ansys software.....	150
Figure 5-9: Displacement vector sum of a cell modeled in Ansys.....	151
Figure 5-10: Sections A, B and C of the simulated cell being studied and compared to one another.....	152
Figure 5-11: Principal stress direction in the transformed coordinate system.....	153
Figure 5-12: Maximum value of the principal stress (tensile) in sections A, B and C detailed in Table 5-3.....	153
Figure 5-13: Average values to find principal stress directions were calculated based on the nodes located on the perimeter of each cross section in the root cell.....	155
Figure B-1: Bending moment just applied to the Arabidopsis root and the same root observed 6 to 7 hours after the bending moment was applied.....	194
Figure B-2: Microtubules orientation measured immediately after (within minutes) the bending load was first applied.....	196
Figure B-3: Microtubules orientation tracked directly after 6 to 7 hours of continuous application of the bending load.....	198
Figure B-4: Another sample showing microtubules orientation along the root cell visualized immediately after and 6 to 7 hours after the bending moment was applied to the root.....	199
Figure B-5: Another selected sample showing microtubules orientation along the root cell visualized 6 to 7 hours after the bending moment was applied to the root.....	201
Figure B-6: Another selected sample showing microtubules orientation along the root cell visualized 6 to 7 hours after the bending moment was applied to the root.....	204
Figure B-7: An example of a root cell losing its microtubules pattern after several hours of being bent with an external bending moment.....	209

Abbreviations

AFM	Atomic Force Microscopy
MT	Microtubules
LSD	Limit State Design
CMT	Cortical Microtubules
CS	Cellulose Synthase
CMF	Cellulose Microfibrils
MF	Microfibrils
CSK	Cytoskeleton
PM	Plasma Membrane
SAM	Shoot Apical Meristem
2D	Two Dimensional
3D	Three Dimensional
DOF	Degrees Of Freedom
PDE	Partial Differential Equations
GFP	Green Fluorescent Protein
MDB-GFP	Microtubule Binding Domain Green Fluorescent Protein
RAM	Root Apical Meristem

Symbols

σ :	Normal stress
σ_1 :	First principal stress
σ_2 :	Second principal stress
σ_{\max} :	Maximum normal stress
σ_{\min} :	Minimum normal stress
$\sigma_x, \sigma_y, \sigma_z$:	Normal stress components along x, y and z axis respectively
τ :	Shear stress
τ_{\max} :	Maximum shear stress
τ_{\min} :	Minimum shear stress
$\tau_{xy}, \tau_{xz}, \tau_{yx}, \tau_{yz}, \tau_{zx}, \tau_{zy}$:	Shear stress components in cartesian coordinate system
θ_p :	Angle defining the maximum normal stress direction
θ'_p :	θ_p in a transformed coordinate system (versus Y axis)
θ''_p :	θ_p in a transformed coordinate system (versus Z axis)
$\theta'_p _A, \theta'_p _B, \theta'_p _C$:	θ''_p in different cross sections (A, B, C) of the cell
$\theta''_p _A, \theta''_p _B, \theta''_p _C$:	θ''_p in different cross sections (A, B, C) of the cell
θ_s :	Angle defining the maximum shear stress direction
F:	Concentrated force applied to cantilever
I:	Moment of inertia
A_0 :	Cross section area
M:	Bending moment
w:	Cantilever width
h:	Cantilever half depth
L:	Cantilever length
eig_1, eig_2 :	Eigenvectors of stress tensor
$\frac{d}{dx}$:	Differential operator
i:	Imaginary number
N_i :	Shape functions
u_i :	Displacement

$u_{\hat{x}}$: Displacement of an element along x axis of a natural coordinate system
 $u_{\hat{y}}$: Displacement of an element along y axis of a natural coordinate system
 $u_{\hat{x}i}$: Displacement of the i^{th} node along x axis of a natural coordinate system
 $u_{\hat{y}i}$: Displacement of the i^{th} node along y axis of a natural coordinate system
 \hat{x} : x component of natural coordinate system
 \hat{y} : y component of natural coordinate system
 \hat{x}_i : x component of the i^{th} node in natural coordinate system
 \hat{y}_i : y component of the i^{th} node in natural coordinate system
 ξ : First component of an element curvilinear coordinate system
 η : Second component of an element curvilinear coordinate system
 $u(\hat{x}, \hat{y})$: Displacement function along x componet of a natural coordinates system
 $v(\hat{x}, \hat{y})$: Displacement function along y componet of a natural coordinates system
 a_1, a_2, a_3, a_4 : Equation constants
 c_1, c_2, c_3, c_4 : Equation constants
 α : First component of a sample curvilinear coordinate system
 β : Second component of a sample curvilinear coordinate system
 ω : Rotation
 ds : Infinitesimal segment of a curve
 ε : Strain
 A, B : Lamé's parameter
 S : A frame structure
 R : Region of space
 φ : Angle between α and x axes
 a, b : ± 1
 Ψ : Curve name
 P, Q, P', Q' : Points name
 G : Green function
 J_0 : Bessel function of order zero
 I_0 : Modified Bessel function of order zero
 M : Selected point on α axis

N : Selected point on β axis
 m : Numerical value of OM distance on α axis
 n : Numerical value of ON distance on β axis
 E : Modulus of elasticity
 E_x, E_y, E_z : Modulus of elasticity of cell wall along x, y and z axes
 G_s : Shear modulus
 ν : Poisson's ratio
 ρ : Radius of curvature
 g : Gravity constant
 Δ : Indentation/ displacement
 k : Equation constant
 $\sigma_{*avg}, \tau_{**avg}, \theta'_{pavg}$: Average values
 λ : Angle
 X_L, Y_L : x-y dimensions of a sample cantilever

Chapter One: Introduction

Structural behavior of a plant segment (in the case of this thesis, the Arabidopsis root cells) at the sub-cellular level can be studied more capably and in depth with the advent of micro visualization technologies. Understanding nature's structural performance (at the micro scale) and replicating similar situations in engineering frame structural design, is the focus of this thesis.

Mechanical engineering and biology seem to be different disciplines with little overlap in the fields of study. The foundation of an engineering analysis is relatively based on mathematics and physics rules and formulations, while in biology such a foundation is more dynamic and involves often not very controllable parameters. This affects results which cannot be easily predicted except by empirical observations. Conducting the type of research presented in this thesis (performing experimental tests on plants and interpreting the behavior by engineering formulas and simulation) highlights the importance of studying such relatively new area of research, since so many valuable findings were uncovered. The work presented bridges disciplines (mechanical engineering and bio-science) with the result being a more in depth and broad analysis.

The role of different agents like light, chemicals, water, and hormones on a plant's micro-structural activities has been extensively studied in literature with little attention given to mechanical forces. There is no doubt that all such agents are either individually, or in a group, contributing to a plant's micro-structural reaction; however, for some reason the key role of external mechanical forces is not considerably studied often in depth as shown in Chapters Four and Five of this thesis.

There are some challenges involved with regards to bridging the two areas of study which were the focus of the thesis. For instance, when it comes to simulating a plant tissue with an engineering software, there is tangible difficulty in mimicking the material behavior and mechanical properties of tissue at cellular or sub-cellular level.

On the other hand, a natural tissue like plant tissue, is considered to have built-in self-optimizing capabilities which is, in part, what inspired the study of structural optimization in some engineering frame structures. There are two main categories of theories in this structural optimization realm; those related to nature (based on Wolff's theory) and those that are purely mathematical (based on Michell theory). No matter how these theories are driven (purely mathematical or from nature), they all date back to more than a hundred years ago. In this thesis, the two aforementioned prominent theories (Michell's and Wolff's) will be considered.. It will be shown that the performance of frame structures modeled based on the theory of combining nature's behavior with mathematical rules (Wolff) gives better results given the problem constraints when compared with analogous results for when applying Michell's theory.

1.1 Main thesis objectives

One of the main objectives of the thesis is to contribute in better understanding the interaction between mechanical forces and a plant's micro-structure response. Attention is more specifically given to the reorientation of microtubules (MT) in Arabidopsis root cells due to the mechanical stresses applied.

Expanding the main concepts and fundamentals of Wolff's theory, from bone micro-structure to encompass plants micro-structure, and verifying the theory is also a

major area of interest. Successfully doing this would endorse Wolff's theory, given various interpretations and appraisals of this theory.

Another objective of the thesis is to employ the self-optimizing property of a natural tissue's micro-structure (e.g. bone or plant) in engineering frame structure design. Such "self-optimizing" ability of these natural tissues is described within Wolff's theorem. This was the motivation to employ Wolff's theory in frame structure design, as any structural optimization leads to time and cost reduction and savings in engineering designs. Performance of frame structures (based on Wolff's theory) was then compared to similar structures based on Michell theory. The compared frame structures were evaluated based on a desirable optimized performance with given constraints. In the presented work, the strength of each model based on the two aforementioned theories, Wolff's and Michell's, is compared.

1.2 Novel thesis contribution

The major novel contribution for the research carried out here was the fact that the effect of external mechanical stresses on microtubules reorientation has never been investigated on the Arabidopsis root cells. It was found for the case of root cells studied that microtubules do move to try to orient themselves *closer to* principal stress directions when a *large mechanical load* is applied; this was verified using both experimental data (in Chapter 4) and numerical simulation (in Chapter 5). The lack of study of this topic might be due to the fact that the Arabidopsis root is a very fragile and difficult to handle specimen, which can easily become damaged while performing the empirical observations or operations. As well, the root is an organ that continuously grows lengthwise, and the experiment has to be performed in a strictly limited time before the

relevant zone of the root sample grows other lateral roots or root hairs, or even before the root gets too long for the Petri dish (which also makes it impossible to move the root and visualize).

1.3 Chapter overview

There are a total of six chapters in this thesis. Chapter 2 is a literature review and the introduction. Chapter 3 focuses on developing engineering frame structures based on Wolff and Michell's theory, and then performance analysis for such structures is undertaken. Chapter 4 contains biological preliminaries for engineers (as non-biologists) as well as the empirical observations and data collection for the plant of interest. This is followed by Chapter 5, where simulations of empirical observations are carried out using engineering software and programming. Chapter 6 is the final and closing chapter, which comprises the conclusion and discussion of the thesis. In the following few paragraphs, the chapter contents introduced in this paragraph are explained in more detail.

Chapter 2, as mentioned above, is a literature review for the research carried out here. It starts with introducing "Wolff's law" as the prominent theory in the field, which was developed based on both scientific and engineering observations and calculations. Such observations were based on studying bone's microstructure. Then Michell theory of structural optimization is introduced which has a mathematical foundation. These two theories are outlined in more details in the next chapter (Chapter 3). Then Wolff's theory is extended from bone micro-structure to plant micro-structure by focusing on the role of mechanical stresses in changing the orientation of the microtubules in the plants (there is also a brief history of similar investigations included in this chapter).

Chapter 3 clarifies in more details the role of principal stresses and the stress trajectories as well as the methodology of how to build engineering frame structures based on Wolff's and Michell's theories. More aspects of Wolff's hypothesis are reviewed, and then steps of constructing a frame structure (cantilever beam) based on such a theory are discussed; followed by a finite element model taking into account the role of stress concentration. After this, features of Michell theory are introduced, along with the formulation and steps to generate a frame structure (a cantilever beam) based on this theory. The two evaluated types of cantilever beams (one produced from Wolff and the other produced from Michell's theory) are compared to each other for performance analysis, and Wolff's law is generally found to produce better results than Michell's theory when loads are applied to structures designed with the two theories in mind.

Chapter 4 describes some biological concepts and terminologies for non-biologists along with the details of the experiment performed on the Arabidopsis root and the visualization techniques. Results of such observations on the root cells are described, and then analyzed with appropriate image processing programs. The main result shown is that microtubules do move to try to orient themselves *closer to* principal stress directions when a *large mechanical load* is applied. Other important findings are that microtubules align themselves transversely to the cell main axis in the cell division zone, and at a 45 degree angle to the cell main axis in the cell elongation zone, in the case of no external applied mechanical load (only internal turgor pressure exist). As well, gravity was found to have a negligible impact on microtubule orientation. The noted alterations in microtubule direction due to load are documented to be later compared with the results of

simulation in the next chapter (chapter 5) to find the possible rationale behind the changes observed.

Chapter 5 of this thesis includes the simulation performed in a finite element program (Ansys) to replicate the empirical test carried out in the previous chapter (Chapter 4) by applying the mechanical bending stress to an Arabidopsis root cell. This chapter starts with the challenges involved in achieving such a simulation. A simulation shown in the chapter beginning is for determining the modulus of elasticity of the cell wall with an Atomic Force Microscopy (AFM) technique. Then the simulation of the Arabidopsis root cell, undergoing a large bending deformation, is carried out using finite element software (Ansys) followed by the stress analysis of the outcome. Such finite element analysis in Ansys is closely assessed against the empirical results achieved in the previous chapter (Chapter 4) to illuminate the underlying principle governing microtubules orientation.

Chapter 6 concludes the research carried out in this thesis. Achieved objectives are discussed more in detail. As well, future work and recommendations on how to improve some features of the research investigations are described.

Chapter Two: Introduction and Literature Review

This chapter is principally concerned with a literature review of Wolff's law, Michell theory and expanded concept of Wolff's theorem in plants. The two mentioned areas of inquiry (Wolff's law and Michell theory) are fundamental to this thesis, and are utilized in Chapter 3 when engineering frame structures are evaluated based on these topics, Chapter 4 when experimentation is carried out to validate Wolff's law as it applies to plants, and Chapter 5 when simulation are carried out to better understand empirical data from Chapter 4.

Maximizing efficiency and load bearing capabilities while minimizing design time and monetary expenditures has always been an essential target for structural engineering designs. Determining the best values for a set of influencing variables in design does not always have an easy solution.

Nature has consistently been an influential source of inspiration for researchers. Algorithms inspired from nature have been studied from decades ago and are getting renewed attraction in the recent years since the simulation problems are becoming more dynamic and intricate. Such algorithms have resulted in competitive advantages and benefits across a range of disciplines from engineering to social sciences. Although finding the best solution is not necessarily guaranteed, adopting structural designs from biological and natural science can provide state-of-the-art solutions for different areas of optimization [1].

In this thesis, the main objective is to bring together the two seemingly different areas of engineering and bio-science. This is achieved by studying the influence of

mechanical forces on the structural re-patterning of plant tissue in sub-cellular level. Such study will facilitate in better understanding a natural tissue's response to its surrounding environment, which could be employed as a template for structural optimization purposes. First and foremost, Wolff's premise will be introduced as one of the most prominent theories relating effects of environmental forces on a natural tissue's (bone) micro-structural behavior. Subsequently, one of the most eminent theories in structural optimization, Michell's theorem, will be presented. Michell's theory is an entirely mathematically driven theory, unlike Wolff's. In the following chapters, performance of structures generated based on Wolff's theory will be evaluated against those generated based on Michell's. Wolff's hypothesis will be then expanded to investigate plant's micro-structural response to mechanical forces, and the hypothesis will be verified and validated by performing some empirical experiments followed by finite element simulation.

2.1 “Wolff's law” and a brief history

Before presenting Wolff's law, it's essential to point out that this theory was originally developed based on femur bone microstructure which is not the main focus of this research. Instead, this theory was considered as a *source* of inspiration from nature (bone microstructure) and to be applied to a *plant* microstructure.

Historically, Wolff's law is a reputable classical example of there being a close correspondence between a natural tissue (bone trabeculae) and an engineering structure (crane-like cantilever). In 1892, a German anatomist named Julius Wolff, after around 25 years of experience in orthopedics and skeleton anatomy, proposed the analogy between the cancellous bone pattern and stress trajectories of a curved crane-like cantilever

resembling a human bone femur. In his seminal work, Wolff revealed that the microstructure of a bone femur, in a self-repair process, adapts to the applied mechanical loading, resulting in an arrangement of the trabeculae with the principal stress trajectories.

Wolff's premise formulating microstructure of the femur bone's morphology has led to the development of Wolff's principle or "Wolff's law" [2]. Among various types of bones containing trabeculae, Wolff allotted his observations to the human proximal femur. In general, there are more extensive and in-depth studies concerning femur than any other types of bone structure. The reason for this is because of the significant role and importance of this bone in daily activities, as well as the large size of the femur bone, as well as the complexity of interior spongy portion of the bone [3, 4, 5, 6].

Despite different interpretations of Wolff's work and disputes about his theory [2, 7], many researchers credit his hypothesis as a seminal work declaring that a bone adopts its microstructure by undergoing morphogenesis in response to average dominant loading environment in a way that a minimal weight structure is achieved [2, 7]. Most disputes about Wolff's principle, originated based on the observations of various bones which led to questioning the orthogonality of the tension-compression trajectories intersections [2]. Regardless of disputes raised about Wolff's work, a noticeable publication in 1917 by an anatomist named J.C. Koch, which has been cited by many contemporary authors has constituted a strong mathematical validation basis [2, 3] for Wolff's law. Koch has declared clearly "the structure of the femur is based upon exact mathematical laws" based on making comparison between a femur and a similar structure having the same external shape and physical properties while sustaining same magnitude and type of loading [3].

Furthermore, he acknowledged that not only the internal architecture of the femur is adapted to its function, but the external shape is also adapted; and any alteration in the load exerted on the bone is followed by the corresponding changes (in both internal and external structure). Some recent studies have also predicted the external geometry and internal density distribution of the proximal femur by engineering optimization methods [8, 9].

Wolff's theory's foundation also rests on the analysis made by an engineer and mathematician named Karl Culmann. Culmann attended a talk presented by an anatomist named Hermann von Meyer regarding the role and significance of cancelli arrangement in a collection of different bones. Culmann realized that such arrangement is very much analogous to his own drawings of structures with similar shape or load. Thus, Culmann depicted his work to von Meyer that the trabecular patterns in a bone seem to be aligned along the principal stress trajectories caused by the external loading that he had calculated [2, 3, 10].

Culmann approximated the upper part of the femur bone with a Fairbairn crane which was similar in the external shape and form. He derived the principal stress trajectories in the crane and concluded that such trajectories are along the trabecular arch as he observed in the frontally sectioned femur. This proved the ability of femur to adopt as a natural structure in supporting a maximum load with a minimum material.

Subsequently, this formed the mathematical foundation of modern theory of the bone adaptation today [3]. Von Meyer investigated different types of bones and illustrated his work in a paper along with Culmann's results. However, his drawings were incorrectly indicating the non-perpendicular angles of the intersecting curves. Eventually, Wolff

developed a more accurate and detailed drawing by using more rigorous tools. His conclusions were highlighting the importance of orthogonal intersections where cancellous bone arch met in the femur head [3]. He cited Culmann's analysis as a mathematical proof declaring that the shape and internal structure of a normal or pathologic bone is regulated by the average static external forces present in the environment [3]. Since then, a large amount of attention was drawn towards Wolff's theory either challenging or accrediting his opinion.

Different applications of Wolff's law can be classified in the following three main aspects [2]:

- 1- Strength optimization of a structure considering the total mass as constraint,
 - 2- Alignment of the trabecular trajectories along the principal stress trajectories
- and
- 3- Self-adjustment of bone microstructure (considering that the tissue cells respond to a mechanical stress)

The first two are the main focus of this research, and part (2) will be extended to plants microstructure.

2.1.1 Principal (maximum-minimum) stress trajectories

Principal stress trajectories are families of curves which are orthogonal to each other; Figure 2-1 shows the principal stress directions and magnitude in each node of a discrete mesh for a cantilever beam with a transverse load at its free end.

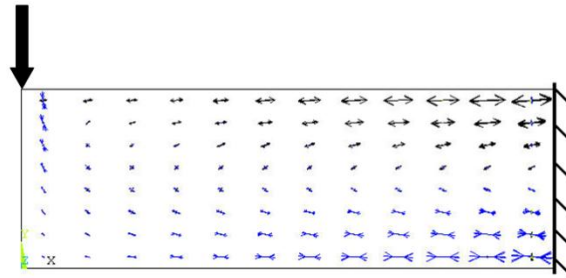


Figure 2-1: A vector field indicating the directions of the principal stresses at nodal points

The method of how these directions are extracted will be explained in the next chapters.

2.1.2 Wolff's hypothesis was more investigated afterwards

Wolff's theory has extensively studied from the time it was first proposed up to the present time. B. Chen et al. conducted an experiment which validated Wolff's law; namely, that bone remodeling is caused by principally mechanical loading and that trabecular trajectories follow the principal stress directions. This was validated by conducting a simulation using a mechanical stimulus, strain energy density, and observed the effect on bone remodeling [11].

Pauwels also increased the understanding of stress distributions within bones in the scientific community with reference to some of the work carried out by Mattheck. Pauwels noted that the arrangement of trabecular bone removes local bending tendencies so that only tension and compression exist. This in turn results in shear stress being minimized and material utilization optimized. In Pauwels work, radiographs were utilized to examine human femur trabecula. He noted that within the femur, the arrangement of

spongiosa provided an optimal average service load. Mattheck had also noted that biological structures tend to provide minimum weight and optimal mechanical strength, and that Von Mises stress tends to be evenly distributed on biological component surfaces. These factors, in turn, reduce mechanical failures in biological structures. Mattheck points out that it may be good to adopt some design principles from nature in man-made designs, since structures in nature offer a unique favorable stress distributions [12].

Huiskes has carried out an innovative research with his colleagues about the effects of mechanical loads on the microstructure of the bone. Mullender and Huiskes performed a computer-simulation for bone remodeling and Wolff's law to see if local controlling processes may explain some of the observed phenomena. Their computer model created structural arrangements similar to trabecular pattern. They found that external loads did cause physical changes in bones by realizing that the trabecular arrangement altered when the load varied. Furthermore, they determined that, as Wolff's law would have predicted, trabecular trajectories did align with principal stress directions, and that this phenomenon could be modeled using an easy regulatory process [13]. Huiskes published a paper in Nature magazine about the influence of mechanical loads on the trabecular bone [14]. He elegantly expressed that trabecular bone configures to facilitate optimal load bearing, in a mathematical sense. Specifically, high stiffness and strength criteria are combined with minimal weight criteria. The trabecular bone that was the focus of the work tends to be porous and it is commonly found in articulating joints and in the spine. He also created a

computational model which was focused on the metabolic processes internal to bone material. This model was used to verify that a feedback exists within the cells' internal processes and mechanical load transfer. The model that was used went a long way towards providing and understanding of how cells maintain a particular trabecular structure which is, in a sense, optimal [14].

However, in his other work he criticized some interpretations of Wolff's law. One of his main criticisms centered on the fact that Wolff's Law was formulated in such a way that it did not take into account, directly, how biological processes function. Biological regulatory processes do not directly follow rules for mathematical optimization when it comes to creating bone material. Even though the bone material has its trabecular trajectories lying along principle stress directions, this is an observed phenomenon which has been confirmed many times (in recent times this confirmation was carried out using FE analysis). It is not, however, a fundamental governing phenomenon the way that Newton's Law of universal gravitation is [15].

2.2 Structural design from mathematical (non-biological) point of view: Michell theory

In this thesis, part of the research work has been dedicated to optimal structural design. Wolff's principle has been a major focus along with Michell theory. A lot of early work on structural optimization was carried out by Maxwell (1869) and later continued by Michell (1904). There are many branches of study in structural optimization, and it can be generally classified into four areas of study. Sizing and material are two areas of focus which tend to be less theoretically mathematical; in contrast, shape optimization

and topology optimization are two areas of focus which tend to involve a lot of mathematical theoretical work.

2.2.1 Shape optimization:

Shape optimization is focused on the shape of material which can be removed from a structure to reduce weight and material usage without significantly affecting the strength and stiffness of the structure undergoing optimization. Some material removal can cause stress concentrations within a structure, and this can have a negative impact on the strength and stiffness of the structure; as such, a key goal while undergoing shape optimization is to avoid stress concentrations. In Figure 2-2 below, circular holes are converted into other shapes which can more readily maintain structural strength and stiffness.

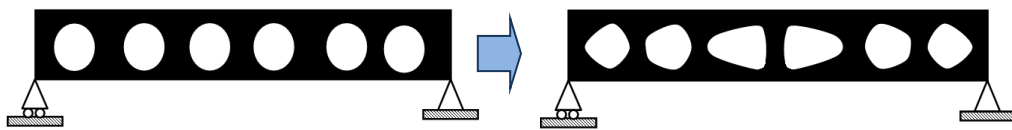


Figure 2-2: A model indicating steps of shape optimization

2.2.2 Topology optimization

The goal of topology optimization is to take a design volume, which is given, and design the stiffest structure possible which occupies a given fraction of the design volume under a certain mechanical loading condition [16, 17]. Another variation of this goal is to find a structure which satisfies a desired function and occupies a given fraction of the design volume specified. Topology optimization is often used in advance of shape and sizing optimization to obtain a template structure upon which a more elaborate design can be configured. Figure 2-3 shows a structural design process using topology optimization [16].

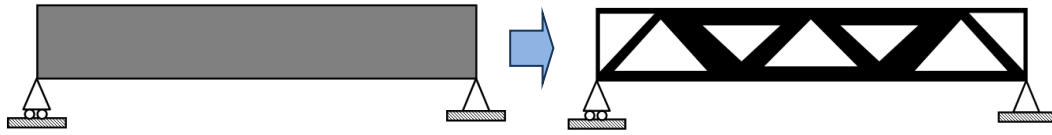


Figure 2-3: An illustration of topology optimization

A great deal of the history of topology optimization can be found in the works of Vanderplaats [18], Sigmund [19] and Rozvany [20]. As well, many researchers have devoted their work for analyzing bone micro-structural adaptation by means of topology optimization [21, 22].

2.2.3 A brief history of Michell theory highlighting its restriction

As will be explained in the following chapters of this thesis, engineering frame structures were modeled based on the Wolff's law and discrete Michell model theory and compared to find the yielding strength of the structures under examination. As mentioned above, in 1904, Michell demonstrated his renowned theory which was a mathematically driven hypothesis, unlike the Wolff's law. He established in his theory the basic requirements for a structure to support a pre-defined set of external loads while having a minimum weight. Michell's work became much more popular in the nineteen fifties, and in 1973 Hemp extended Michell truss theory to make it more rigorous. In his work, Hemp utilized a theoretical development of slip-lines for specified conditions (perfectly plastic solids within a plane). Slip-lines theory is also known as the theoretical development of Hencky-Prandtl nets) [23]. In his classical theory, Michell demonstrated that for an engineering structure to have a minimum mass (and of course volume) under a given mechanical loading situation, all the structural members must be strained by the same strain magnitude, while each element is in simple tension or compression [24, 25].

Since then, Michell's theorem was employed for different purposes such as elastic design problem and Limit State Design (LSD), two problems that are known to be mathematically related [26]. The research presented in this thesis is focused on the elastic design problem only. Michell's theory was developed for a system composed for extremely thin tension and compression elements with a continuous mass distribution. In contrast, real world applications for designing engineering structures generally require a finite number of discrete elements each with cross section area proportional to the force magnitude [24, 25].

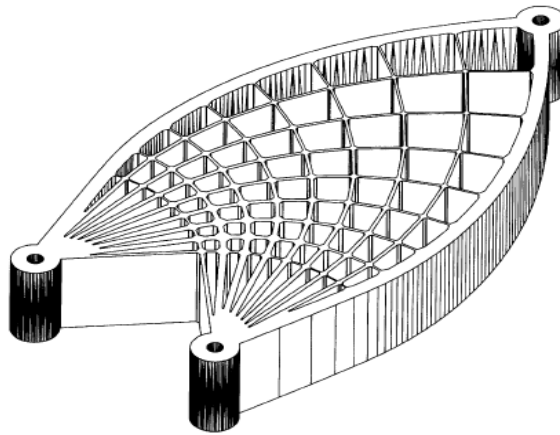


Figure 2-4: A 3D reconstruction of Michell topology (taken from [24])

In this thesis, the discrete approximation to the Michell model was employed. The use of Michell's theorem to obtain an optimal layout was not practical enough for many applications, and as a result Prager and Rozvany (1977) pioneered a more general idea of Michell's optimum layout theory [27, 28].

For an optimal frame structure design, if the objective function is the minimum mass or the ultimate strength of the structure, then an arrangement of structural members (e.g. rods) is sought to equilibrate a given set of external loads. Most of the research

around the optimum layout theory can be classified in two major types: continuum structures and skeletal structures (e.g. trusses, grillages, beams, etc.) [27]. The latter is the main interest of the present research work in this thesis.

In 1974, Prager proved that the solutions for the problem of optimum layout designs of a Michell truss can be non unique [29]. Michell truss is a truss structure with a stress constraint and having the minimum mass. Rozvany showed the validity of Prager's arguments of the non-uniqueness of solutions for the Michell truss structures. He believed that Prager's example was accurate if the truss members were confined to a smaller portion of the design plane [30]. He later addressed various weak points of the Michell's truss theory and mentioned some limitations and the classes of problems in which this theory is applicable. Rozvany showed that Michell's work (1904) only provided optimal layout information for a small number of cases, when $\sigma_0^+ \neq \sigma_0^-$. In many cases, Hemp's ideas are more suited to a larger number of cases for optimal design [31]. Rozvany, in his other work revealed some more exceptions for the orthogonality in the case of intersecting compression and tensile trajectories [23].

Rossow and Taylor postulated the idea of topology optimization which utilized a continuum approach in 1973. When utilizing this topology optimization strategy, the design area of significance could be either a truss or frame based design area, or a design area composed of continuum elements such as cubes, triangles and quadrilaterals (the truss or frame based design areas utilize discrete elements). When discrete elements are utilized, design criteria for structural members include the position and number of elements as well as their connectivity. When continuum structures are utilized, design

criteria for the internal and external shape of boundaries, as well as the selection of inner gap spaces, are used to try to satisfy predetermined criteria for the design [16].

Most often, Michell's defined structures, which are idealized (such as trusses), are not realistic for many potential designs. However, a simplification of these idealizations (such as what is displayed in Figure 2-5) may produce a realistic design.

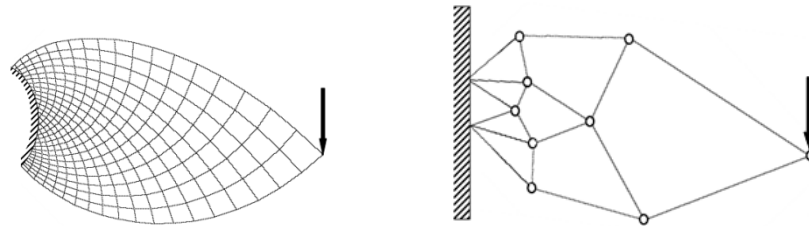


Figure 2-5: *Left*) a Michell structure *Right*) similar structure when made simpler

What is given above shows that even though Michell's methodology was, in many cases, not realistic, simplified versions of the methodology he outlined were effective in some cases. One of these cases where the simplified methodology was usually effective involved steel pipes which are welded to form a normal truss. Even though constructing a truss in this manner is very cost effective, such structures are not generally visually pleasing [32].

2.3 Extending Wolff's theory from bone to plant tissue

As mentioned above, Wolff's theory was originated based on the observation carried out on femur bone. It is valuable to expand the notion of such theory to plants and to verify it by performing empirical methodology. Below is a brief summary of the research works studying the effects of mechanical stresses on the plants morphology in sub-cellular level.

2.3.1 The role of mechanical forces in botany

Despite the fact that a great deal of effort has been continuously devoted to the understanding of remodeling of biological tissues such as bone, cartilage and muscle, much less work has been given to the interaction between mechanics and botany. In this research, Wolff's law was adapted and extended from bone research to study plants micro-structural behavior.

2.3.2 The rationale behind selecting plants

Animals are more dynamic and more difficult to constraint under a specific given laboratory condition. Plants are known to respond to their mechanical environment in ways that are perhaps more drastic, more rapid and more significant than animals; at the same time plants are more accurately tracked and measured as changes occur. Animals are more complicated in terms of their internal chemical interactions, and it is also harder to control their daily activities that might affect the average mechanical load applied to their bones. This was one of the motivations for selecting plants as they seemed more promising for the present research and it was determined they would likely produce data with significantly less noise. Although Wolff's theory is dedicated to animals bone structure in a macro-scale, in this research this theory is tailored for plants in a micro-scale [33, 34, 35].

2.3.3 Central role of mechanical stresses versus other cues

It is believed that plants adapt their micro-structural components in such a manner as to optimize their structural efficiency for the environment in which they reside. Such adaptation normally occurs as feedback to the environmental cues such as light, chemical substances, gravity, drought, electrical field, hormones and other features in the

surroundings of a plant [36, 37]; many of the abovementioned environmental impacts have been thoroughly characterized and investigated for several years. However, likely the central influencing factors affecting plant microstructures are mechanical stresses [38, 39]; furthermore, the role of such mechanical stresses has not been as comprehensively studied.

2.3.4 Microtubules

When it comes to plants microstructure, typically the roles of Cortical Microtubules (CMT), Cellulose Synthase or Cellulose Microfibrils (MFs) are the main features of most research works (Cellulose is the structural element of the cell wall in green plants - more biological terminologies are detailed in Chapter 4). For the work presented in this thesis, the main focus is cortical microtubules. One reason is due to the experimental restrictions since with the current tools and the available plant type, microtubules were the most visible candidate structures given the facilities and tools available. Another reason for the choice of plant structure chosen is that cortical MTs are used by most cells when maintaining the orientation of cellulose MFs which are recently synthesized; this is verified by a large array of data analysis from experimental work.

MTs have many roles within plants. Cyr cited Wymer's work as evidence that cortical MTs are capable of behaving as sensors and transducers; in the former case they monitor force, and in the later they communicate to cellulose synthase important spatial data [40, 41]. Considering the small size of the microtubules, what we see under the microscope is mostly a bundle of MTs not a single MT.

Microtubules are one of the elements of cytoskeleton (CSK) in plant cells and act as cells structural components. The cytoskeleton, which is made of protein, acts as

"scaffold" or "skeleton" for cells contained inside the cytoplasm. The cytoskeleton is a dynamic three dimensional structure that maintains the cells shape. Microtubules are involved in two essential roles in the plant morphogenesis; one is the orientation of cellulose microfibrils and the other one is defining the division plane.

2.3.5 History of plants micro-structural adaptation to mechanical forces

In this section, a brief history of research highlighting plants response (at the micro-structural level) to environmental stresses will be discussed.

There are various studies analyzing a plant's reaction to mechanical loads from different points of views having different objectives [42- 55]; here the focus will be given to the "mechano-sensory" feature of microtubules [56]. The term mechano-transduction refers to the mechanism of converting biophysical force (e.g. mechanical energy) to a biochemical response [65, 66].

In 1938 Castle for the first time presented that mechanical stress signals might provide directional information for individual plant cells to align their cellulose fibers [43]. Green and King later investigated the effect of stress on the orientation of microtubules specifically [57]. Williamson showed that microtubules can affect the direction of future cell expansion and morphogenesis. He also acknowledged the fact that the microtubules orientation arrangement is proportional to changes in a source providing directional information to the cell. He also believed that in the presence of the chemical and electrical gradient, mechanical stresses have relatively a more direct impact on the cell morphogenesis in comparison to chemical and electrical factors; one example of mechanical stimuli is turgor pressure which is the driving force for all cells during the growth stage [58]. Turgor pressure is defined as the pressure applied on the cell wall by

the water inside the cell. Preston also studied the orientation of cellulose as a result of mechanical forces and electrical fields [58]. He predicted that microfibrils orientation is affected by the transverse and longitudinal loads. Turgor pressure in most plant cells (with non-spherical shape) causes the cell wall to experience anisotropic mechanical forces. The minor and major axes of a cell are influenced by such mechanical forces. He proposed that cortical microtubules could orient themselves when force was transmitted through the plasma membrane. When turgor pressure is applied to a cell, the cell will tend to lengthen. The cell remains cylindrical, as its walls become reinforced in a manner that limits growth in a circumferential direction. He originally proposed the possibility of microtubules not getting directional information for re-orientation; however he was convinced that microtubules do get directional information to adjust their orientation. He outlined that in addition to the fact that chemical, electrical or other signals could affect microtubules orientation, mechanical forces could have a large impact. Mechanical forces stem directly from turgor pressure, which drives growth in cells, and thus such pressure directly impacts morphogenesis in plants; also, electrical and chemical influences are less direct and not as significant for plant growth.

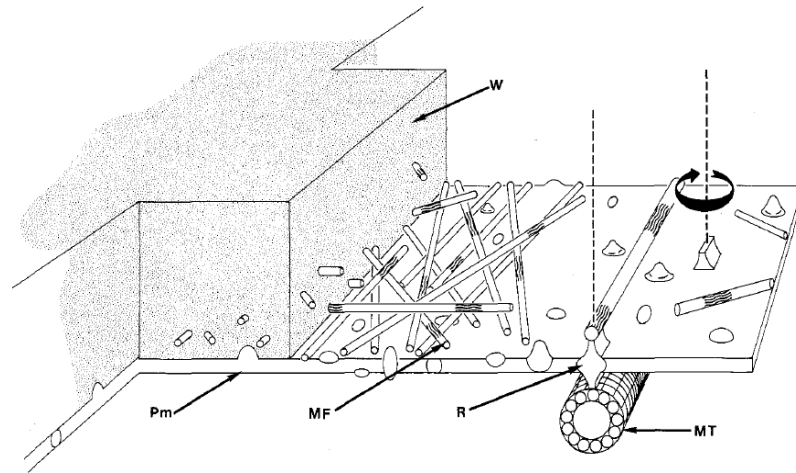


Figure 2-6: A picture demonstrating the cell wall (W), Microtubules (MT), Microfibrils (MF) and Plasma Membrane (PM) [taken from 43]

Williamson determined that the directional information source MTs use for their alignment is outside of the cell; this is contrary to many of the previous theories based on MT self-organization. The mechanism that was postulated is based on wall information transfer towards the cortical cytoplasm [43].

In other similar research carried out by J. Lucas and S.L. Shaw, which is more recent (2008), they explained that the microtubules pattern can be represented as a model for cellulose microfibril extrusion. However, as outlined in other research, they believed that the mechanism behind how the microtubules are oriented into specific patterns still remains a mystery [59].

Figure 2-6 shows the relative location of microtubules, microfibrils and plasma membrane in the cell wall, while Figure 2-7 helps to better demonstrate the arrangement and pattern of the microtubules, microtubules bundles, cellulose synthase and cellulose microfibrils with respect to each other.



Figure 2-7: Arabidopsis Hypocotyl cells with cellulose synthase complexes shown; these complexes are aligned with cortical microtubule bundles (taken from [59]).

Hejnowicz has a paper which is somewhat different from most other research from an analytical point of view. He determined an angle λ , which was defined between the cortical microtubules direction and the longitudinal direction of the cell. He studied the epidermal cells of *Helianthus annuus* (a kind of sunflower) hypocotyls.

He unveiled that there exists a periodic change in an angle λ with respect to time meaning that λ angles have a cyclic change.

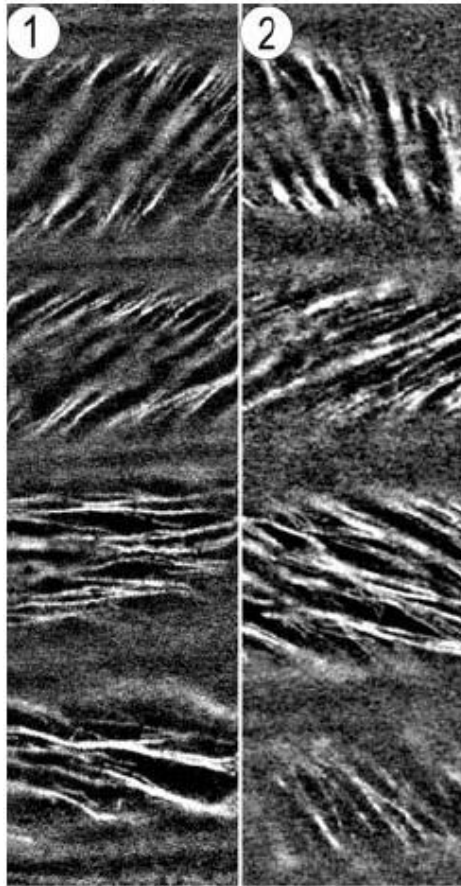


Figure 2-8: Different λ angles in neighboring cells (taken from [60])

He determined that the fact that there exists symmetry in such rotating cycle, with regards to the morphological directions, delineates the principal directions of a tensor quantity, which is possibly in charge of controlling the cycling [60, 61].

Hejnowicz has other motivating research showing the influence of tensile stress on the orientation of cortical microtubules that makes MTs align along the maximum stress in cell walls. [62, 63]. Bichet gave details on cortical microtubule patterns with a perpendicular orientation to the elongation axis of the cell while having same orientation

as cellulose microfibrils. The research conclusion for this work was that the reorientation of cortical microtubules is associated with growth [45].

In a scope from a micro-to-macro (cell level-to-the entire plant) structural point of view, Dumais described how the growth of a plant requires shape forming. He outlined that the existence of the aptitude in plants in sensing and transferring mechanical signals implies the potential interaction between chemistry and physics of the plant. For a more comprehensive understanding from the process of growth and development in plants, he believed that it is essential to synthesize the fundamentals of mechanics with molecular science; emphasizing that mechanical forces might have a key and central role in conducting some biological phenomena. In a research paper he investigated plant tissue shape forming under the effect of mechanical buckling and was convinced that the rippling shape of a grass leaf is an example of patterning by means of mechanical forces (more specifically buckling) [64]. The comparison made between the wavy looking grass blade and a knitting sample is illustrated in Figure 2-9. This proves that mechanical buckling has influenced the plant tissue.

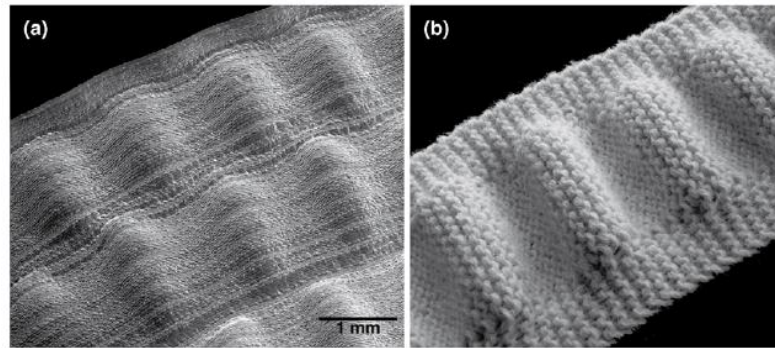


Figure 2-9: Mechanical buckling deformations influence on the plant tissue (a) wavy looking grass blade (b) A knitting sample with rippling in the center (taken from [64])

Dumais’s research shows that mechanical forces are substantial aspects in the development of plants [64].

There are some research works studying the effects of gravity on the micro-structure of the plant. A clinostat is a device which is used to reduce or even negate the effects of gravity on the growth and development of plants. The terms “gravitropism” and “gravimorphism” are used to describe the effects of gravity on growth and development respectively. M. Saiki et al used a clinostat to study the effects of gravity on plant growth. When rice seedlings were taken from a “normal” gravitational environment and moved to a clinostat, a change was noticed in the epidermal cells. More specifically, within half an hour the cortical microtubules were oriented more transversely [67].

Ranjeva et al. as well studied gravity effects on microtubules orientation. One finding was that the cortical microtubule may help act as a stabilizer by sensing strain and helping to counter some of the gravitational effects acting on plants. If gravity vector is considered as an external force applied to the plant, microtubules act as a strain-gauge;

thus changing the direction of the gravity will be followed by the re-orientation of the plant's growth which involves microtubules in the sensation mechanism [68].

Hardham et al. have also accomplished research proving the alterations in microtubules arrangement in *Arabidopsis* epidermal cells by utilizing a micro needle [69].

In another recent paper (2007), Elsner studied cortical microtubules (CMTs) when subjected to chiral mechanical load. Specifically, the consequence of applying a mechanical torque to hypocotyls was observed by tracking the orientation of CMTs.

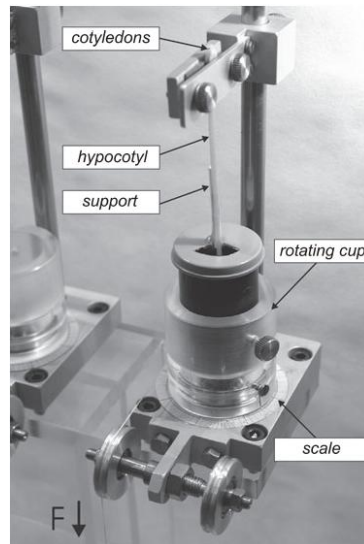


Figure 2-10: Hypocotyl of sunflower under rotational torque examine. (taken from [70]).

When compared to the cell's long axis direction, control (untouched) and immobilized (but untwisted) specimens had cMTs that were generally transverse whereas twisted specimens had cMTs that were generally oblique.

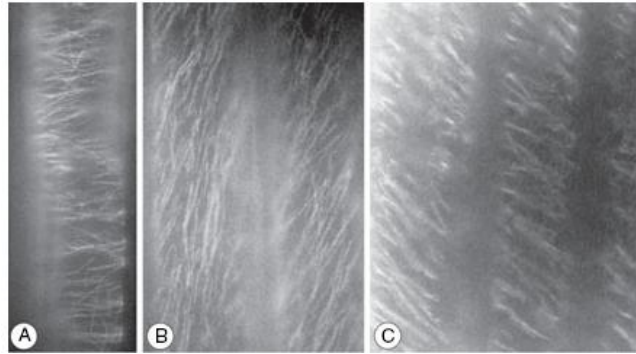


Figure 2-11: Cortical microtubules orientation in a sunflower hypocotyls being (A) transverse and (B-C) oblique (taken from [70]).

Such data suggest that cortical microtubules are directly related to the changes in tissue stress [70].

The effects of electrical fields and mechanical fields were studied by J. M. Hush and R. L. Overall in 1991; these fields were not so strong as to cause injuries to the plants. Reorientation of cortical microtubules was observed in pea roots such that the new orientation of the microtubules was in a plane generally perpendicular to the field applied [71].

Fisher and Cyr examined the cytoplasm of cells when changes in gravity were applied. Specifically, tension and compression forces were applied to plants and the changes to protoplasts were observed (Protoplast is a colorless material that contains and surrounds other parts of a cell. Protoplasts are living parts of a cell -including protoplasm- that had their cell walls removed.). The “protoplasts” generally become longer in the direction of the force applied or perpendicular to the force applied. The authors (Fisher and Cyr) came to the conclusion that plants acted in a manner such as to ensure optimal growth [72].

In 1974, Philip M. Lintilhac examined cell plate orientation when axial load was applied. Given a certain stress environment, he found a preferred orientation of cells during their attempt to maximize the ability of a cell to manage shear stress based on a unique orientation of a cell free from shear stress. Lintilhac found a relationship relating the principal stress trajectories and cell wall arrangement [73].

Hamant and his colleagues inspected microtubules in the shoot apex of a plant and its influence on morphogenesis. They showed that microtubules align themselves along the principal stresses as anticipated. They identified (by measuring the “average” of wall stresses) that a feedback mechanism is mainly responsible for aligning microtubule directions along the axis of maximum stress. They studied the shoot apex to determine that the principal stress directions have the same arrangement with orientations of cortical microtubules [74].

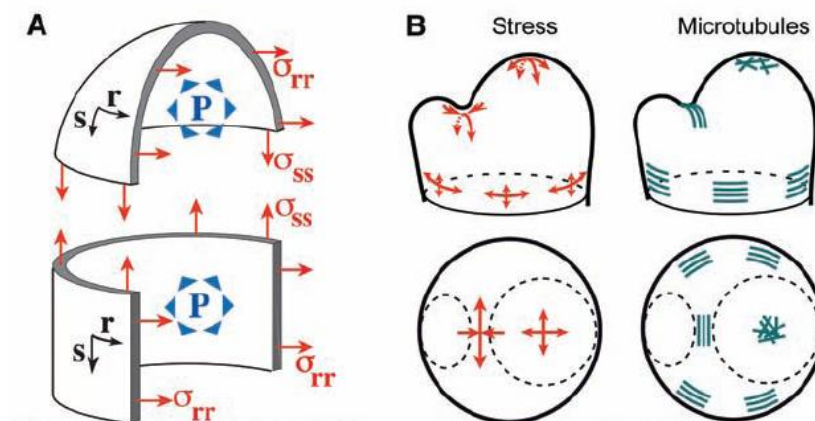


Figure 2-12: Proposed stress patterns for the meristem. *a*) Stresses in a pressure vessel *b*) Microtubules orientations (taken from [74]).

Hamant, in another paper with J. Trass, underlined the importance of interaction between biochemistry and mechanics and discovered the role of mechanical signals. This further strengthened the undeniable contribution of stress patterns in the future cell shape and division although it is not clear yet whether the cell wall or maybe plasma membrane is involved in the signaling mechanism [57].

Uyttewaal et al studied the role of biochemistry and biophysics in morphogenesis, and a couple of different patterning mechanisms were explained. Both of these two mechanisms are integrated together inside a plant, even though they are sometimes not coupled. The first mechanism keeps growth rates under control using mostly auxin-based signaling. The second mechanism keeps anisotropic growth rates under control (and possibly contributes to patterning growth rates) using mechanical-based signaling while utilizing microtubules [75].

Dumais showed that a “mechanical signal” could be involved as part of a morphogenetic feedback mechanism to regulate the alignment of cortical microtubules [76].

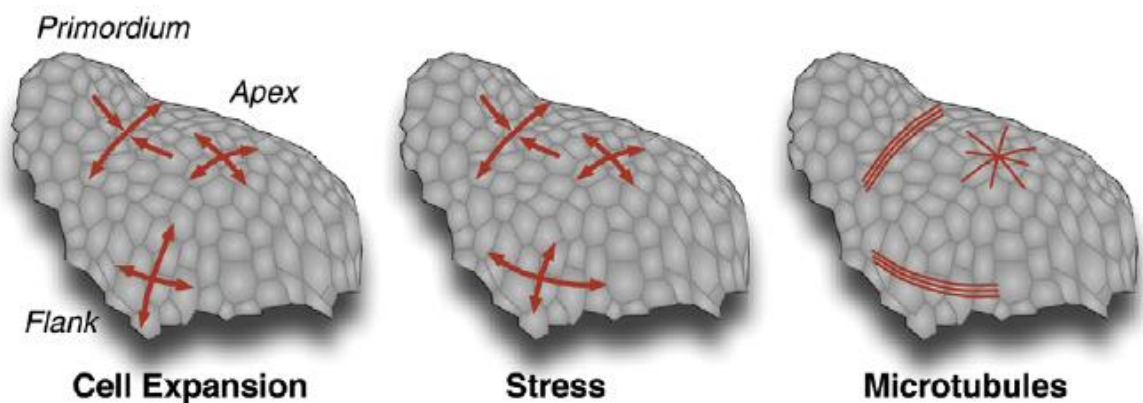


Figure 2-13: A shoot apical meristem (SAM) showing the directions of cell expansion, principal stresses, and microtubules (Taken from [76]).

Zhou and his colleagues similarly proved that alterations in microstructural growth were often due to applied mechanical forces. There was a greater tendency for cells under induced mechanical load to divide and elongate in a direction at right angles to applied principal stresses [77].

Many researchers believe that cell wall strain produces stress, which is what causes cortical microtubules to become oriented (along the direction of maximum stress) [74, 40]. Cyr stated that turgor pressure, although hydrostatic and therefore isotropic, generates vectored stress transmission in plant cells because of cell geometry and mechanically anisotropic cell walls. As a result of force transfer between plant cells, structurally important information can be transferred from cell to cell [40]. MT-cuing mechanisms have been studied in different research works. In one experimental study conducted by Hush and Overall, plant root cell MTs changed orientation to be orthogonal to forces applied after having been exposed to lateral compressing load. Another similar study was carried out by Clearly and Hardham, who utilized 5 to 20 minutes of pressure at 50 MPa on *Lilium* leaves; cellular cortical arrays generally reoriented. It is clear from the studies conducted that MT are not only influenced by mechanical loads but also their arrays can reorient themselves partly due to the influence of mechanical forces. Wymer et al. conducted multidisciplinary research between biologists and mechanical engineers in 1996. They studied the effect of centrifugal forces on the orientation of microtubules in protoplasts and concluded that microtubules orientation become aligned with the vectors of such forces. They were convinced that microtubules act like biophysical sensors [78, 40, 79, 80].

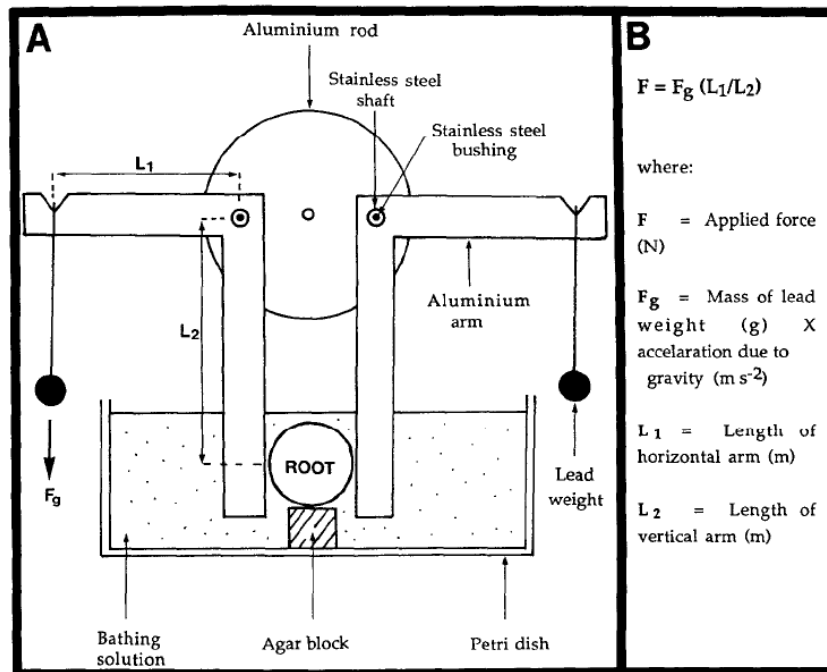


Figure 2-14: Schematic picture showing apparatus employed to apply force to the pea roots [taken from 79]

In 1997, Fischer and Schopfer investigated multiple effects of mechanical forces along with light and auxin treatment in the maize coleoptiles. They applied bending stress to Coleoptile segments, which was achieved by bending them over stainless steel pins that were curved 60° and mounted vertically; same segments were used as control sample and were placed on straight pins. Mechanical bending stresses, auxin, as well as red and blue light were used to investigate cortical microtubule re-orientation (in longitudinal and transverse direction); this re-orientation was observed for maize coleoptile specimens at their outer epidermal wall. Mechanical loading was in the form of cell extension or compression triggered by bending. The researchers outlined in their results that change in growth caused by either mechanical forces, auxin or light will affect MT orientation. In

their research they were convinced that MT's change in orientation was a result of mechanical stress or rate of growth fluctuations [81].

Effects of wounds on the cell polarity and as a result on the microtubules orientation was studied by Hush et al. The research they conducted showed that plant tissue cell polarity changes could be anticipated from MT changes in orientation. They proposed that the mechanism behind such significant change might be the electric field produced by the ionic wound current and also change of mechanical stress field. After observing MT orientation five hours after wounding the plants, the researchers found a few patterns in the wounds; those cells located near the wound tip had longitudinal MTs, nearby cells located within the wound corner had oblique MTs, cells located at wound edges had transverse MTs, and cells at the junction of the stele and cortex had longitudinal MTs. These junctions were located near the edge of the wound [82].

2.4 Chapter Conclusion

Wolff's law and Michell theory have been thoroughly explored, and the manner in which they relate to plant microstructure has also been evaluated in detail in this chapter. This knowledge will be used in subsequent thesis chapters to develop the body of the thesis around how these theories are applicable to various areas of study; specifically, in a structural engineering and biological context.

In the next Chapter of this thesis, Wolff's law and Michell theory are used in engineering frame structural design. A goal of this chapter is to demonstrate how biologically inspired theories can apply to engineering to help achieve material and cost savings. This extends the applicability of the research presented from only the biological realm into the structural design realm as well.

Chapter Three: Engineering Frame Structures and Principal Stresses

This chapter is largely concerned with how the internal arrangement within structures influence the relative magnitude of the stresses developed internally. This chapter helps to demonstrate how biologically inspired theories can be applicable to other areas of study (in the case outlined in this chapter, structural engineering). Principal stresses and their trajectories will be explained more in detail, along with how to derive such trajectories for a given condition. The two major theories mentioned in Chapter 1 of this thesis “Wolff’s law” and the “Michell Theory” will be explained in detail and compared to one another performance wise.

Getting the most optimized and best performance from a structure is a mixture of engineering, technology, mathematics and science. There are many different theories focusing on the structural optimization when it comes to engineering and bio-science. Among these theories, Wolff (science related) and Michell (engineering related) were among the most prominent. This is the main reason that these two theories were of interest in this research. Bringing together these two seemingly different theories from bioscience and engineering will allow for more research focus on this topic, which is not described in literature sufficiently. Although, utilizing natural structures as a starting point for engineering design has been closely studied since more than a century ago, there has been many different opinions and hypotheses developed with different interpretations giving credit or challenging an idea, and in this thesis there is a more thorough discussion about this topic to help better understand it.

3.1 What is Wolff's premise known as "Wolff's law?"

Before introducing Wolff and his influential theory, a frontally sectioned femur bone is illustrated for a better understanding of bone's internal structure for engineers as per Figure 3-1. Trabecular bone is the spongy part of the interior bone tissue which resembles a network of fibers. The exterior surrounding of the femur bone is denser and called cortical bone. Such design of the bone provides a strong structure with the advantage of keeping the weight as small as possible.

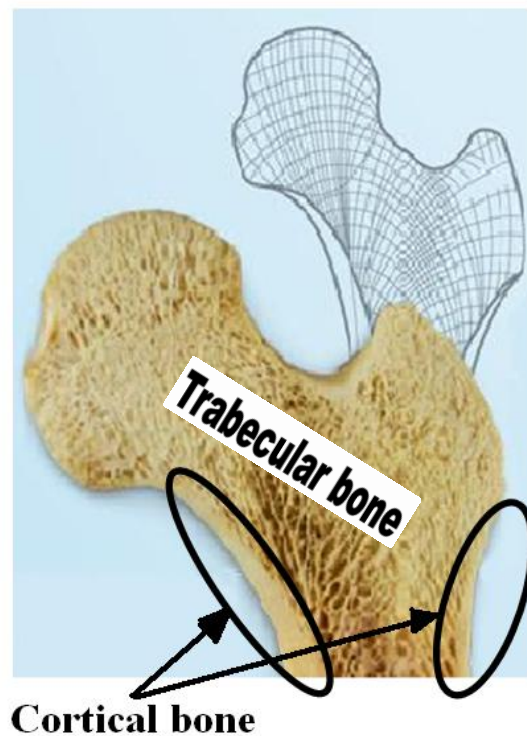


Figure 3-1: A frontally sectioned view of a femur bone. The spongy looking part is called trabecular bone and the more dense peripheral area is called cortical bone. Such design has both benefits of reducing the bone's weight while maintaining the maximum strength for load tolerance [taken from <http://www.answersingenesis.org/articles/am/v4/n4/architects> and modified].

In simple words, Wolff's law is one of the most distinguished theories highlighting similarities between a natural tissue (bone microstructure) and an engineering structure (crane-like beam). Julius Wolff was an anatomist and surgeon, and his works were one of the milestones in skeleton anatomy and orthopedics. He suggested the analogy between the trabecular bone pattern in a femur bone and the principal stress trajectories of a crane-like cantilever. He showed that the micro-structural elements in a femur bone (known as trabecula) adapt their arrangements with respect to the principal mechanical stresses (compression or tension) trajectories as shown in Figure 3-2.

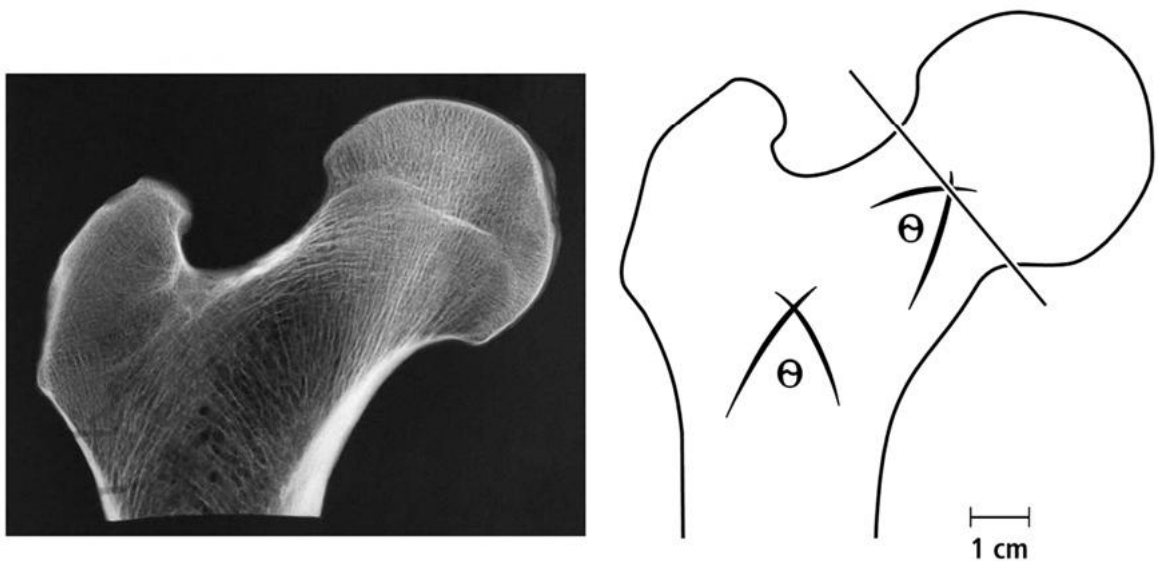


Figure 3-2: A human femur bone frontally sectioned. This was as a standard sample in most of Wolff's observations (taken from [2]).

Wolff's theory was in fact originated from K. Culmann and Von Meyer's studies in 1866. Culmann was a notable engineer and evaluated the analogy between the trabecular bone arrangement in a human first metatarsal bone and the principal stress trajectories of a cantilever beam [83]. Since he was an engineer, he suggested the

outcome of his observations to Von Meyer who was an anatomist. These two researchers also made the same comparison between the human proximal femur bone and a crane-like beam. There was a main difference between Culmann's and Von Meyer's drawings: Von Meyer's drawings of femur bone trabecular trajectory lines do not form orthogonal intersections while Culmann's drawings of such trajectory lines obviously meet with 90 degree angles. However, Von Meyer hasn't clearly entailed the non-orthogonality of the intersecting curves.

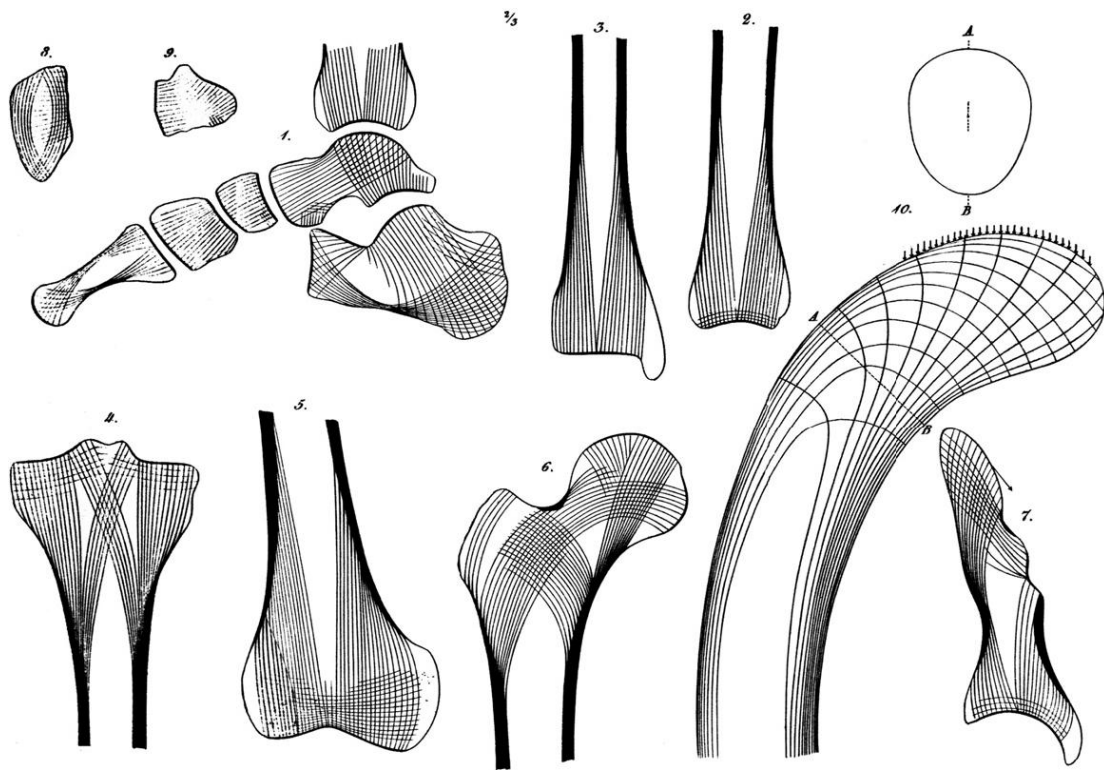


Figure 3-3: Culmann and von Meyer's drawings illustrating trabecular patterns for different specimens of human bones. Stress trajectory lines on an arched beam are also shown (taken from [2]).

Later on, when Wolff made more observations and studied more in detail, he was convinced that such analogy between the pattern of stress trajectories in Culmann's

crane-like beam and the trabecular arrangement in the human femur bone cannot be just a coincidence. In 1870, he expanded his theory known as “Wolff’s law” and also demonstrated that these trajectories intersect at right angles [2].

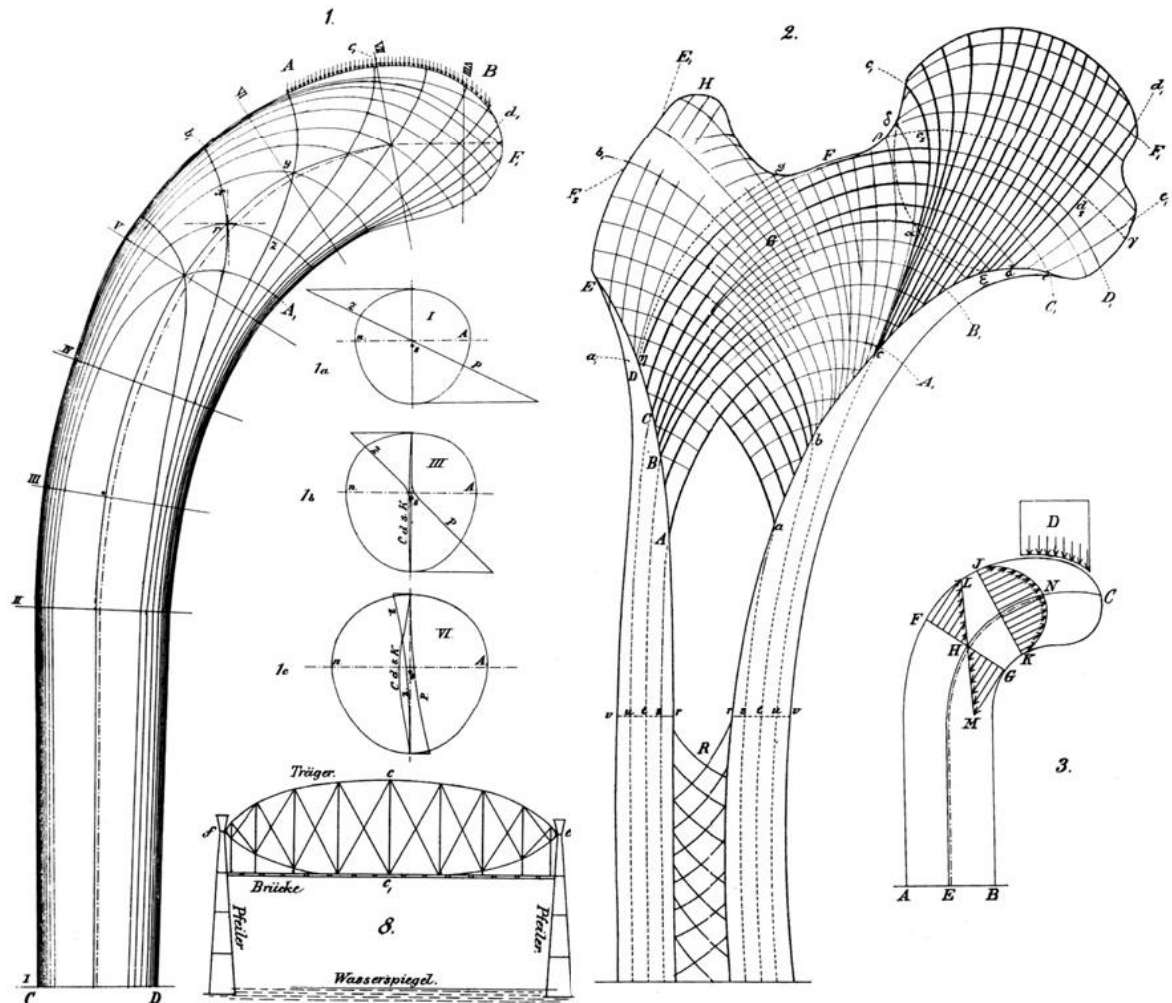


Figure 3-4: Wolff’s drawings comparing femur bone trabecular arrangement with an arched beam based on Culmann’s original work (taken from [2]).

Wolff was also aware of the fact that such geometric arrangements (curves meeting at right angles) could be only a rough approximation for real world scenarios.

This means that since a bone is a live dynamic tissue experiencing a variety of loading pattern, the trabecular bone arrangement could be reflecting the effect of “average” load system.

Since then Wolff’s hypothesis has been accredited or challenged by many researchers as more detailed in Chapter 2 of this thesis. Most of the disputes that Wolff’s theory was facing were those questioning the orthogonality of the intersecting curves. Apart from all such disagreements about Wolff’s view, a prominent research work in 1917 by an anatomist named J.C. Koch appears to have established a sturdy mathematical validation foundation for Wolff’s hypothesis [2, 3]. Koch made a comparison between a femur bone and an equivalent structure having the same external shape. He stated that “the structure of the femur is based upon exact mathematical laws” [3]. He even went one step further and stated that not only the internal architecture of the femur bone, but also the external profile, is adapted to the functional loading. This means that any variation in the exerted mechanical stresses on the bone is closely followed by an equivalent change in both internal and external structure.

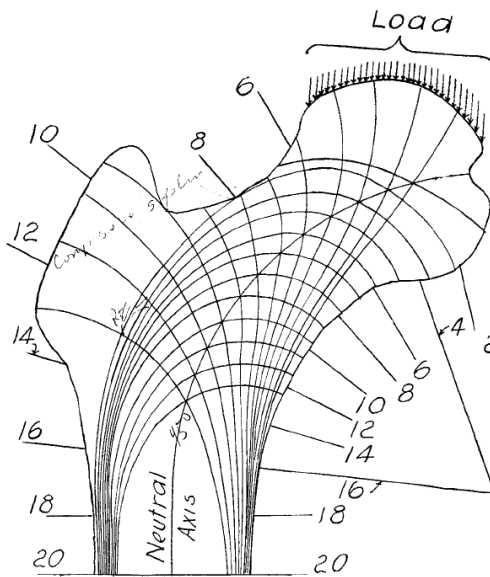


Figure 3-5: Koch's mathematical analysis illustrating the stress trajectories (tension/compression) in the femur bone (taken from [3]).

3.2 Principal stress trajectories

3.2.1 Principal stresses

Consider a continuum body experiencing a system of external forces having stress distribution in a given point as per Figure 3-6. The state of stress in this point will be defined by the stress tensor in Cartesian coordinate system.

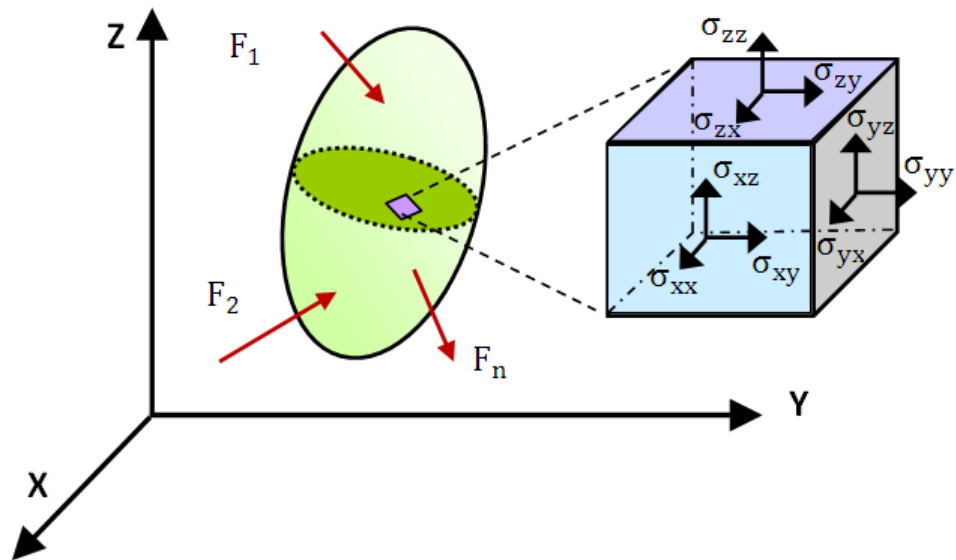


Figure 3-6: State of stress in a selected point of a continuum body under a system of external forces

The stress tensor has nine components; three of which are the normal stresses and the other six components are shear stresses.

$$\boldsymbol{\sigma} = \begin{bmatrix} \sigma_{xx} & \sigma_{xy} & \sigma_{xz} \\ \sigma_{yx} & \sigma_{yy} & \sigma_{yz} \\ \sigma_{zx} & \sigma_{zy} & \sigma_{zz} \end{bmatrix} \equiv \begin{bmatrix} \sigma_x & \tau_{xy} & \tau_{xz} \\ \tau_{yx} & \sigma_y & \tau_{yz} \\ \tau_{zx} & \tau_{zy} & \sigma_z \end{bmatrix} \quad \text{Equation 3-1}$$

Eigenvalues of a tensor are actually invariants that their values do not depend on the coordinate system selected. The eigenvalues of a stress tensor are called the principal stresses. Mohr's circle is a graphical method representing the state of stress at a point. Mohr's circle also assists in finding the principal (maximum-minimum) stresses values along with their directions as briefly explained here. The derivation for the principal stresses is undertaken here by using the proper equation and illustrating it in Mohr's circle in 2D only.

As is common engineering knowledge from the fundamentals of Mechanics of Materials, for a given state of plane stress $\begin{bmatrix} \sigma_x & \tau_{xy} \\ \tau_{xy} & \sigma_y \end{bmatrix}$ in a selected point, the principal stresses will be defined as Equation 3-2:

$$\sigma_1 = \sigma_{max} = \frac{(\sigma_x + \sigma_y)}{2} + \sqrt{\left[\frac{(\sigma_x - \sigma_y)}{2}\right]^2 + \tau_{xy}^2}$$

$$\sigma_2 = \sigma_{min} = \frac{(\sigma_x + \sigma_y)}{2} - \sqrt{\left[\frac{(\sigma_x - \sigma_y)}{2}\right]^2 + \tau_{xy}^2}$$

$$\tau_{min,max} = \pm \sqrt{\left[\frac{(\sigma_x - \sigma_y)}{2}\right]^2 + \tau_{xy}^2} \quad \text{Equation 3-2}$$

Utilizing the above equations, one can find the “value” of the principal stresses. The “direction” of such stresses is defined as per Equation 3-3:

$$\theta_p = \frac{1}{2} (tg^{-1}[2\tau_{xy}/(\sigma_x - \sigma_y)])$$

$$\theta_s = \frac{1}{2} (tg^{-1}[-(\sigma_x - \sigma_y)/(2\tau_{xy})]) \quad \text{Equation 3-3}$$

θ_p is the angle that the maximum “normal stress” plane forms with the X axis and θ_s is the angle that the maximum “shear stress” plane makes with the X axis. Note that $\theta_s = \theta_p \pm 45^\circ$.

The presented mathematics are better facilitated and understood by employing Mohr’s circle as a graphical tool as shown in Figure 3-7.

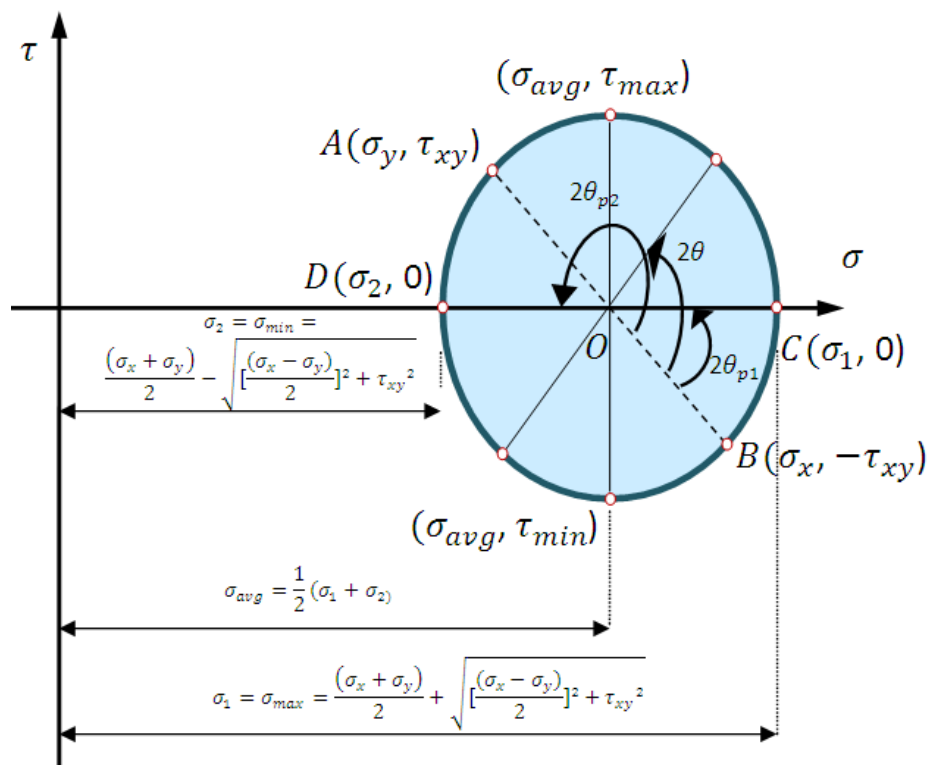


Figure 3-7: Mohr's circle for a given stress condition at a point. By defining points A and B, maximum and minimum stresses will be identified as Points C and D on the circle.

A transformation from a regular coordinate system to the principal directions is demonstrated in Figure 3-8:

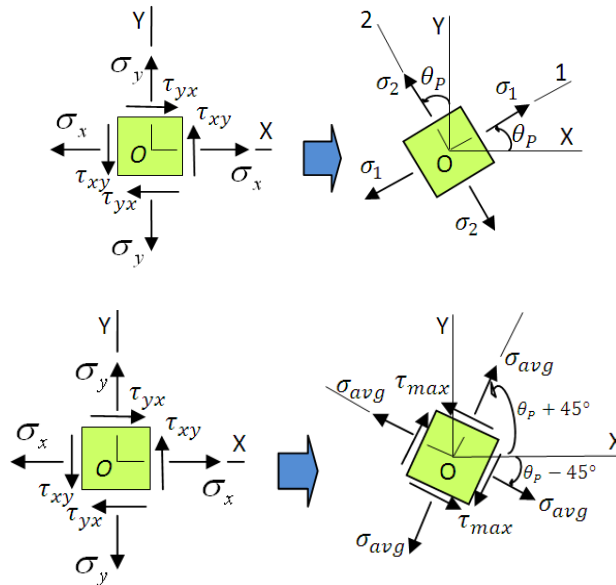


Figure 3-8: Normal and shear stresses being transformed from a given coordinate system to the principal directions

3.2.2 Principal stress curves known as stress “trajectories”

Principal stress “trajectories” are in reality a system of curves which are intersecting each other with a 90 degree angle as shown in Figure 3-9. Each family of curves representing tension and compression in the beam along with the neutral axis are also recognizable in this figure. Every point of a “solid line” represents the direction of the principal *tensile* stresses, while “dashed lines” identify the direction of the principal *compressive* stresses.

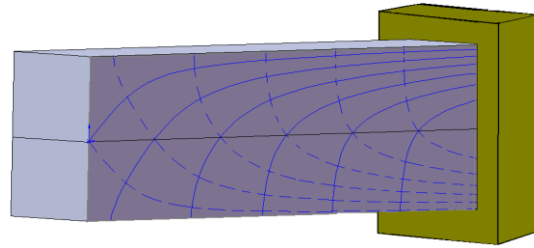


Figure 3-9: Stress trajectories illustrated in a continuum cantilever beam having a concentrated load at the free end. Each point on a solid line defines direction of the principal tensile stress, whereas dashed lines identify the direction of the principal compressive stress.

Following is a brief description of the rationale behind creating principal stress trajectories, which will be pursued more in details in the following sections through the use of relevant equations and Matlab code showing how to construct them.

Consider the element in Figure 3-10, which is in an arbitrary point of a cantilever beam in XY plane. The cantilever has a concentrated transverse force (F) at the free end of the beam with a rigid support at the other end. Dimensions of the beam are as follow: length L , depth $2h$, width w , cross section area A_0 and moment of inertia of the section I .

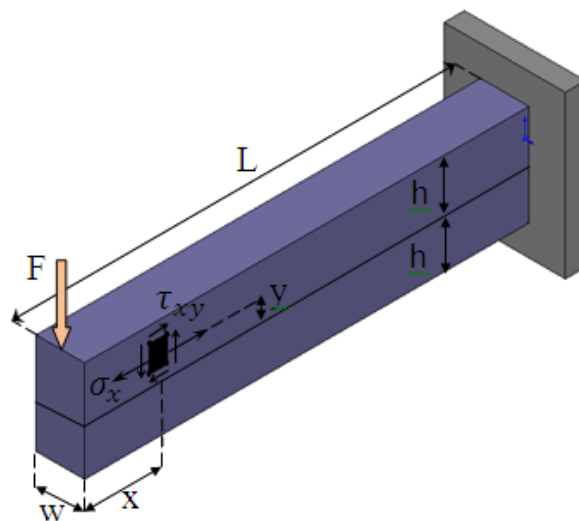


Figure 3-10: An arbitrary element in the XY plane of a cantilever beam under a concentrated transverse force.

The state of the stress in the element shown in Figure 3-10 will be as follows:

$$\sigma_x = \frac{Fxy}{I} = \frac{3Fxy}{A_0h^2} \text{ and } \tau_{xy} = \frac{3F}{2A_0} \left(1 - \frac{y^2}{h^2}\right) \quad \textbf{Equation 3-4}$$

Principal stresses can be calculated by employing sets of Equation 3-2 and Equation 3-3. One can determine the numerical amount of σ_x and τ_{xy} since the values of the other parameters in Equation 3-4 are known. However, it is preferred to provide a solution parametrically (to be more generalized) by introducing $\sigma_n = \frac{Mh}{I}$ where M is the bending moment acting at a point. Figure 3-11 gives details of calculation performed for finding the ratio σ_{\min}/σ_n and σ_{\max}/σ_n in two different sections A and B of the beam.

	Section A			Section B		
y/h	σ_{\min}/σ_n		σ_{\max}/σ_n	σ_{\min}/σ_n		σ_{\max}/σ_n
1	0.0		1.0	0.0		1.00
0.8	-0.01		0.81	-0.001		0.80
0.6	-0.04		0.64	-0.003		0.60
0.4	-0.09		0.5	-0.007		0.41
0.2	-0.16		0.36	-0.017		0.22
0.0	-0.25		0.25	-0.063		0.063
-0.2	-0.36		0.16	-0.22		0.017
-0.4	-0.5		0.09	-0.41		0.007
-0.6	-0.64		0.04	-0.60		0.003
-0.8	-0.81		0.01	-0.80		0.001
-1.0	-1.0		0.0	-1.00		0.0

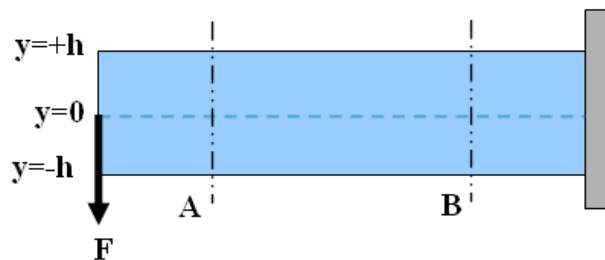


Figure 3-11: *Top*-Principal stresses distribution for section A and B of the beam. *Bottom*- A cantilever beam having a transverse single load at its free end. Principal stresses have been measured for 11 points on each section A and B.

As described in the table in the previous figure, the presented ratios, along with the principal directions have been computed for 11 different elements all located in each of the two cross sections (A or B). If such analysis is expanded to include more elements in each cross section, as well as more cross sections across the whole beam, then stress trajectories will be found as shown in Figure 3-9. One set of such stress trajectories are tangent to the principal axes and correspond to σ_{\min} and the other set of stress trajectories are tangent to the principal axes and correspond to σ_{\max} .

3.2.3 Building stress trajectories in Matlab

As described using Equation 3-4, a stress tensor in an arbitrary element for what is shown in Figure 3-10 will be as per Equation 3-5:

$$\begin{bmatrix} \sigma_x & \tau_{xy} \\ \tau_{xy} & \sigma_y \end{bmatrix} = \frac{3F}{4wh^3} \begin{bmatrix} 2xy & h^2 - y^2 \\ h^2 - y^2 & 0 \end{bmatrix} \quad \text{Equation 3-5}$$

Thus, principal stresses are the eigenvalues of the above stress matrix which are defined as follows:

$$\begin{bmatrix} \sigma_1 & 0 \\ 0 & \sigma_2 \end{bmatrix} = \frac{3F}{4wh^3} \begin{bmatrix} xy + \sqrt{(h^2 - y^2)^2 + x^2 y^2} & 0 \\ 0 & xy - \sqrt{(h^2 - y^2)^2 + x^2 y^2} \end{bmatrix} \quad \text{Equation 3-6}$$

And the eigenvectors will be given as follows:

$$\begin{aligned} eig_1 &= \left(\frac{1}{h^2} \right) \left(xy + \sqrt{(h^2 - y^2)^2 + x^2 y^2} \right) \mathbf{i} + (h^2 - y^2) \mathbf{j} \\ eig_2 &= \left(\frac{1}{h^2} \right) \left(xy - \sqrt{(h^2 - y^2)^2 + x^2 y^2} \right) \mathbf{i} + (h^2 - y^2) \mathbf{j} \end{aligned} \quad \text{Equation 3-7}$$

It is important to mention that the eigenvectors in Equation 3-7 depend only on x , y and h , and they are independent of the force applied (F). As mentioned before, stress

trajectories are tangent to the eigenvectors of the aforementioned matrix in Equation 3-5; thus they are determined by the following differential equations [84]:

$$\frac{dy}{dx} = \frac{xy \pm \sqrt{(h^2 - y^2)^2 + x^2 y^2}}{h^2 - y^2} \quad \text{Equation 3-8}$$

The explicit form of the solutions for such differential equations (Equation 3-8) can be obtained in reference [84]. Once again, the stress trajectories only depend on the *direction* of the principle stresses and not on the *magnitude*. These trajectories are orthogonal to each other and by taking either the plus sign or the minus sign in Equation 3-8, the two sets of curves representing tensile or compressive principal stresses will be achieved. Furthermore, for every element chosen on the beam, there exists a pair of these curves, and if they were all depicted, then instead of having Figure 3-9, an entirely black cantilever due to so many lines being drawn on the figure would be depicted (so as to obfuscate the view of any individual line).

The differential equations in Equation 3-8 were utilized in a numerical iterating algorithm with the initial conditions starting on a given point on the neutral axis of the beam and terminating on the cantilever's boundaries. The stress trajectories were produced by using a program in the Matlab programming environment and then results were exported to a Finite Element software (Ansys) for optimization analysis, which will be more explained in the following sections. Appendix A has the context of the Matlab program to create the compressive and tensile stress trajectories. This program is called "Matlab Program #1".

Figure 3-12 has a sample output of the aforementioned Matlab program (for tensile and compressive stress trajectories) for the input value of cantilever dimensions $L=100$ and $2h=30$; this program ran for 300 iterations:

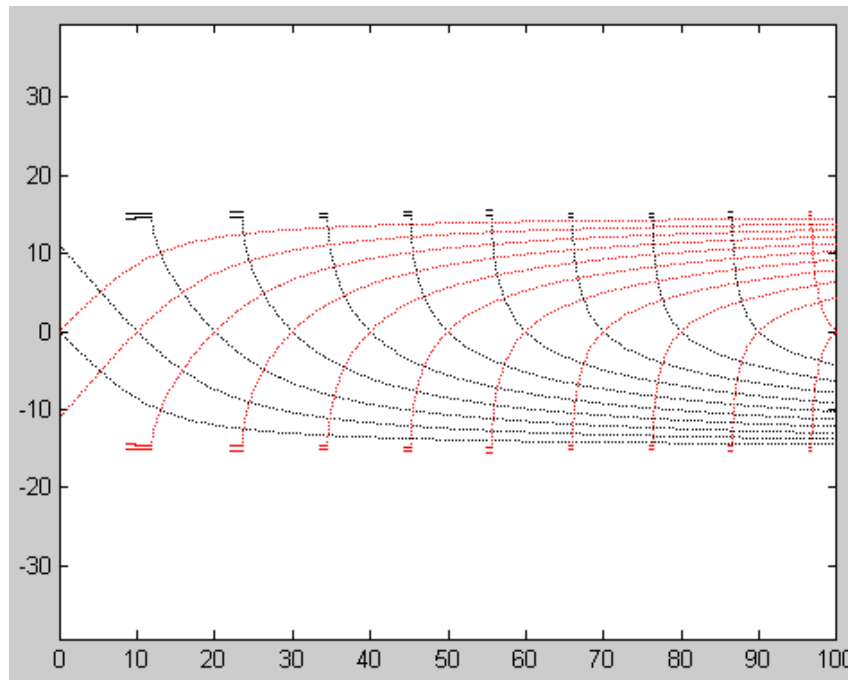


Figure 3-12: Tensile (*red*) and compressive (*black*) stress trajectories for a cantilever beam with single transverse force at the free end of the beam; built in the Matlab programming environment.

As previously described, for each point on the cantilever beam, there is a pair of stress curves. Those illustrated in Figure 3-12 are ones selected to go through some designated points on the neutral axis of the beam. This figure could show a different set of trajectories if other arbitrary points were selected on the beam. The criterion for choosing these points is based on having equal distances between the points on the neutral axis.

The achieved data in the previous figure are now set to be exported to a CAD software for further analysis. Thus, after constructing these stress trajectories in Matlab, they were exported to Solidworks software for illustration and future structural performance analysis. As described in the appendix for Matlab program #1, each curve point obtained from this program is saved in a separate data file, which will be readable by SolidWorks program. Figure 3-13 illustrates the 2D and 3D reconstructed model obtained:

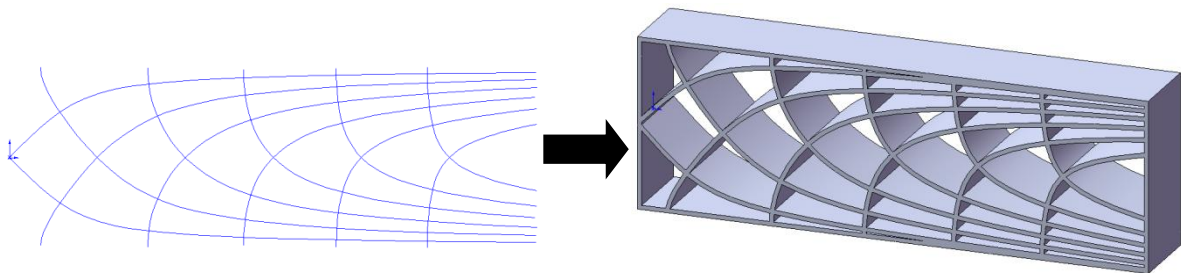


Figure 3-13: Generating stress trajectories in SolidWorks software in 2D and 3D by means of Matlab program producing the curve points.

3.2.4 Role of stress concentration

From a stress analysis point of view, one of the most significant distinctions between a real world phenomena and a mathematical simulation is stress concentration. In the previous section, stress trajectories were constructed mathematically based on a Matlab program; however in reality, such trajectories are affected by stress concentration in the system under the influence of a concentrated load, a given support condition, manufacturing imperfections, geometry, etc. Extracting the stress trajectories for a relatively more complicated system (as opposed to what was outlined for the previous section) acted upon by a given system of forces (rather than a single load) on a beam

having an arbitrary structural shape or support condition will only be achievable by means of Finite Element Analysis.

In this section, the procedure of how to derive the principal stress trajectories from a finite element analysis is discussed, which is dissimilar to the process explained in the aforementioned section and is more intricate. Stress trajectories are created by means of isoparametric interpolation among the nodal quantities obtained from a Finite Element Analysis in Ansys software.

3.2.4.1 Isoparametric interpolation:

As is common engineering knowledge, a shape function is a mathematical formula which assists to interpolate data outside a mesh grid where there is no given point to identify the mesh. An isoparametric element, coming from its name (iso=same), utilizes a similar set of shape functions to describe both the element geometry and displacement interpolations; more specifically, displacement functions are utilized to describe the element geometry.

There are advantages and limitations in employing an isoparametric formulation when it comes to structural mechanics. One advantage is that same steps for all the isoparametric elements are applied and the shape functions are very quickly created. As well, it's not required to separate or categorize elements with a straight or curved side. Limitations of this technique will consist of weak performance (being overly-stiff) of low-order isoparametric elements. As well, the method is not extendable to problems with index variation more than 1 (for example plate bending or shells) which is not a concern in this thesis.

Assume a two dimensional (2D) element having n nodes in a plane stress condition. Isoparametric representation of such an element will be described as follows. Equation 3-9 and Equation 3-10 describe an element geometry and displacement interpolation respectively:

$$1 = \sum_{i=1}^n N_i, \quad \hat{x} = \sum_{i=1}^n \hat{x}_i N_i, \quad \hat{y} = \sum_{i=1}^n \hat{y}_i N_i \quad \text{Equation 3-9}$$

$$u_{\hat{x}} = \sum_{i=1}^n u_{\hat{x}i} N_i, \quad u_{\hat{y}} = \sum_{i=1}^n u_{\hat{y}i} N_i \quad \text{Equation 3-10}$$

Where $\{\hat{x}_i, \hat{y}_i\}$ defines the location of each node.

This will be as follows in a matrix form:

$$\begin{bmatrix} 1 \\ \hat{x} \\ \hat{y} \\ u_{\hat{x}} \\ u_{\hat{y}} \end{bmatrix} = \begin{bmatrix} 1 & 1 & \dots & 1 \\ \hat{x}_1 & \hat{x}_2 & \dots & \hat{x}_n \\ \hat{y}_1 & \hat{y}_2 & \dots & \hat{y}_n \\ u_{\hat{x}1} & u_{\hat{x}2} & \dots & u_{\hat{x}n} \\ u_{\hat{y}1} & u_{\hat{y}2} & \dots & u_{\hat{y}n} \end{bmatrix} \begin{bmatrix} N_1 \\ N_2 \\ \vdots \\ N_n \end{bmatrix} \quad \text{Equation 3-11}$$

Where N_i are shape functions, u_i displacement and (\hat{x}, \hat{y}) are the natural coordinate system.

The above equations for a 4-Node bilinear quadrilateral element after equalizing geometry and displacement will be as follows:

$$\begin{bmatrix} 1 \\ \hat{x} \\ \hat{y} \\ u_{\hat{x}} \\ u_{\hat{y}} \end{bmatrix} = \begin{bmatrix} 1 & 1 & 1 & 1 \\ \hat{x}_1 & \hat{x}_2 & \hat{x}_3 & \hat{x}_4 \\ \hat{y}_1 & \hat{y}_2 & \hat{y}_3 & \hat{y}_4 \\ u_{\hat{x}1} & u_{\hat{x}2} & u_{\hat{x}3} & u_{\hat{x}4} \\ u_{\hat{y}1} & u_{\hat{y}2} & u_{\hat{y}3} & u_{\hat{y}4} \end{bmatrix} \begin{bmatrix} N_1 \\ N_2 \\ N_3 \\ N_4 \end{bmatrix} = \begin{bmatrix} 1 & 1 & 1 & 1 \\ \hat{x}_1 & \hat{x}_2 & \hat{x}_3 & \hat{x}_4 \\ \hat{y}_1 & \hat{y}_2 & \hat{y}_3 & \hat{y}_4 \\ u_{\hat{x}1} & u_{\hat{x}2} & u_{\hat{x}3} & u_{\hat{x}4} \\ u_{\hat{y}1} & u_{\hat{y}2} & u_{\hat{y}3} & u_{\hat{y}4} \end{bmatrix} \begin{bmatrix} \xi_1 \\ \xi_2 \\ \xi_3 \\ \xi_4 \end{bmatrix} \quad \text{Equation 3-12}$$

Where (ξ, η) is the element curvilinear coordinate system.

Consider two bordering elements; for the isoparametric element to satisfy continuity along the boundary, the displacement functions should satisfy the

compatibility in their common boundary [85]. Now consider an element having total eight Degrees Of Freedom (DOF) two at each node as shown below:

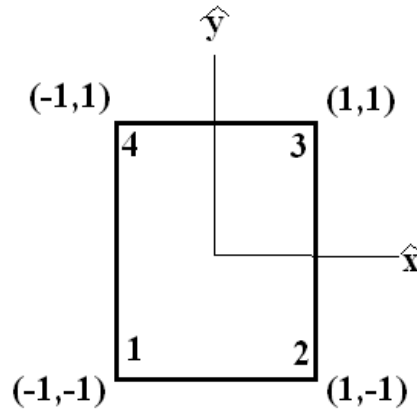


Figure 3-14: A linear square element shown in natural coordinates system (\hat{x}, \hat{y}) .

The displacement functions are identified as follows:

$$u(\hat{x}, \hat{y}) = a_1 + a_2\hat{x} + a_3\hat{y} + a_4\hat{x}\hat{y}$$

$$v(\hat{x}, \hat{y}) = a_1 + a_2\hat{x} + a_3\hat{y} + a_4\hat{x}\hat{y} \quad \text{Equation 3-13}$$

Details of extracting and developing of all these equations in this section are well explained in reference [85].

All the constants a_i in Equation 3-13 can be found by substituting the nodal values. By such substitution, Equation 3-14 will be achieved:

$$u(\hat{x}, \hat{y}) = N_1(\hat{x}, \hat{y})\hat{u}_1 + N_2(\hat{x}, \hat{y})\hat{u}_2 + N_3(\hat{x}, \hat{y})\hat{u}_3 + N_4(\hat{x}, \hat{y})\hat{u}_4$$

$$v(\hat{x}, \hat{y}) = N_1(\hat{x}, \hat{y})\hat{v}_1 + N_2(\hat{x}, \hat{y})\hat{v}_2 + N_3(\hat{x}, \hat{y})\hat{v}_3 + N_4(\hat{x}, \hat{y})\hat{v}_4 \quad \text{Equation 3-14}$$

Where

$$N_1(\hat{x}, \hat{y}) = \frac{1}{4}(1-\hat{x})(1-\hat{y}) \quad N_2(\hat{x}, \hat{y}) = \frac{1}{4}(1+\hat{x})(1-\hat{y})$$

$$N_3(\hat{x}, \hat{y}) = \frac{1}{4}(1 + \hat{x})(1 + \hat{y}) \quad N_4(\hat{x}, \hat{y}) = \frac{1}{4}(1 - \hat{x})(1 + \hat{y}) \quad \text{Equation 3-15}$$

Equation 3-15 denotes the non-dimensional shape functions or N_i . The value of N_i becomes unity at the i^{th} grid point in the system, and becomes zero at the other three points.

Consider a quadrilateral element with its four nodes defined in the global coordinates system (x,y) as shown in Figure 3-15. This element is hereby examined by utilizing the curvilinear coordinates system (ξ, η) .

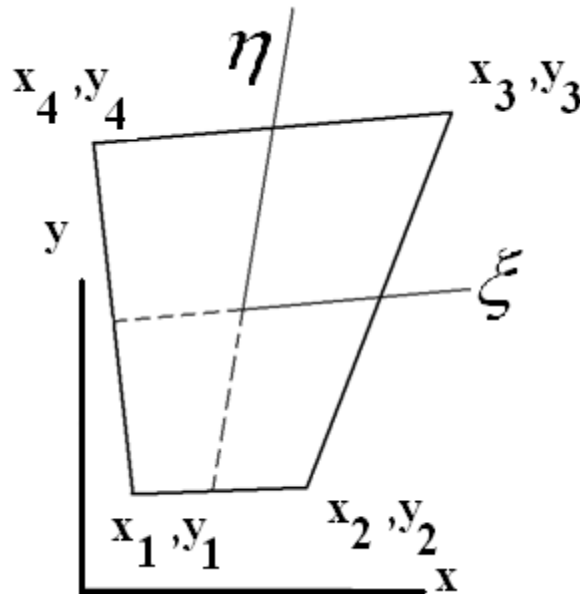


Figure 3-15: A square element mapped into quadrilateral in the curvilinear coordinate system (ξ, η)

The shape functions will be employed to map the square element shown in Figure 3-14 in isoparametric coordinates (ξ, η) to the quadrilateral shown in Figure 3-15 in the same form to identify the following:

$$x(\xi, \eta) = c_1 + c_2\xi + c_3\eta + c_4\xi\eta$$

$$y(\xi, \eta) = c_1 + c_2\xi + c_3\eta + c_4\xi\eta$$

Equation 3-16

As well:

$$x(\xi, \eta) = N_1(\xi, \eta)x_1 + N_2(\xi, \eta)x_2 + N_3(\xi, \eta)x_3 + N_4(\xi, \eta)x_4$$

$$y(\xi, \eta) = N_1(\xi, \eta)x_1 + N_2(\xi, \eta)x_2 + N_3(\xi, \eta)x_3 + N_4(\xi, \eta)x_4$$

Equation 3-17

These equations will be employed in the following section of the thesis to create principal stress curves in Matlab programming environment by utilizing nodal data outputs in Ansys software.

3.2.4.2 Generating stress trajectories in Matlab via Ansys output

Consider the following cantilever beam created in XY global coordinate system:

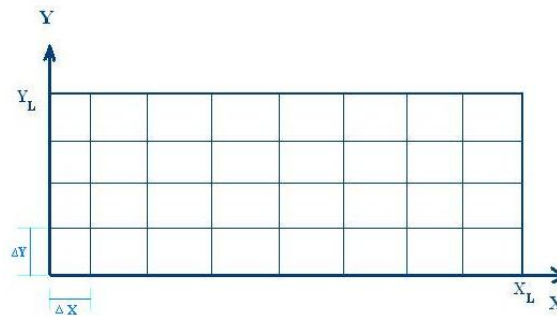


Figure 3-16: A cantilever beam in global coordinate system.

The above figure and Equation 3-14 to Equation 3-17 are the basis of Matlab programs #2 and #3 (detailed in Appendix A) to generate the stress trajectories based on a Finite Element model created in Ansys software.

The first program (Matlab program #2) will take the dimensions of the beam (X_L, Y_L) in XY plane, along with the desired refinement of the mesh in each direction

$(\Delta x, \Delta y)$. This program will sort and classify the nodes and their corresponding nodal output for almost any Ansys post-processing data to be useable to develop stress trajectories in the other program (#3). As detailed in Matlab program #2, Ansys post-processing nodal solutions to be sent to the Matlab program will include XYZ components of the node, principal stresses components of the nodes and normal and shear stresses components of the nodes. Refer to Appendix A for more details about this.

The third program (Matlab program #3) is user friendly and will produce stress trajectories after asking the user of how many trajectories they desire to obtain. Appendix A has more details of this program (program #3), which only generates compressive stress trajectories. For tensile stress trajectories, the same program was utilized with a different indexing.

Below is a sample output to draw 6 stress trajectories for the following data input to both Ansys and Matlab programs as per Figure 3-16: $X_L=120$, $Y_L=40$, $\Delta X = 10$, $\Delta Y = 5$.

The depth of the depicted cantilever does not affect the results, and the value of depth was chosen as 60 units for this specific example.

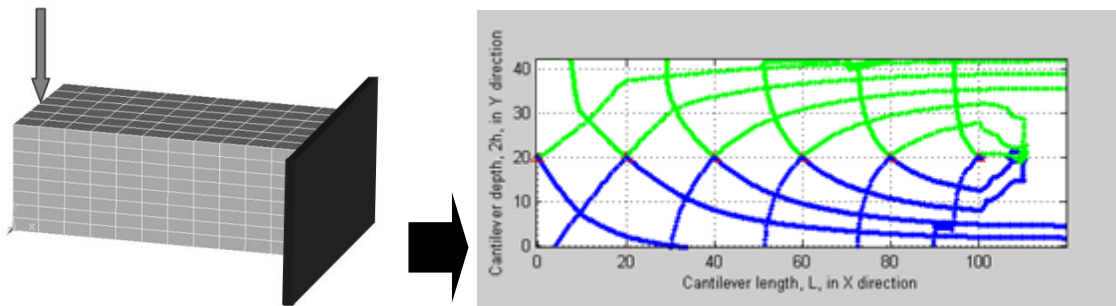


Figure 3-17: Stress trajectories illustrated by means of Matlab program for a sample beam analyzed in Ansys software. Nodal quantities were imported to Matlab from Ansys.

By having the stress trajectories curve points produced in the Matlab program #3, all the data will be exported to SolidWorks software first. Then the resultant output will be exported to Ansys after removing the undesirable points outside the cantilever's domain. Figure 3-18 illustrates a sample 2D model obtained. Effects of stress concentration are noticeable where the single load F was applied as per Figure 3-10. As is observable in both Figure 3-17 and Figure 3-18, the tensile and compressive stress curves are slightly distorted (especially where the force F is applied) and they are not completely symmetrical as a result of stress concentrations and boundary conditions.

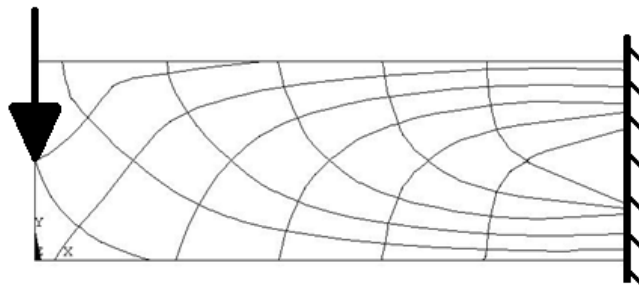


Figure 3-18: Stress trajectories generated in Ansys by means of Matlab and SolidWorks software. Effects of stress concentration and boundary conditions are noticeable.

While comparing Figure 3-13 with Figure 3-18, it is evident that there is an obvious difference in the results when the principal stress trajectories derived from the mathematical technique and principal stress trajectories extracted from the finite element analysis are compared. Frame structures constructed based on Figure 3-18 (finite element analysis) have less strength than those constructed based on Figure 3-13 (mathematical analysis) due to the distortion in the curves caused by the stress concentration. Therefore, the frame structures extracted from the finite element analysis (Figure 3-18) will not be compared in the future with frame structures modeled based on the Michell theory. This is because the frame structures constructed based on the mathematical techniques (Figure 3-13) are better candidates with higher strength.

The capabilities of the previously noted algorithm, detailed in Matlab program #3, have to be validated for another cantilever beam with a rectangular hole inside of it. The same steps in the previous analysis are taken, and the results are depicted in Figure 3-19. The curves acquired from the algorithm in Matlab program #3 oscillate near the hollow section of the beam, and in doing so they generate some undesirable curve points. However there are only very few minor modifications necessary to the above algorithm to make it feasible to develop the principal stress trajectories, which are depicted in Figure 3-19:

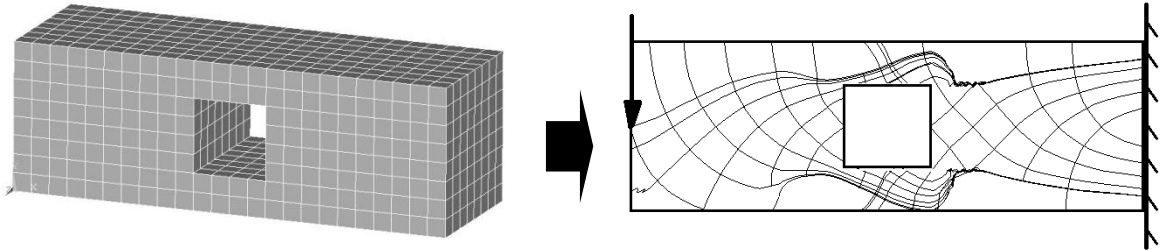


Figure 3-19: Principal stress trajectories of a cantilever with a rectangular opening in the middle of the beam, rigid support and a concentrated force at the free end of the beam. Effectiveness of the algorithm is demonstrated as the stress curves react to the stress distribution around the hole.

These results reveal the effectiveness of the above algorithm to determine the principal stress trajectories after the geometry of the beam was altered [86].

In the following section, Michell theory will be introduced and some frame structures will be generated based on this theory and compared to some of the above structures (which were based on Wolff's theory).

3.3 Michell theory

As briefly described in Chapter 2, Michell was a distinguished engineer and his theory was mathematically driven, as opposed to the Wolff's law which was mostly based on experimental observations. Michell established the requirements for a structure to carry a pre-defined set of external forces while maintaining a minimum weight. His calculations revealed that under a specified set of mechanical forces, the structure will have the minimum mass if all the structural elements have exactly the same amount of strain magnitude; either taking compression or tension strain [24, 25].

Michell theory was developed for a system of extremely dense and infinitesimal tension and compression elements having a very compact mass distribution of the structural members. It is important to note that the real world applications of such theory

should be based on a restricted number of discrete members, especially when it comes to designing of engineering frame structures. This is the main reason that a *discrete approximation* to the Michell was considered [27, 28]. The material utilized for such analysis should perform the same stress–strain relationship for tension and compression stresses. This would allow an equal strain magnitude to be maintained under load alterations. Thus the cross section of the elements should be proportional to the forces applied to them to satisfy having equal strain condition.

The majority of the contemporary research in structural optimization can be classified in two main categories: continuum structures and skeletal structures (like beams, trusses and grillages) [28]. The second is of central interest for this thesis work.

Consider designing an optimal frame structure, with the objective function to be minimizing the overall mass or the ultimate strength of the structure. In this case, the goal will be acquiring the best arrangement of the structural elements (e.g. rods) to equilibrate a specified set of external forces.

3.3.1 Michell’s theory formulation

Consider a frame structure represented as \mathbf{S} to be optimized in a defined region of space \mathcal{R} , under a given set of forces. Presume that there is a frame structure represented as \mathbf{S}^* which satisfies these conditions:

- a) If σ is the material “allowable stress” for tension and compression, the stresses in all of the structure’s elements are equivalent to $\pm\sigma$.
- b) There is a “virtual deformation” of the region \mathcal{R} with zero displacement on the support, and having strains value of $\pm\varepsilon$ for all the \mathbf{S}^* elements, where ε is a small positive number and none of the strains in \mathcal{R} exceed ε .

Michell's theory stipulates that the total mass (or volume) of the structure \mathcal{S}^* is less than or equal to that of any other frame structure \mathcal{S} in the region \mathcal{R} having same set of external forces [26]. Details of the proof of such theorem can be found in references [87] and [88].

It is obvious that the components of the optimum structure \mathcal{S}^* must be along the principal strain curves in the virtual deformation; otherwise, a direction could be defined for which the strain magnitude will be greater than ε thus contradicting the condition (b) above. As well, each pair of tension and compression intersects orthogonally at a node.

3.3.1.1 Virtual deformation

Consider a frame structure in 2D plane, where the Cartesian coordinate system is denoted as (x, y) , the curvilinear coordinate system (α, β) and the components of virtual displacement defined as (u, v) as per Figure 3-20. Also, ω is the rotation at point (α, β) .

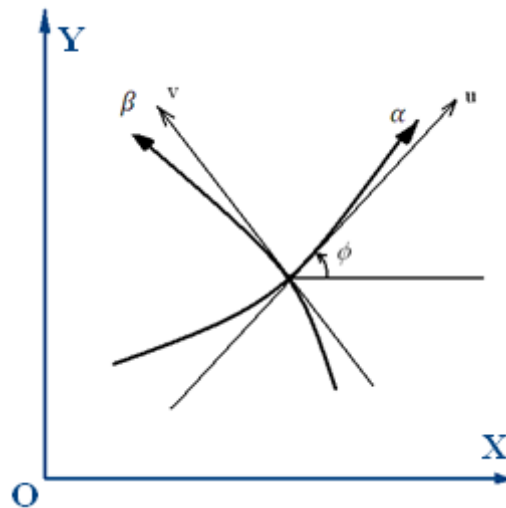


Figure 3-20: Cartesian and curvilinear coordinate system (Taken from: [26])

Michell curves (or the principal strain curves) outline a family of orthogonal curves defined with an infinitesimal segment of the curve ds as below:

$$ds^2 = A^2 d\alpha^2 + B^2 d\beta^2 \quad \text{Equation 3-18}$$

Where A and B are functions of α and β having positive value known as Lamé's Parameters. Strains along α axis are tensile thus will be indicated as $+\varepsilon$ and along β axis are compressive and defined as $-\varepsilon$, and shear strain is also zero.

The following equations relate the displacement components, strains and rotation in the curvilinear coordinate system:

$$\frac{1}{A} \frac{\partial u}{\partial \alpha} + \frac{v}{AB} \frac{\partial A}{\partial \beta} = \varepsilon$$

$$\frac{1}{B} \frac{\partial v}{\partial \beta} + \frac{u}{AB} \frac{\partial B}{\partial \alpha} = -\varepsilon$$

$$\frac{B}{A} \frac{\partial}{\partial \alpha} \left(\frac{v}{B} \right) + \frac{A}{B} \frac{\partial}{\partial \beta} \left(\frac{u}{A} \right) = 0$$

$$\frac{1}{AB} \left[\frac{\partial}{\partial \alpha} (Bv) - \frac{\partial}{\partial \beta} (Au) \right] = 2\omega \quad \text{Equation 3-19}$$

By introducing the parameter φ as being the angle between the positive direction of α axis and a fixed reference axis (x axis of Cartesian coordinate system in this case), Equation 3-19 will be simplified as below:

$$\frac{\partial \varphi}{\partial \alpha} = -\frac{1}{B} \frac{\partial A}{\partial \beta}, \quad \frac{\partial \varphi}{\partial \beta} = \frac{1}{A} \frac{\partial B}{\partial \alpha} \quad \text{Equation 3-20}$$

By solving the sets of Equation 3-19 for u and v derivatives $\left(\frac{\partial u}{\partial \alpha}, \frac{\partial u}{\partial \beta}, \frac{\partial v}{\partial \alpha}, \frac{\partial v}{\partial \beta} \right)$, and also cancelling A and B derivatives $\left(\frac{\partial A}{\partial \beta}, \frac{\partial B}{\partial \alpha} \right)$ as per Equation 3-20, the following is resultant:

$$\begin{aligned} \frac{\partial u}{\partial \alpha} &= A\varepsilon + v \frac{\partial \varphi}{\partial \alpha} , & \frac{\partial u}{\partial \beta} &= -B\omega + v \frac{\partial \varphi}{\partial \beta} \\ \frac{\partial v}{\partial \alpha} &= A\omega - u \frac{\partial \varphi}{\partial \alpha} , & \frac{\partial v}{\partial \beta} &= -B\varepsilon - u \frac{\partial \varphi}{\partial \beta} \end{aligned} \quad \text{Equation 3-21}$$

Finally, by eliminating u and v between the two sets of equations in Equation 3-21, and then removing ω in the achieved equation, Equation 3-22 will be obtained:

$$\frac{\partial^2 \varphi}{\partial \alpha \partial \beta} = 0 \quad \text{Equation 3-22}$$

The above Equation 3-22 denotes the geometrical restraint on the Michell layout curves which is known as the “*compatibility equation*” for the Michell virtual strain system.

3.3.1.2 Developing Michell curves

Michell curves could be generated by either analytical or graphical techniques.

Below is a brief summary of how to construct such curves by analytical method and then graphical method will be explained followed by the appropriate Matlab program to build the curves. Details of how to derive the equations in this section can be found in reference [26].

As shown in Figure 3-21, there exist four different arrangements of Michell layouts, depending on the angle between the tensile and compressive curves.

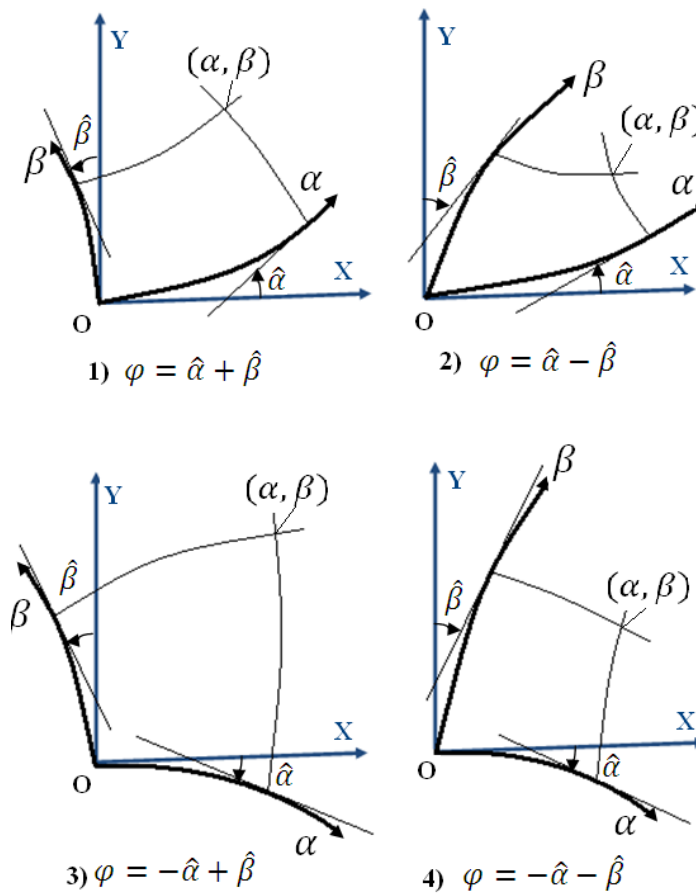


Figure 3-21: Angles between compressive and tensile strain curves could lead to four different arrangements of Michell curves. $\varphi = a\alpha + b\beta$ where a and b are equal to ± 1 (Taken from: [26]).

Following from Equation 3-18, and knowing that the angle φ was formed between the tangent lines of the two coordinate systems (Cartesian and Curvilinear), following equations will lead to layout curves [26]:

$$\cos \varphi = \frac{1}{A} \frac{\partial x}{\partial \alpha} = \frac{1}{B} \frac{\partial y}{\partial \beta}$$

$$\sin \varphi = \frac{1}{A} \frac{\partial y}{\partial \alpha} = -\frac{1}{B} \frac{\partial x}{\partial \beta}$$

Equation 3-23

By integrating the above equations for Cartesian coordinate components (x, y) , the following equations will be obtained:

$$x = \int^{(\alpha, \beta)} (A d\alpha \cos \varphi - B d\beta \sin \varphi)$$

$$y = \int^{(\alpha, \beta)} (A d\alpha \sin \varphi + B d\beta \cos \varphi) \quad \text{Equation 3-24}$$

If the values of A and B are determined, then the above Equation 3-24 will lead to the Michell layout curves. Below is a brief note on determining such values and more details can be acquired in reference [26]. One technique used for finding A and B values is by integrating the equation below and employing Riemann's method.

$$\frac{\partial^2 H}{\partial \alpha \partial \beta} + abH = 0, \quad (a, b = +1 \text{ or } -1) \quad \text{Equation 3-25}$$

Riemann's method is a solution to the Problem of Cauchy which is applicable to linear, hyperbolic, PDE (Partial Differential Equations) of the second order for an unknown function of two independent variables like $\bar{U}(x, y)$.

According to Riemann's method, if the value of H and one of its derivatives (e.g. $\frac{\partial H}{\partial \alpha}$) are defined along the curve ψ in Figure 3-22, then the other derivative (e.g. $\frac{\partial H}{\partial \beta}$) will be known on this curve (ψ). Thus the value of H at an arbitrary point like $S(\xi, \eta)$ will be defined as in Equation 3-26.

As shown in the above equations (Equation 3-23 to Equation 3-28) for the analytical method, it is apparent that it's not always practical to solve these equations and integrations to draw the Michell curves; thus the graphical method (as described below) will be a preferred technique in this research.

For constructing Michell curves using the graphical method, recall Equation 3-22. This equation implies that φ is a function of α and β :

$$\varphi = f(\alpha) + g(\beta) \quad \text{Equation 3-29}$$

Equation 3-29 could be interpreted as showing that a change in angle φ for a finite change of α along α axis (e.g. $\frac{\partial\varphi}{\partial\alpha}$) is independent of β , and a change in angle φ for a finite change of β along β axis (e.g. $\frac{\partial\varphi}{\partial\beta}$) is independent of α . This means, in simple words, that given any of the two coordinate axes of one family (e.g. α axis), the coordinate axes of the other family (e.g. β axis), are related using a constant angle of $\Delta\varphi$. Figure 3-23 illustrates this statement known as Hencky's theory:

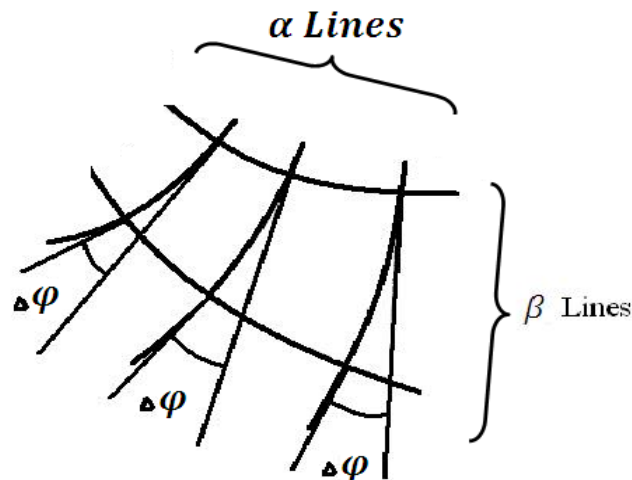


Figure 3-23: Family of α lines intersecting family of β lines at a constant angle ($\Delta\varphi$)

This illustrated property makes it possible to depict Michell curves graphically once the boundary conditions are defined.

Consider point P (m, n) in the curvilinear coordinate system (α, β) as illustrated in Figure 3-24.

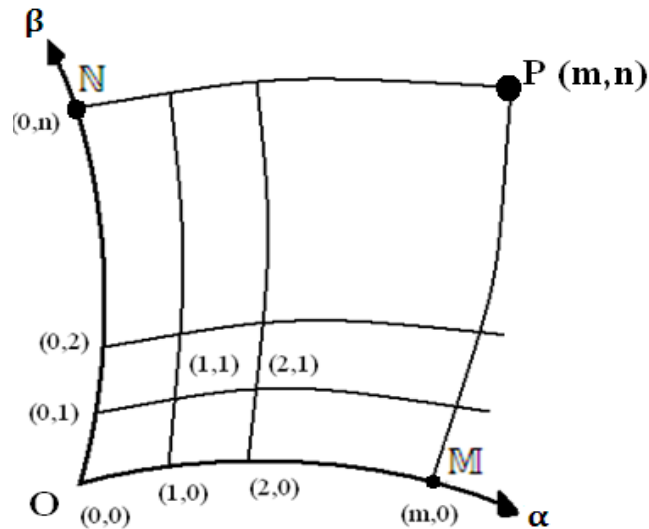


Figure 3-24: An arbitrary point in the curvilinear coordinate system (α, β)

Based on Hencky's theory stated and previously mentioned (for having constant $\Delta\varphi$), and considering the α and β lines intersecting at point P (m, n) in Figure 3-24, the following can be stated:

$$\varphi(m, n) - \varphi(0, n) = \varphi(m, 0) - \varphi(0, 0) \quad \text{Equation 3-30}$$

If the fixed Cartesian coordinate system (x, y) is selected in a way to be tangential to the curvilinear coordinate system (α, β) then the angle $\varphi(0, 0) = 0$ and Equation 3-30 will be simplified to:

$$\varphi(m, n) = \varphi(0, n) + \varphi(m, 0) \quad \text{Equation 3-31}$$

The above equation will give the value of $\varphi(m, n)$ at any point since the values of $\varphi(0, n)$ and $\varphi(m, 0)$ angles are known.

Figure 3-25 *left*, illustrates an example of creating Michell curves step by step using points defined as $(0,0)$, $(1,0)$, $(2,0)$ and $(0,1)$, $(1,1)$, $(2,1)$ as per Equation 3-31.

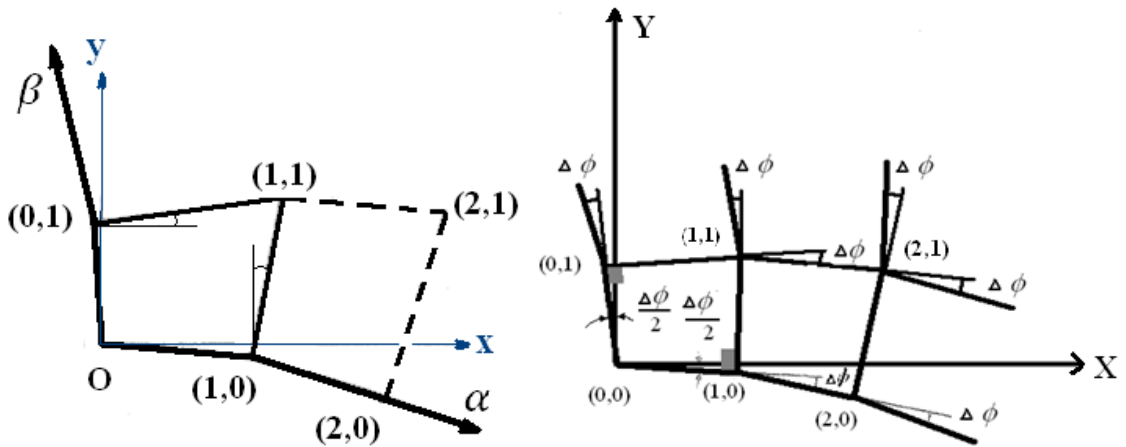


Figure 3-25: Producing Michell curves step by step

As shown in Figure 3-24, if the curvilinear coordinate axes α and β are divided in a way that the value of $\Delta\varphi$ between the points $(0,0)$, $(0,1)$, ..., $(0,n)$ and $(0,0)$, $(1,0)$, ..., $(m,0)$ will be constant, then the change of angle along any of these layout curves at any intersecting point will be a constant ($\Delta\varphi$), as per Hencky's aforementioned theory. Therefore, Michell's layout can be built without calculating the value of φ at every intersection. Figure 3-25 *right*, demonstrates this graphically.

Appendix A has the details of a Matlab program written to produce Michell layout based on the graphical method explained. This program is self-explanatory and utilizes what is graphically depicted in Figure 3-24 to Figure 3-26 for the users to understand the steps.

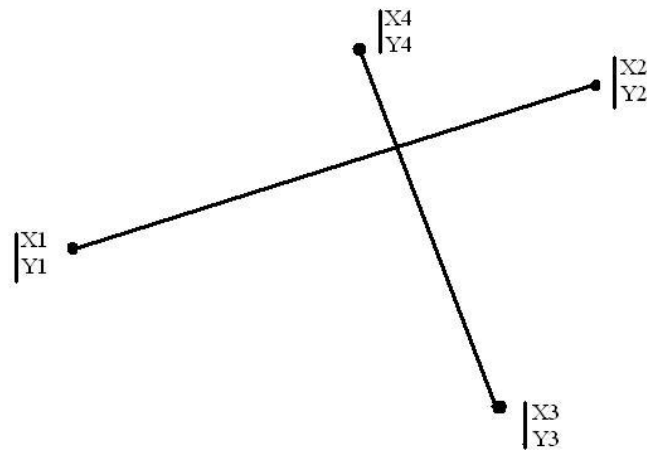


Figure 3-26: First step used to create Michell layouts by means of the Matlab program #4 (Appendix A).

Below is an example for an output of the Matlab program #4 (detailed in Appendix A) for different input parameters. This program is utilized for the following values:

Angle $\Delta\varphi = 15^\circ$, distance \overline{OM} on Alpha axis=40, distance \overline{ON} on Beta axis= 40, desired number of nodes along Alpha axis, $m=10$, desired number of nodes along Beta axis, $n=10$.

Figure 3-27 is the outcome of Matlab program #4 (detailed in Appendix A) using the abovementioned parameters as input:

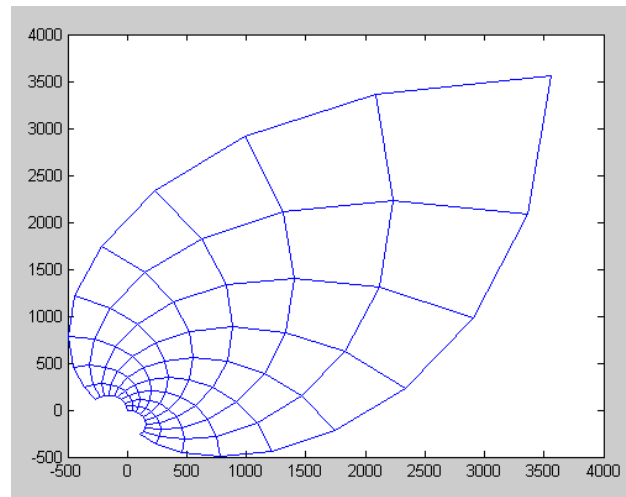


Figure 3-27: Michell layout generated in Matlab programming environment by means of graphical method for the following parameters input to the program: $\Delta\varphi = 15^\circ$, $\overline{OM} = 40$, $\overline{ON} = 40$, $m=10$, $n= 10$.

A second program is performed for the following values:

Angle $\Delta\varphi = 5^\circ$, distance \overline{OM} on Alpha axis=40, distance \overline{ON} on Beta axis= 40, desired number of nodes along Alpha axis, $m=10$, desired number of nodes along Beta axis, $n= 10$.

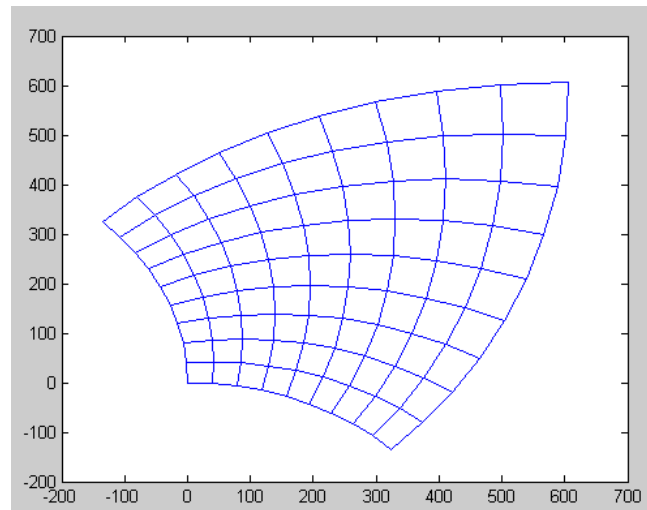


Figure 3-28: Michell layout generated in Matlab programming environment by means of graphical method for the following parameters input to the program: $\Delta\varphi = 5^\circ$, $\overline{OM} = 40$, $\overline{ON} = 40$, $m=10$, $n= 10$.

As shown in these two figures, the effects of changing the parameters are noticeable in the resultant Michell layout. Especially when it comes to generating a cantilever frame structure whose components follow Michell's curves layout, various trials and error sets should be performed to obtain the desired beam's geometrical properties (like aspect ratio).

For performance comparison analysis of the frame structures produced based on Michell layout, the produced structures were transferred to SolidWorks software after the nodal points were created in the Matlab program #4 detailed in Appendix A. Each node's XY component was created in this Matlab program and then exported to SolidWorks software, and finally the model was transferred to Ansys for further analysis.

The next step in the analysis uses Michell trusses obtained in this section to be compared to the frame structures generated based on Wolff's theory (section 3.2.3 of this thesis). The following section gives more detail for such a comparison.

3.4 Strength assessment of frame structures modeled based on Michell and Wolff theories

In this section, a performance comparison will be carried out between two different types of frame structures: structures modeled based on principal stress trajectories and Wolff's theory as described in section 3.2 of this thesis, and frame structures modeled based on Michell's theorem as described in section 3.3 of this thesis.

All these frame structures are in plane, and the cantilever elemental members are composed of identical rods all joined together. At the free end of the cantilever, there is a single transverse force applied, and the other end of the beam has a rigid support with zero degree of freedom. A static equilibrium condition without a pre-stress loading is considered for analysis.

In order to have a consistent performance comparison of the cantilevers produced based on Wolff's and Michell's theories, each of these two pairs of beam models should have the same geometry, aspect ratio, total mass and also relatively the same mass distribution.

For the Ansys software simulation, the material for each cantilever is homogeneous, isotropic and linear elastic. Modulus of elasticity for each of these models is $E=200$ Gpa with a Poisson ratio of $\nu = 0.3$. Element type was chosen as "BEAM3" with equal real constant values for both models. BEAM3 has 3 DOF at each node and is a uni-axial element having compression, tension, and bending simulation abilities.

Several cantilever models were generated based on Wolff and Michell's theory and each set of corresponding models were compared together. Those frame structure modeled based on the Wolff's law had in average slightly larger total mass (by 6.5%) and a very negligible higher aspect ratio (by 1%) as compared to their peer Michell cantilevers (mass and aspect ratio are supposed to be close to identical for comparison).

An example of a cantilever modeled based on the Wolff's hypothesis (where beam elements follow principal stress trajectories), is shown in left hand side of Figure 3-29 and a cantilever based on Michell analysis is on the right:

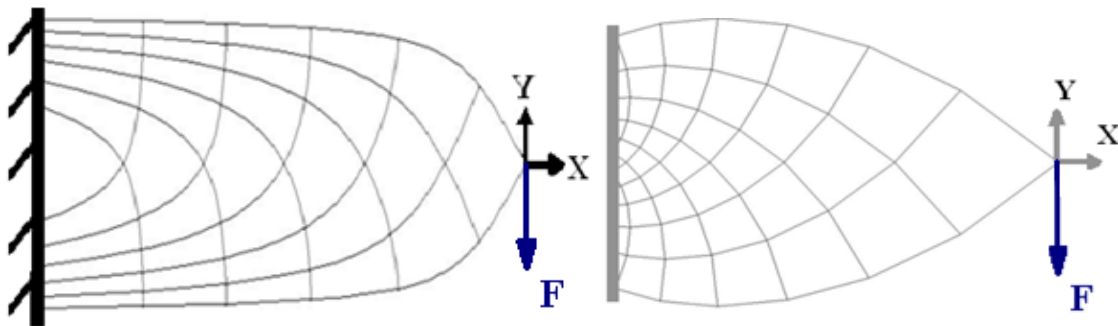


Figure 3-29: *Left*- example of a cantilever beam generated based on the Wolff's premise (beam elements follow principal stress trajectories), *Right* - an example of a model of a cantilever obtained based on Michell's theorem having identical aspect ratio, total mass and fairly the same mass distribution

The analogous Michell frame structure for the comparison is created by performing several iterative trial and error approaches and by adjusting the parameters ($\Delta\phi$, OM , ON , m and n) shown in Figure 3-24 and Figure 3-25. The resultant beam is similar to the one illustrated in the right hand side of Figure 3-29. As mentioned above, mass distribution (per unit area) has to be relatively the same for both of the models. A constraint for such comparison between the two cantilevers performance is the material yield strength.

Final results of the comparison made between the two aforementioned models confirms that when the cantilever model based on the Wolff's premise is compared to the corresponding cantilever model based on the Michell's theory, enhanced performance is achieved by Wolff's theory (element members arrangement follow the principal stress trajectories). This means that the value of the maximum allowable strength of the beam increases around 10% to 18% for a cantilever modeled based on the Wolff's hypothesis. In addition, there is another significant challenge while drawing the cantilever models based on Michell's theory. Given Equation 3-31 and Figure 3-25 to extract Michell frame structure graphically, and the fact that the nature of constructing such cantilever is trial and error based using five parameters ($\Delta\phi$, OM , ON , m and n), it is obvious that it's very tedious to obtain the desired geometry and aspect ratio of a beam. These five parameters are independent, which applies a great deal of restrictions for obtaining the preferred displacement, aspect ratio and as a resultant total mass of the structure. Thus by modifying these five independent parameters, a variety of cantilevers are obtained with hard to predict aspect ratios as shown in Figure 3-30.

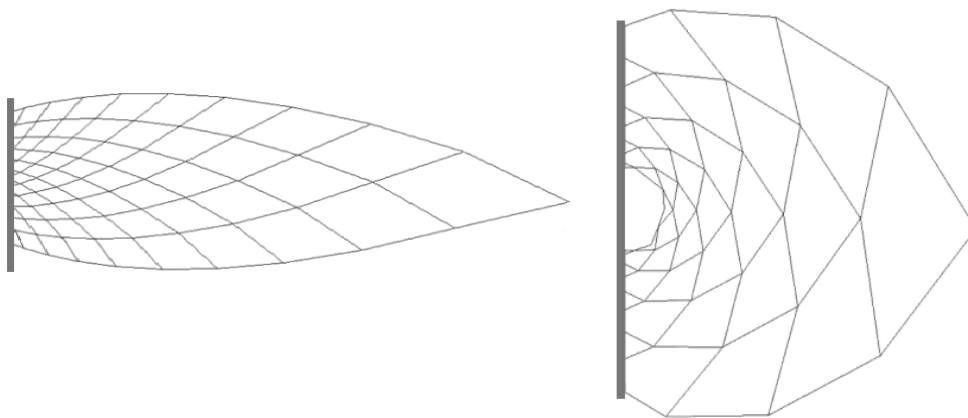


Figure 3-30: Changing the five independent parameters $\Delta\phi$, OM , ON , m and n , will result in multiple cantilever models with unpredictable aspect ratios

For this reason, satisfying dimensional borders and restrictions is somewhat impractical or considerably time consuming given the trial and error nature of constructing Michell layouts as per the methodology employed here. As also mentioned in chapter 1, there are some other limitations in employing Michell's theory, like the non-uniqueness of the solutions for optimal layout designs of a Michell truss [29]. Therefore, creating the cantilever models based on the Wolff's hypothesis will provide us with a more extensive design domain without almost any concern regarding the predefined dimensional or mass restrictions. As well, by employing Wolff's theory in designing the abovementioned cantilevers, a more economical and time efficient procedure will be gained [89, 90]. In simple words, when it comes to an optimization problem with the objective function of increasing the yield strength of a frame structure (in this case cantilever beam), those structures whose elemental members' arrangement follow the principal stress trajectories (constructed based on Wolff's method explained in section 3.2) are a preferred option to structures created based on Michell's theory (detailed in section 3.3).

3.5 Some Notes about How Thesis Chapter 3 is Associated to Chapter 4 and 5

Here is a brief description on how Wolff's theory, Michell theory (structural optimization) and plants microstructures are associated together:

- Michell theory is mathematically driven and it is one of the most prominent theories in structural optimization. On the other hand, Wolff's theory is one of the most distinguished theories which originated from both experimentation and mathematical studies. The effort to bring bio-science and engineering more closely together is the reason why these two

prominent theories were selected to be compared against each other. The main relationship between the experimentation conducted and these two theories is that in all three cases, some attempts are being made to achieve structural efficiency. For Wolff's law, the structural efficiency stems from the fact that a bone self-optimizes according to its loading environment. This has a close correspondence with the thesis experimentation, which demonstrates a similar phenomenon for plants. Michell theory represents another avenue, based on mathematics, for determining the most optimal structural efficiency.

- The fundamentals of Wolff's theory are based on *bone's* micro-structure. As mentioned in this chapter (Chapter 3), Wolff's theory details the effects of mechanical loading on the micro-structure of the *bone*. As mentioned in section 1.1 of this thesis (main thesis objectives), one of the objectives is to expand Wolff's theory to the domain of plant micro-structure. Following, the effect of external mechanical forces on the micro-structure of a *plant* will be studied (Chapter 4 and 5). The experimental results will be used to validate the use of Wolff's theory in the domain of plant micro-structural behavior.
- As will be shown in Chapters 4 and 5, the effects of external mechanical forces on the micro-structure of a plant will be studied. A common investigative question is: after finding how the mechanical loads interact with plant micro-structure, then what are the benefits/ applications of such study, and where can the findings of this study be employed? The main

answer is that by employing such results one can improve the strength of frame structures in engineering applications, once an appropriate internal arrangement of the elements is selected (which is the core idea in Chapter 3).

Chapter Four: Biological Preliminaries and Experimental Tests

In this chapter, at the beginning, some biological fundamentals and terminologies will be described for engineers. Then details of the experimental tests performed to track and record Microtubule direction in the Arabidopsis root cell when mechanical loads is applied will be explained. In these experimental tests, Microtubule orientation was defined in different sections of the root cell, when the root was free of any external mechanical forces (still having internal turgor pressure). As well, the effect of gravity is studied followed by studying the influence of an external mechanical bending moment on the Microtubules orientation.

One might ask: why study plants and their behavior when responding to external environmental factors? As mentioned earlier in Chapter 2, one reason is that plants are inactive, which makes it easier to control the desired lab test environment and parameters. As well, plants have more prompt reaction to environmental loadings (in the range of few hours) while other tissues like bones need days and maybe months to adapt their microstructure and react to external loading. Thus plants are ideal specimens to model and investigate their form-function interaction.

Investigating a plant's micro-structural behavior from an engineering point of view is not a very simple task. When it comes to biology, there are very many unpredicted or unknown parameters involved in the plant response to certain stimuli, which are not necessarily very understandable for biologists or engineers. As well, some engineering theories and hypotheses might not be very obvious to biologists or practical enough to be applied in the field of biology. This makes the process of understanding

plant behavior from an engineering point of view somewhat difficult. More specifically, for the purpose of simulating a plant (or plant cell) with software to investigate mechanical loading effects, various simplifications and assumptions are involved to approximate a real world scenario.

The key point is that plants and their behavior, as many other living tissues, can't infringe basic chemistry or physics laws [91]. The effect of mechanical forces has always been observed in a macro scale, e.g. the wind load bending a tree stem in the direction of the wind blow as shown in Figure 4-1. As observed in this figure, the roots tend to be longer and thicker on the right hand side of the root (bearing tension stress) which adds more reinforcement to the surrounding soil. On the contrary, the compression side (left hand side) has roots which tend to be smaller and shorter [92].

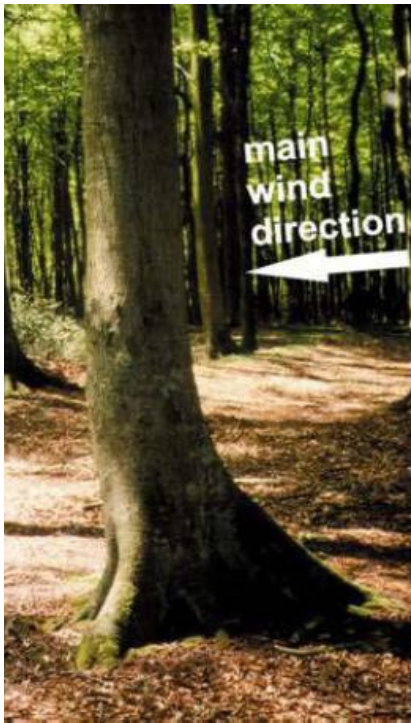


Figure 4-1: A tree trunk deformed under the strong wind condition. Based on the main wind direction (right to left arrow), the roots tend to be longer and thicker as they undergo the tension stress which causes more reinforcement to the surrounding soil. On the compression side the roots tend to be smaller and shorter (taken from [92]).

Seemingly, such effects (like adaption to wind loading) in a micro scale are conceivable and need to be verified.

Material properties of biological tissues could be altered depending on their age or function. This could be directly related to the cell walls. Newly born and younger plant cells tend to be more elastic, while older cells are less elastic. Material properties of each organ in the same plant are different. Even for a particular part of a plant, material properties could change during the growth stages or if subjected to variable amount of force applied [91]. Interestingly, there is evidence that the tensile strength of Cellulose Micro-Fibril is comparable to that of structural steel [93].

Some researchers believe that studied plants response to mechanical forces dates back to even before 1938 Castle's investigations (please refer to Chapter 2 section 2.3.5). It is believed that in 1878 Vochting was the first who discovered such relation. He realized that by hanging his experimental specimen fruits from a fence, stems of such fruit will have more vascular tissues than the normally grown fruit on the ground. As mentioned in Chapter 2 of this thesis, many similar attempts have been repeated to study the relation between mechanical forces and the equivalent plant reaction. Some researchers indorsed such direct relation and other refuted this. Niklas [91] believed that one reason that some similar experiments had different outcomes was the fact that researchers didn't consider normalizing the mechanical forces utilized in their experiment; this means that experiments having similar force magnitudes, material properties but different plant dimensions would have different mechanical outcomes.

In addition, many plant materials cannot be clearly identified as an ideal solid or ideal fluid; although engineering materials themselves are not theoretically ideal. The fact that material properties of biological tissues (including plant cells) alter during growth and developmental stages, highlights their difference with classical engineering structures

and analysis method. Thus, understanding how engineering fundamentals are extendable to biological science is an important asset in this area of research.

In the presented research for material simulations, ideal solids are assumed. Another approach is to perform simulations by means of utilizing visco-elasto-plastic materials, but this other approach is unproven and needs to be further investigated [91].

4.1 Microtubules

Inside each plant cell there exists an aqueous solution named the Cytoplasm. The Cytoplasm is jelly-like and has the role of holding most of the sub-cellular organs together. The cytoskeleton is a structure inside the Cytoplasm which is considered to be cell's "scaffolding" or "skeleton". Microtubules are hollow tubes which are one of the elements of Cytoskeleton and have important role in sustaining cell's structure. Each Microtubule itself is made of a protein called tubulin as shown in Figure 4-2:

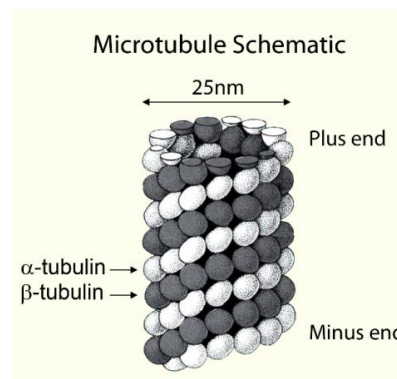


Figure 4-2: Microtubule schematic structure- each Microtubule is made of protein called tubulin (taken from [http://www.google.ca/imgres?imgurl=http://www.cytoskeleton.com/media/wysiwyg/MT_schematic_2.jpg&imgrefurl=http://www.cytoskeleton.com/tubulins&h=1712&w=1944&sz=395&tbnid=c7bP9iUIuSQhbM:&tbnh=90&tbnw=102&prev=/search%3Fq%3Dmicrotubule%2Btubulin%26tm%3Disch%26tbo%3Du&zoom=1&q=microtubule+tubulin&usg=__fUa2AmH9pJDXHMErPlanHikLwcl=&docid=IYk94oHPiIQUIM&sa=X&ei=_f4QUqqaBoPHiwK31YGCg&ved=0CEwQ9QEwBA&dur=706])

Microtubules are highly dynamic, their diameter is around 25 nanometers and their length is in micrometer order, which could reach as high as 25 μm . Microtubules length can vary as required by the cell (e.g. adjusting to spatial positioning or performing mechanical work) [94]. In simple words, such variation in the Microtubules length is called polymerization if it's an assembly process (Microtubule growing in length) and is called de-polymerization if it's a disassembly process (Microtubules shrinking in length), as demonstrated in Figure 4-3. Such growth and shrinking is driven by losing and receiving tubulins from each end of the Microtubules.

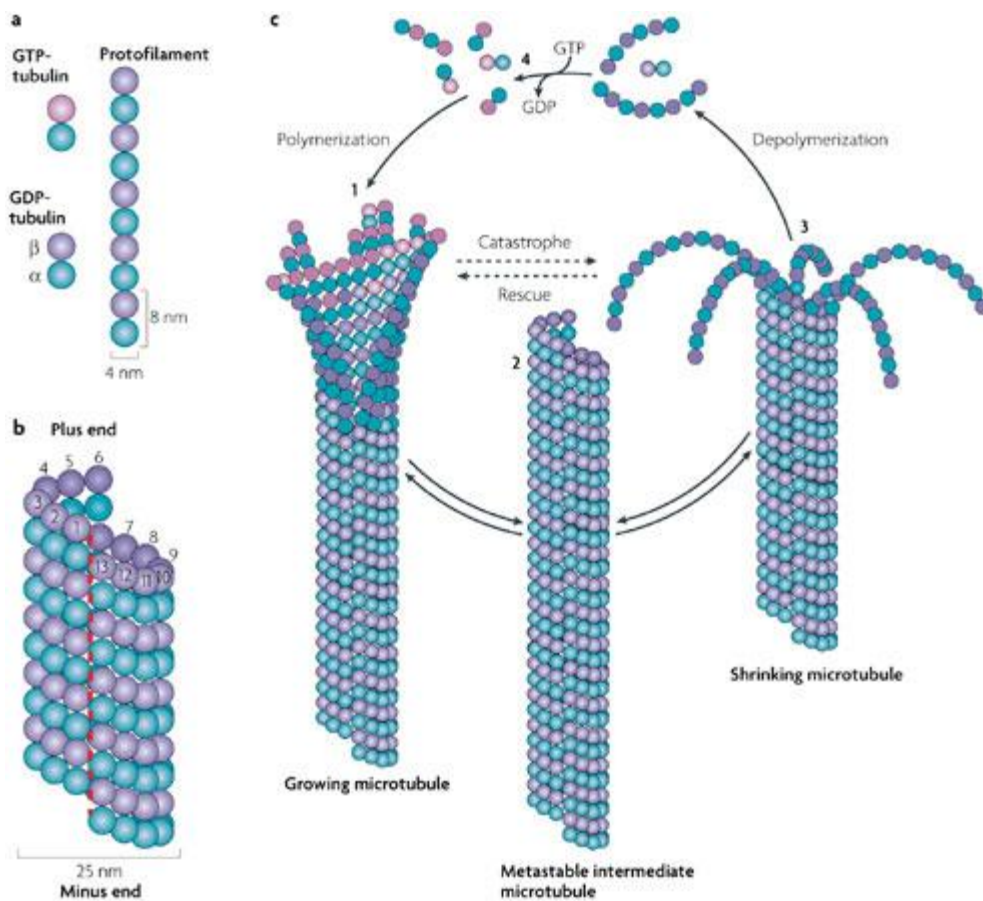


Figure 4-3: Microtubule polymerization and de-polymerization process [taken from http://www.nature.com/nrm/journal/v9/n4/box/nrm2369_BX1.html]

The Microfibrils (MF), as shown in Figure 2-6 in Chapter 2, is composed of very fine fibers in the cell wall with diameter in the range of nanometers. This figure also shows the location of both the Microfibrils and the Microtubules in the cell wall. As mentioned before, Microtubules influence Microfibrils deposition and this doesn't affect the shape of a cell instantly [95, 96]. The shape of a plant cell is typically imposed by the cell wall [97, 98, 99].

4.1.1 Why Microtubule and why orientation of Microtubule?

One might ask why the orientation of the Microtubules might be of interest among other seemingly analogous organs inside a cell (e.g. Microfibrils or Cellulose Synthase). As mentioned in the Chapter 2 of this thesis, Lucas and Shaw in their research showed the arrangement and pattern of the Microtubules, Microtubules bundles, Cellulose Synthase and Cellulose Microfibrils with respect to each other, all together in one schematic as shown in Figure 4-4:



Figure 4-4: Cellulose Synthase and Microfibrils, along with Microtubules in a newly born (*left*) and mature (*right*) cell. Cellulose Synthase (dotted lines) have the same arrangement as Microtubules (solid lines). Most likely, the direction in which Microfibrils are deposited is defined by the Microtubules orientation. Individual Microtubules form bundles of Microtubules (taken from [59]).

As seen above, Cellulose Synthase, Microfibrils and Microtubules have the same orientation. It is believed that Microtubules are the key factors in directing the orientation of the Microfibrils and Cellulose Synthase; however the mechanism is not very well understood [100]. For this reason, the study of Microtubules was chosen for the research. Another point about Microtubules is that what one sees under the microscope is not actually an individual Microtubule, it's in fact a bundle of them. Each individual Microtubule is bound to its peers to form a bundle.

Figure 4-5 is a schematic drawing of a plant cell wall showing the local spatial arrangement of Microtubules, Microfibrils and Cellulose Synthase with respect to the plasma membrane. The plasma membrane, also known as cell membrane, is a biological lipid bi-layer which separates the internal part of the cell from the external surroundings. The plasma membrane is distinct from a cell wall and its relative position is between the cell wall and center of a cell, as shown in Figure 4-6.

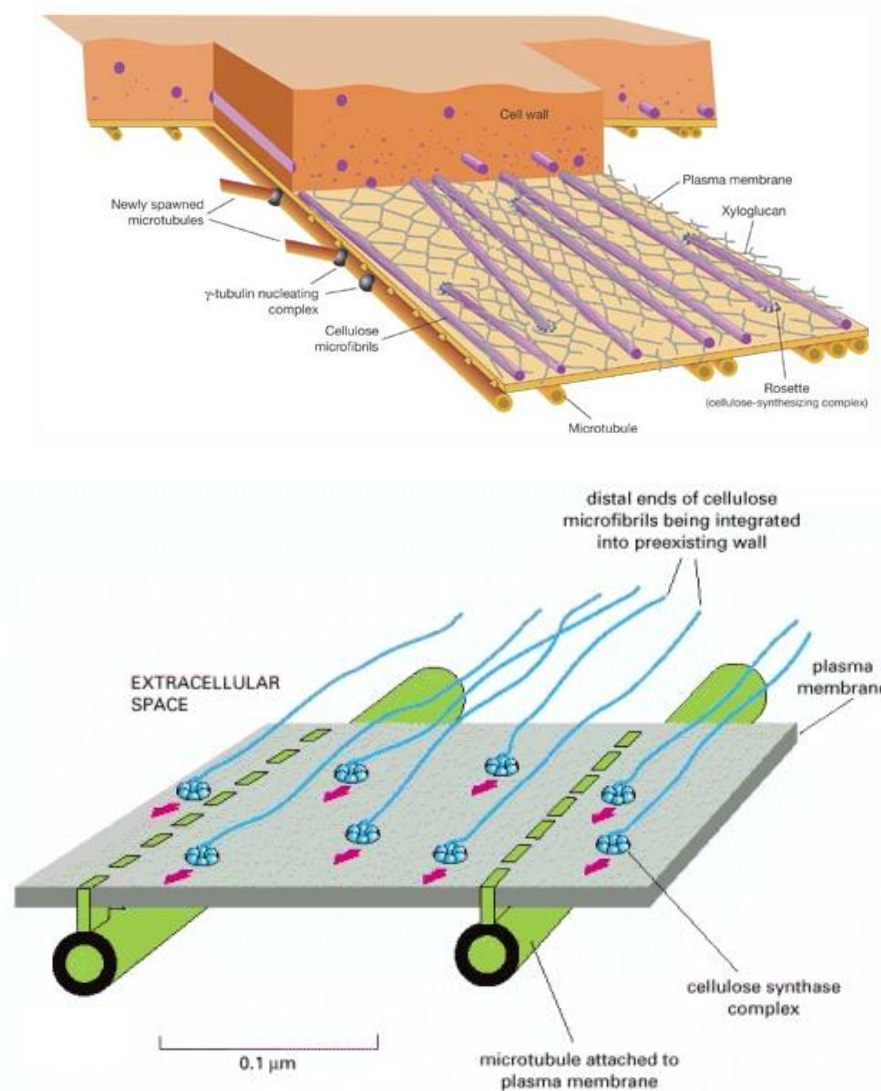


Figure 4-5: Positional location of Microtubules with respect to Plasma Membrane. It is believed that the orientation of Cortical Microtubules might direct the orientation of Cellulose Microfibrils. (Top: taken from <http://www.nature.com/ncb/journal/v7/n10/full/ncb1005-927.html> Bottom: taken from <http://www.ncbi.nlm.nih.gov/books/NBK26928/>)

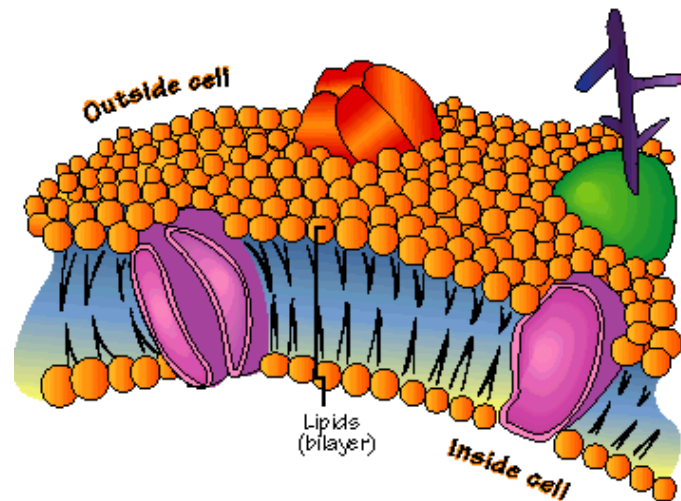
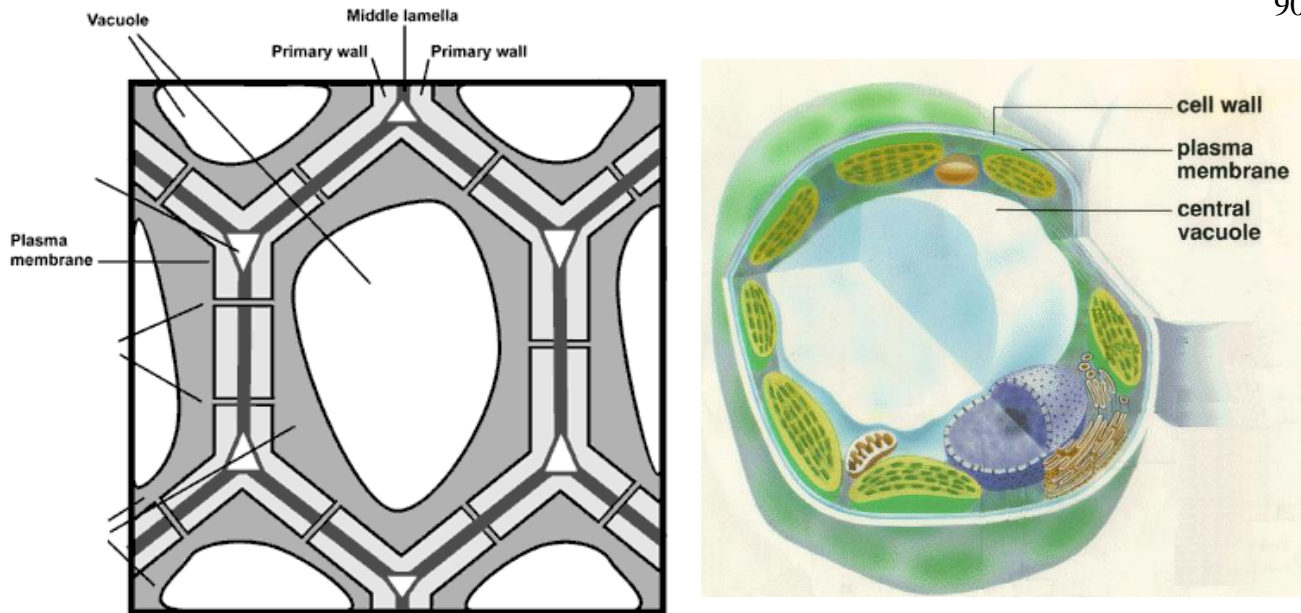


Figure 4-6: A general outline of a typical plant cell. Position of Plasma Membrane is shown relative to the cell wall (taken from http://www.odec.ca/projects/2004/mcgo4s0/public_html/t4/Analogies.html, <http://www.crc.uga.edu/~mao/intro/outline.htm> and http://library.thinkquest.org/C004535/cell_membranes.html)

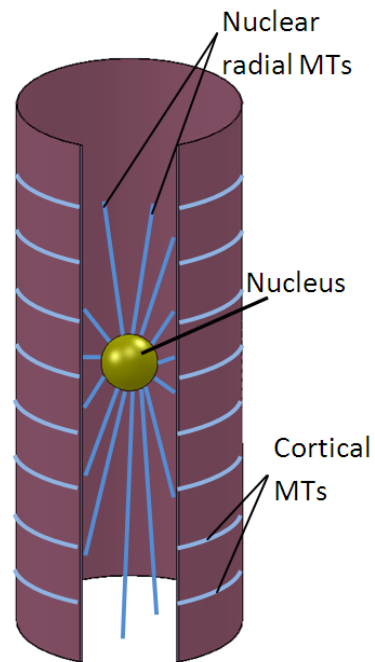


Figure 4-7: Microtubules positions versus Cortical Microtubules

4.2 Arabidopsis plant

The plant considered in this research is called *Arabidopsis Thaliana*. *Arabidopsis* is a very delicate and tiny flowering plant which is extensively used as a model in plant biology. The *Arabidopsis* plant provides essential advantages for a variety of research in the area related to genetics or molecular biology.



Figure 4-8: Arabidopsis Thaliana plant

The specimen studied in this research specifically is a transgenic Arabidopsis. This means that the Arabidopsis under investigation is genetically modified in a way that when placed under microscope laser light, Microtubules will be tracked by the green fluorescent light emission. Such emissions are emitted from another protein (called MBD-GFP) that binds to Microtubules [101]. MBD-GFP stands for Microtubule-Binding Domain-Green Fluorescent Protein. Such green fluorescent reflection is not found in the wild plant varieties, and it is very convenient to have a fluorescent “marker” on Microtubules for tracking the changes in orientation. Microtubule-Binding Domain-Green Fluorescent Proteins (MBD-GFP) show a bright green fluorescence reflection when subjected to blue light.

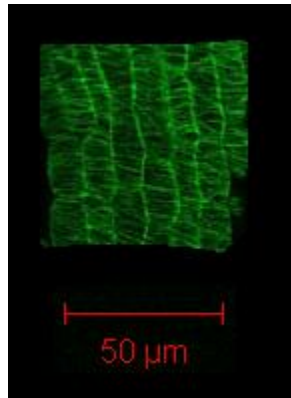


Figure 4-9: Microtubule bundles in Arabidopsis cell. The thin and transverse green lines represent Microtubules, and the thicker vertical ones are the cell wall.

4.2.1 Why Arabidopsis and why Arabidopsis root?

There are quite a few advantages that make Arabidopsis a popular specimen for study in cell biology. One of such advantages is the life cycle. It only takes three to four days from cultivation to germination and around six weeks from germination to a mature plant. Easy and convenient access to the seeds in stock is another advantage, along with the easy method of cultivation in relatively limited facilities and space. In addition, since the mutant Arabidopsis reflects fluorescent light emission from a laser beam, our specimen studies does not need dyeing, which is a significant noise avoiding factor in the experiment.

The plant roots' main role is providing nutrition for the plant, as well as holding up the physical structure of the plant. The Arabidopsis root is a very suitable candidate to study the plant behavior, as it has a simple structure even though it's a very hard to handle organ. Figure 4-10 shows the simple structure of an Arabidopsis root cross-section. The focus in this research is only on the epidermal layer of cells as shown below. Epidermal layer is the outermost layer in the cross section of a root.

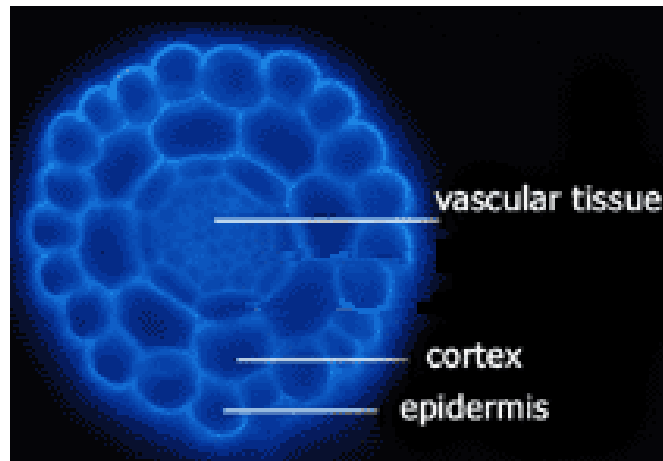


Figure 4-10: Cross-sectional view of an Arabidopsis root. [taken from <http://www.mcdb.lsa.umich.edu/labs/schiefel/research/index.html> and modified]

One reason for considering the epidermal layer is the efficiency of image taking procedure as the interior tissues can often not be accessed. For a confocal microscope, images are taken as two dimensional (2D) slices in planes approximately perpendicular to the laser beam. A three dimensional (3D) model is constructed by combining the 2D slices. Epidermal cells are only sharing sides with neighboring cells directly next to them. For this reason, any possible undesired noise from other cells around will be a minimum.

There are a lot of research works performed on the upper portion of Arabidopsis denoted the Shoot Apical Meristem (SAM) compared to Root Apical Meristem (RAM) (bottom portion of the plant). Figure 4-11 shows the location of SAM and RAM sections of the plant:

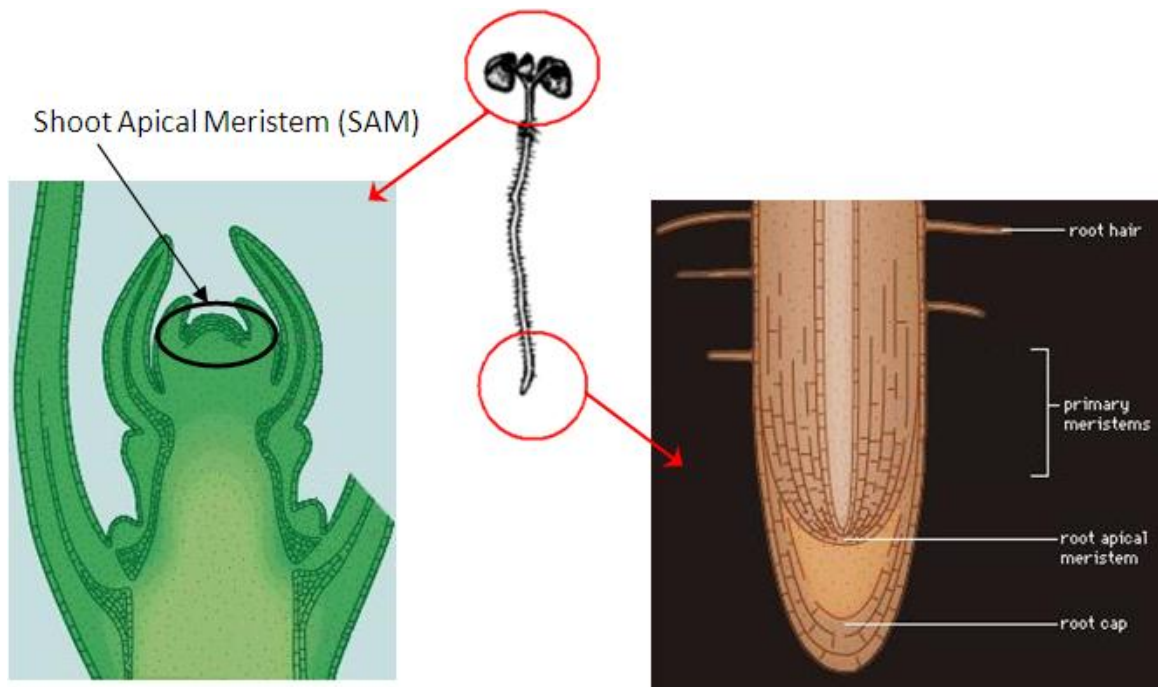


Figure 4-11: Root Apical Meristem (RAM) versus Shoot Apical Meristem (SAM) position in a plant [taken from <http://www.britannica.com/EBchecked/media/376/Apical-meristems>]

RAM growth is relatively more controlled than SAM in terms of dimensional increase (specially length of the root), and SAM cells are generated in two directions. This means that cells divisions in root, which are quite predictable and lateral, are not generated for SAM growth.

4.2.2 More about Arabidopsis in this research

In this research, we preferred the Arabidopsis species aged between about seven to fifteen days for experimentation. The reason was mostly the length of the Arabidopsis root to be easier to handle under the microscope when aged between seven to fifteen days, given the size of petri dish and the area under the microscope lens. Older and more

mature *Arabidopsis* plants could also be studied as well, but since the focus of our research was on roots, and the roots keeps elongating while growing, it would be very difficult to visualize longer specimens under a microscope. As mentioned earlier, the *Arabidopsis* root is a very tender and difficult to handle organ; thus a long root when reaching the edges of a petri dish, would start bending along the shaped edges. In this case, to make it possible to observe the root under the microscope, the root should be pulled towards the center of the petri dish (with forceps), and the root should be, at the same time, rotated on the surface of media. This reduces the accuracy of the data collected as the cells can no longer be in the same orientation as they had naturally grown and will rotate and bend in 3D space. Using younger specimens, as mentioned, avoids this problem.

Figure 4-12 illustrates different sections of a mature root.

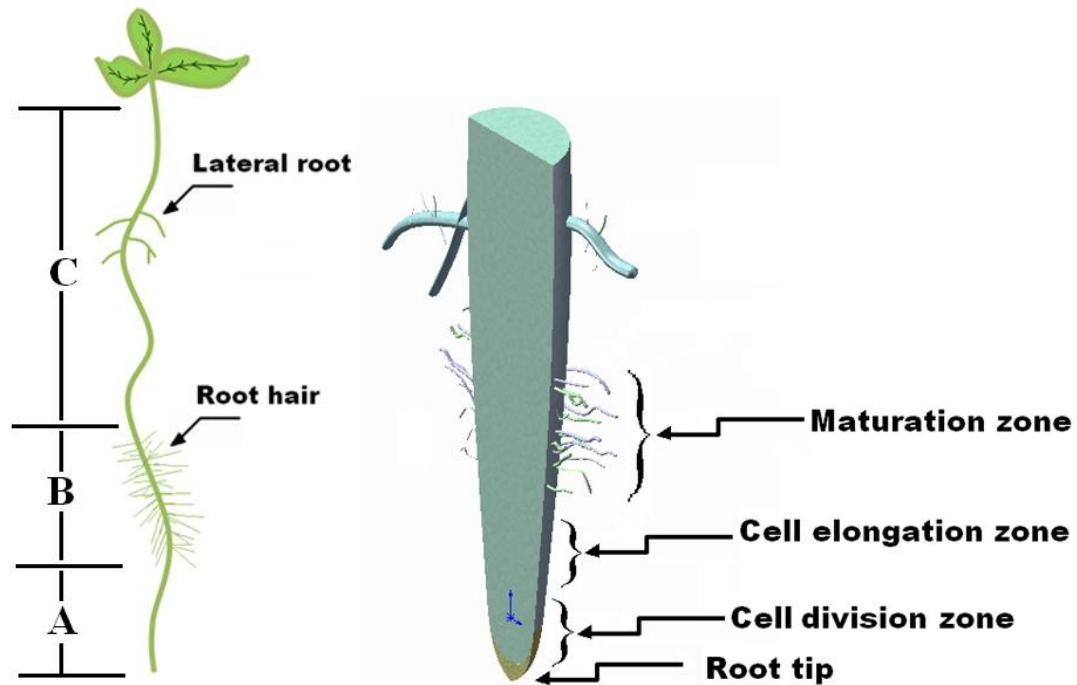


Figure 4-12: Left- a typical Arabidopsis root Right- a close-up view of the root

As shown in the previous figure, it can be seen that in the area defined as “C” there are a lot of lateral roots grown on the main root itself. All of these lateral roots are initiated at postembryonic stages of the plants growth. When such an area was observed under the microscope, there was not in fact a dominant pattern of Microtubules orientation in this area. Given the existence of this many lateral roots, it would also not be easy to visualize the main root itself. The area defined as “B” was also not favored for study due to the existence of root hairs. The difference between the lateral roots and root hairs is that each lateral root is an organ, in some cases with sub-roots branching from the lateral root that themselves have Microtubules inside. In contrast, a root hair is just a single cellular structure.

For investigating and tracking the Cortical Microtubules orientation, a region from between 1 or 2 mm off the root tip (Area “A”) up to maximum 10 or 15 mm off the root tip was selected, as illustrated in Figure 4-12. Length of area “A” was on average 5 to 7 millimeters, and if the media had enough water it could be as long as 15 millimeters. This is because the more watery media (or a media with higher nutrient concentration) would have fewer root hairs produced. Another rationale behind the preference of such region (around cell elongation and maturation zone) over the rest of the root is that approximately the first 0.5 to maximum 2 mm of the root tip is the meristematic zone of the root where the cell division occurs.. The cells in this zone are still in the early stages of growth and cell development.

The maturation zone, as mentioned, is not a much desired region to study the epidermal cells, due to existence of root hair.

In the root regions with lateral roots, or even sometimes in the maturation zone where cells are relatively more mature or aged (Area “B” or “C”), turgor pressure loss is almost inevitable; refer to Figure 4-12 and Figure 4-13. A reduction in the water content of the medium or the cell tissue also occurs after a certain elapsed time. This also results in the diminishing of the cell wall’s elasticity, which results in the erect shape of the cell no longer being maintained [91]. Accordingly such regions are not ideal to study the CMT’s reorientation for two reasons. Firstly, there is a lack of a dominant pattern and in contrast a randomness for the CMT’s orientations. Secondly, when the bending stress is applied to such regions, there doesn’t seem an immense resistance to the applied stress, and the root very slowly and hesitantly proceeds towards the essentially erect non-stressed position, unlike the younger cells with higher turgidity which are more stiff.

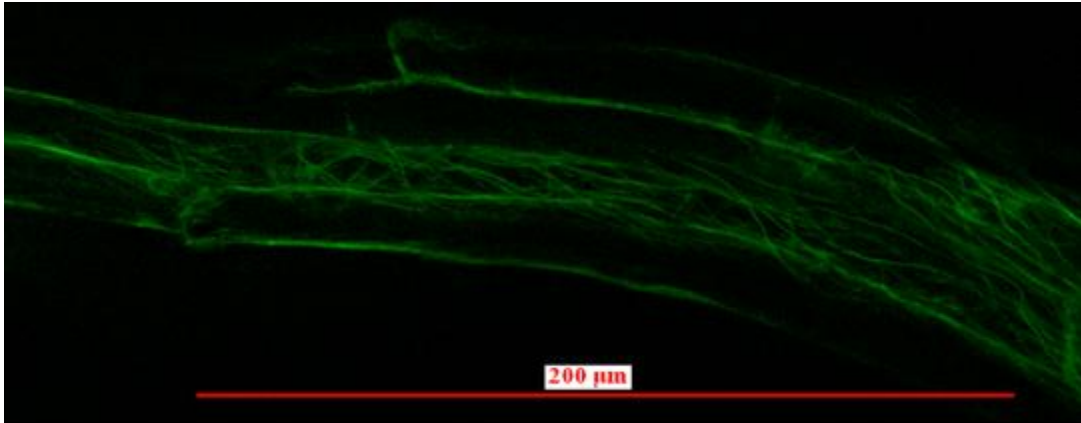


Figure 4-13: Typical expected Microtubules arrangement in region B or C. There exists no dominant pattern in the orientation.

Figure 4-14 depicts a typical dominant pattern observed in different sections of a root:

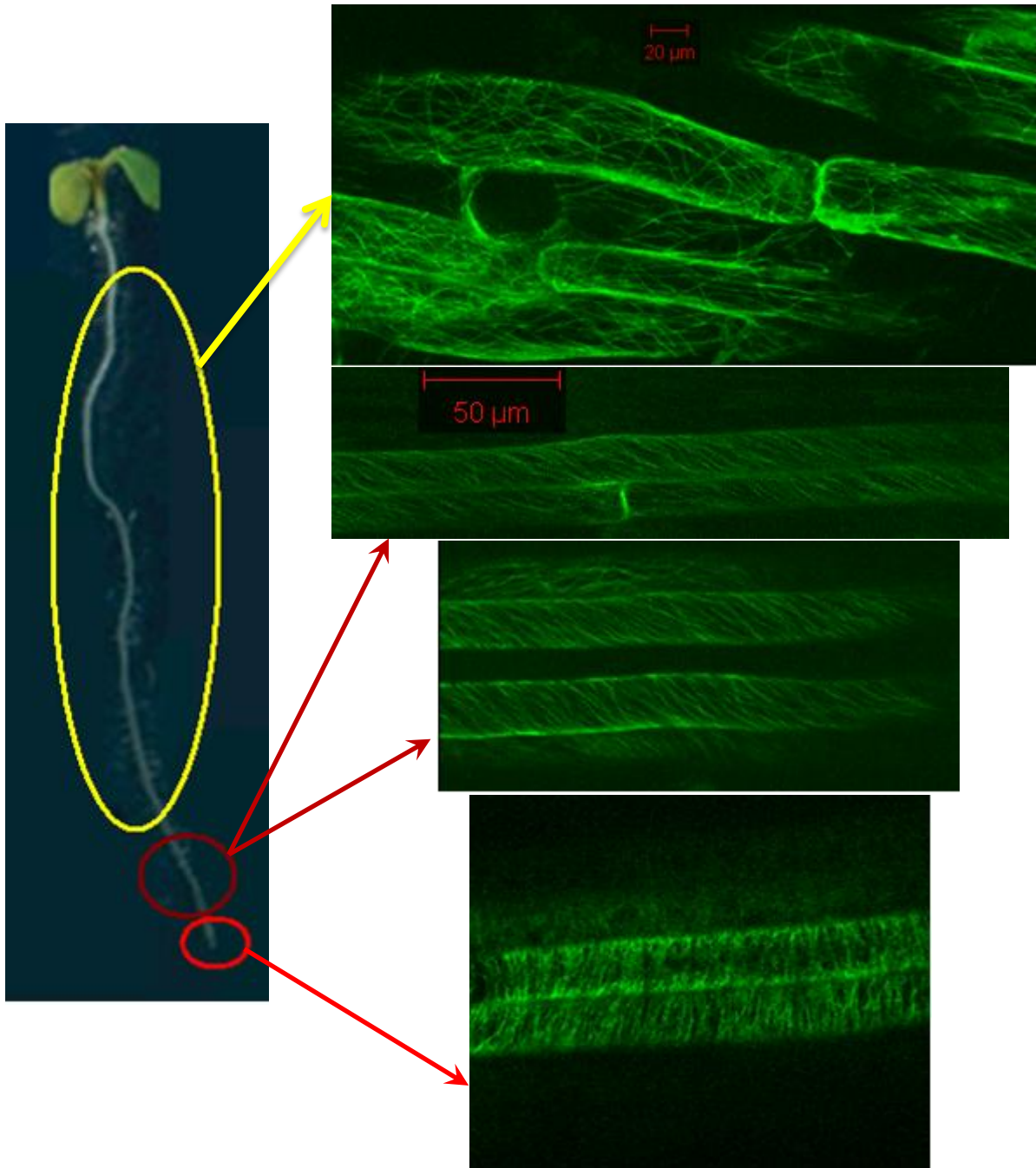


Figure 4-14: dominant Microtubules pattern observed in different sections of a root

Figure 4-15 shows both a real and a schematic depiction of the length of Arabidopsis root grown in a vertical petri dish over time.

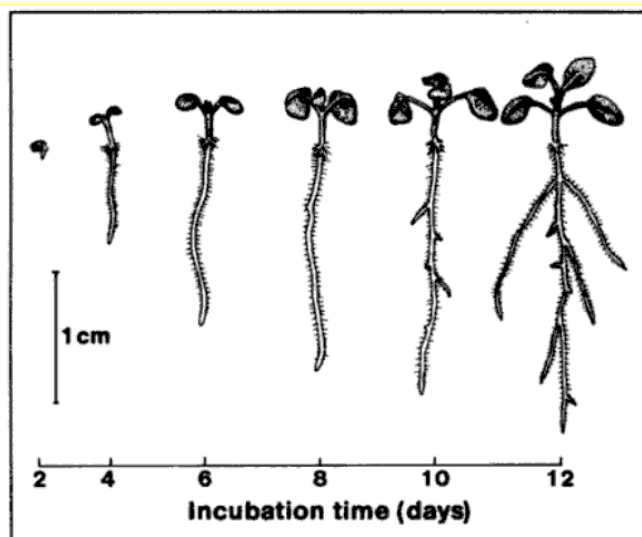


Figure 4-15- a: Schematic illustration of Arabidopsis length and growth rate over time (taken from [91])

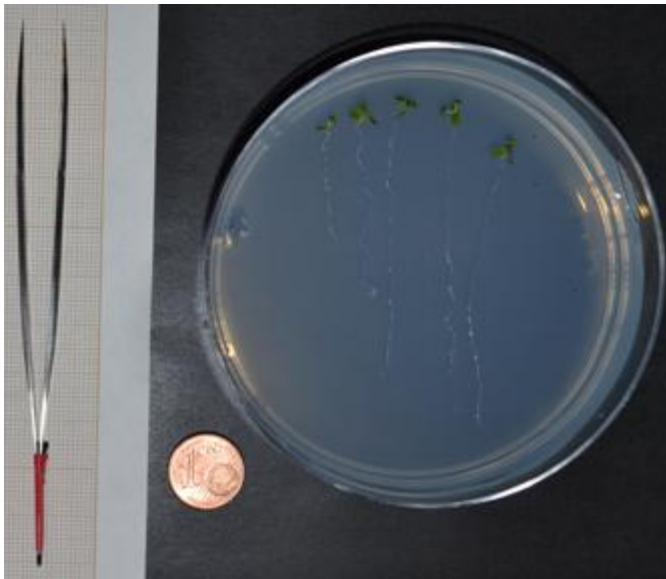


Figure 4-15-b: Real world images of mature Arabidopsis seedlings grown vertically in agar media

Arabidopsis root growth rate varies in different sections of the root which are depicted in Figure 4-12. However on average the total length of the root will grow between 5 to 9 mm per day.

4.3 Materials and methods

In this section some details of how the experiment was performed are explained. The following procedure (in the next three paragraphs) is a common practice in biological science.

Transgenic Arabidopsis seedlings were sterilized with 1 ml of a solution composed of 440 mg of Dichlor (Dichloro- isocyanuric acid, Sigma D-2536), 5 ml H₂O and 45 ml Ethanol 95% for 5 to 10 minutes. After decanting the sterilization solution and washing the seeds with 1 ml of Ethanol 95% and repeating all these steps for one more time, seeds were dried out under the hood and could be used a day after. This entire process had to be performed under a controlled sterilized chamber to avoid any unwanted dirt that might contaminate the seedlings. The sterilization process is necessary to avoid any future mold growth in the Petri dish, and if such process is not performed properly the seedlings may be either killed or not sterilized so as to be suitable for experimentation.

Arabidopsis seeds were then cultivated in a half-MS (Murashige and Skoog) medium, and were grown in a Sanyo growth chamber. The growth chamber had an average temperature of 24 °C, relative humidity of 44% with 16 hours of illumination and 8 hours of darkness. The chamber consisted of 7 neon lamps with 5 (50 $\mu\text{mol m}^{-2} \text{s}^{-1}$) light intensity. Five of the neon lamps (Osram Biolux L36W/72-965) were for the purpose of simulating the natural sun light and the other two (Sylvania GRO LUX F36W/GRO-T8) were for promoting photosynthesis process in the plant.

The Petri dishes in which Arabidopsis seeds were cultivated were maintained vertically the whole time in the growth chamber so that the Arabidopsis roots would grow on the outer surface of the agar medium.

4.3.1 Visualizing preparation

To observe a sample root under the confocal microscope, the Petri dish containing the Arabidopsis root was transferred under the lens without any need for dyeing or major change. The only thing that a confocal microscope requires is a few drops of water (or in some cases oil) under the lens so that the object would be visible. However since Arabidopsis root is very delicate, and as a result a very light organ, a few drop of water can easily make the root lose its surface contact with the agar media upon which it is sitting. Direct water drops cause the root to hover around the Petri dish. To solve this problem, a cover slip had to be directly applied on the root. The friction between the cover slip and the agar media would keep the root relatively fixed in its position. Although this is the only practical method to avoid the root from moving around, there are two significant challenges for this method. One challenge is that when covering the root with a cover slip, the surface of the cover slip has to be perfectly bonded to the root (at least in the area of interest). A small amount of air (like an air bubble) stuck between the cover slip and agar media would create a large amount of visual noise that blocked the whole process of visualization, as shown in Figure 4-16. A second challenge is that since the root is in direct contact with the dry surface of the cover slip, there is a short limited time span in which visualization should be performed, otherwise the vulnerable root cells might die due to drought.

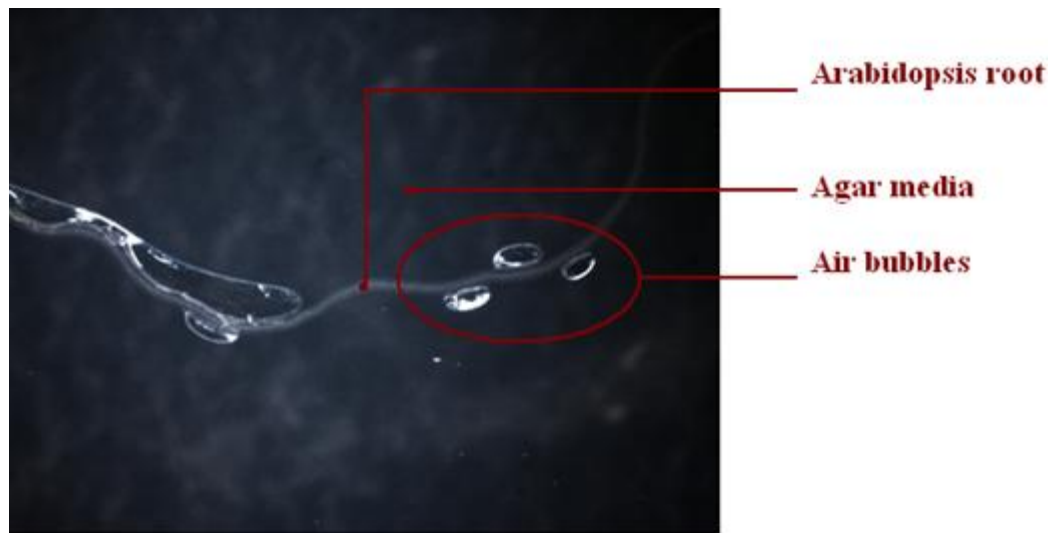


Figure 4-16: Air bubbles trapped between the cover slip surface and agar media.

This vital and limited time was especially of importance when the tracking of the Microtubules orientation had to be performed repeatedly after certain hours; since the risk of destroying the cells with the dryness caused by cover slip would be higher given the repeated nature and long time span of the experiment.

Once the cover slip is fixed properly holding the root on agar media, then water droplets can be applied on the cover slip.

4.3.2 Applying mechanical bending stress

For the purpose of applying mechanical loadings, very thin rods with about 0.3 mm thickness and 3 to 7 mm length were employed. These very fine rods, which have almost the same cross section diameter of the Arabidopsis root, make it possible to apply mechanical stresses to the root, while assuring that the plant is handled properly with no damage to the cells. To apply the mechanical bending stress to the root, a few small

pieces of thin rods were utilized as scaffolds around the root to keep the final bent shape of the root for about six to seven hours. The thin rods are touching the cells which are around a few cells away from the one which is bent and studied. Based on this, any possible signal transmission from the cells attached to the thin rods to the bent cell is negligible and does not affect microtubules orientation at all. The required time of 6 to 7 hours noted was selected based on the experiment itself, as well as what found in literature [102- 105]. These thin rods are slowly inserted inside the agar media in a perpendicular direction to the media surface around the root to prevent the root from sliding on the slippery surface of the media.

It is preferred that the intact root does not have a wave shape in the area of interest to avoid any possible miscalculation in the orientation of Microtubules. These natural wavy patterns in the Arabidopsis root are quite common which may sometimes occur due to obstacle touching, gravity direction alteration, or other environmental stimuli.

Bending stress was applied evenly by moving the sub-apical region of the root tip on the flat surface of the half-MS media by means of steel pins, as shown in Figure 4-17. Application of such bending force continued until the root would form an arch with about 200 to 600 μm radius of curvature. Maximum bending load could not be easily measured, as it was reached by trial and error. The role of such thin rods might be comparable to the supports of a beam in a three or four point bending test, as illustrated in Figure 4-17, except that in this experiment, high deformations are experienced.



Figure 4-17: a sample Arabidopsis root under mechanical bending stress applied by three surrounding thin rods. Such thin rods act like scaffolding elements ensuring the root will not move on the agar media surface.

If such scaffolds are not placed around the root, then the Arabidopsis root will have a tendency to return back to its original straight shape. As explained before, such a tendency is specific of younger and newly born cells. Older cells will either not return to

the original shape, or very hesitantly and slowly move back towards the original shape without fully returning.

It is very important to make sure that after applying the bending stress, the root is still healthy and growing as in a normal condition. For tracking Microtubules orientation after applying mechanical load, the images were taken after around 6 to 7 hours after the stress was applied so that Microtubules would have enough time to rearrange. Figure 4-18 shows the observations made right after applying the bending force and 6 to 7 hours after applying the load:

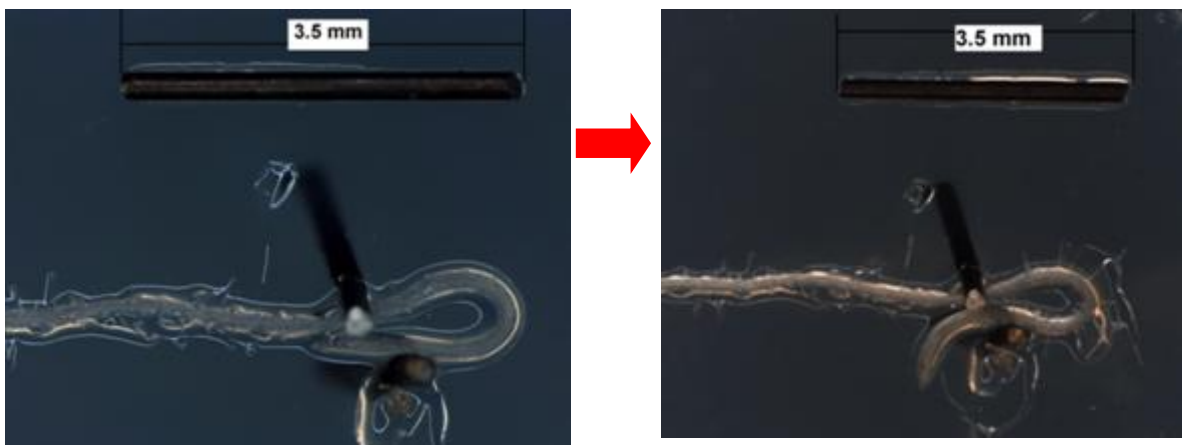


Figure 4-18: Tracking Arabidopsis root appearance after applying the bending load
Left- root immediately after the bending stress is applied right- six to seven hours
after bending stress is applied.

As shown in Figure 4-18, the Arabidopsis root kept a normal growth pattern even though the root was undertaking the bending force. As well, root hairs were slowly growing on the outer surface of the root in the area where external load was applied. This confirms that Arabidopsis root was healthy and in a normal growing condition.

It is worthwhile to mention that there are some studies focusing on the role of mechanical bending on the lateral root initiation (somewhat comparable to Figure 4-18) which is not included in the scope of this research [105, 104].

While applying mechanical bending loading to the root, it is also very crucial not to destroy the vulnerable cells of the root in the area where load is applied. More specifically, when the root is undergoing bending stress, the region with the lowest radius of curvature has got the highest deflection and can be the first place to get injured under the load. As well, it is always essential to know that the cells under investigation are healthy and normal cells. Fortunately, it is quite simple to recognize a healthy cell in Arabidopsis root from a destroyed or unhealthy one. As illustrated in Figure 4-19, Microtubules in a damaged cell will not be visible within the area where it is smashed or destroyed.

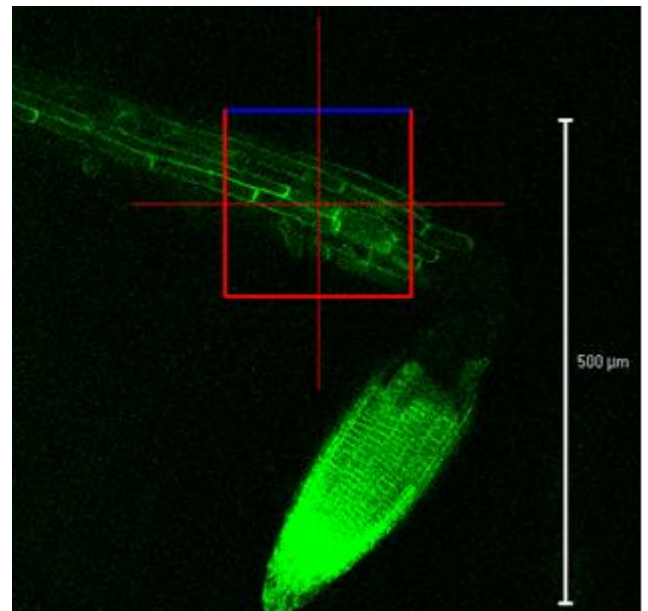


Figure 4-19: Arabidopsis root destroyed under the excessive bending load applied. Microtubules in such area are not visible anymore.

4.3.3 Some details of imaging process

Micrographs in this research were captured via a laser confocal microscope. Principles of how a confocal microscope functions is very simple as illustrated in Figure 4-20. Confocal microscopy was developed to overcome some of the restrictions in fluorescence microscopy. In fluorescence microscopy, the light (from the light source) is uniformly distributed over the whole specimen. In contrast, confocal microscopy utilizes “point illumination”. It means that a small breach in a plane in front of the light detector removes the out-of-focus signals (Figure 4-20). Since only light caused by fluorescence near the focal plane (Figure 4-20) is detectable, the resolution of images is quite better than that of fluorescence microscopy.

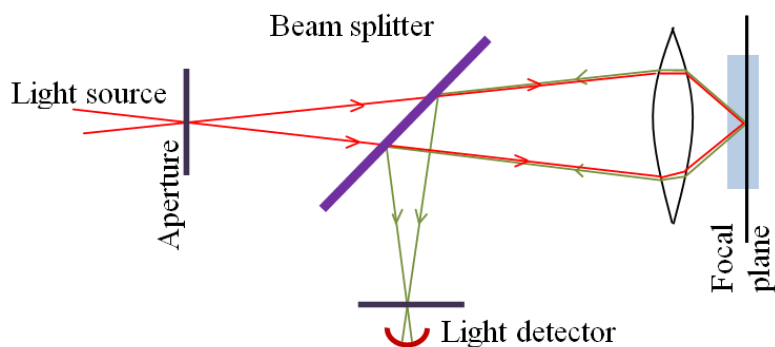


Figure 4-20: Basics of how a confocal microscope works.

Observations in this research were performed by using a Zeiss LSM upright laser-scanning confocal microscope. This microscope was equipped with a 40×water-corrected objective and appropriate filters for the detection of fluorescence signal of Green Fluorescent Proteins (GFPs). The settings were as follow: an Argon laser beam with

wavelength of 488 nm (maximum power 30 mW, output of 50%, transmission set between 35 to maximum 55%) and emission filter LP 505 was utilized in this experiment. Images from confocal microscopy were quantitatively assessed by an image-processing program named “ImageJ” (<http://rsb.info.nih.gov/ij/>) to investigate the orientation of Microtubules. Since ImageJ has an open architecture, Dr. A. Boudaoud has written a code as a plug-in to this software that makes it possible to extend some of the desired abilities of ImageJ for the research conducted [106]. This coded ability was measuring the dominant orientation of a group of Cortical Microtubules by defining the area of interest in the images. This capability was employed in this thesis.

After drawing a polygon around the preferred region of study on the image (Figure 4-21), and subsequently initiating the mentioned Microtubules tool, a log output will provide some information that includes the overall average orientation of the region, in angles from -90 to 90 degrees. The quality of the Cortical Microtubules orientation based on a score from zero to one is also output. All obtained results were quantitatively studied, and the obtained numerical data were processed using Microsoft Excel, as explained in the following sections of this thesis.

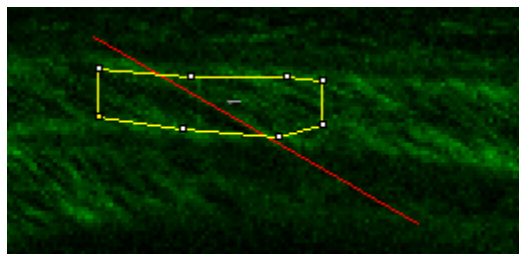


Figure 4-21: ImageJ software utilized in measuring the dominant orientation of Microtubules in the area of interest (inter part of the yellow polygon)

4.3.4 Measuring radius of curvature for each cell

As will be explained in the following sections, for analyzing Microtubules arrangement, one of the parameters to measure is the radius of curvature of each individual cell after the bending load is applied. Given the vulnerable nature of the Arabidopsis root, measuring the magnitude of the force applied is quite challenging; as an alternative, studying the radius of curvature was more practical.

To achieve this, images from ImageJ were transferred to SolidWoks software. Since the real size of the cell will look unrealistic after being transferred to SolidWoks, each image should have a proper scale bar. This yellow scale bar, as shown in Figure 4-22, is created and marked in ImageJ. In SolidWoks software, three arches will be curve fitted by means of '3 Point Arc' on the inner surface (R1), mid surface (R2) and outer surface (R3) of a cell image as shown below.

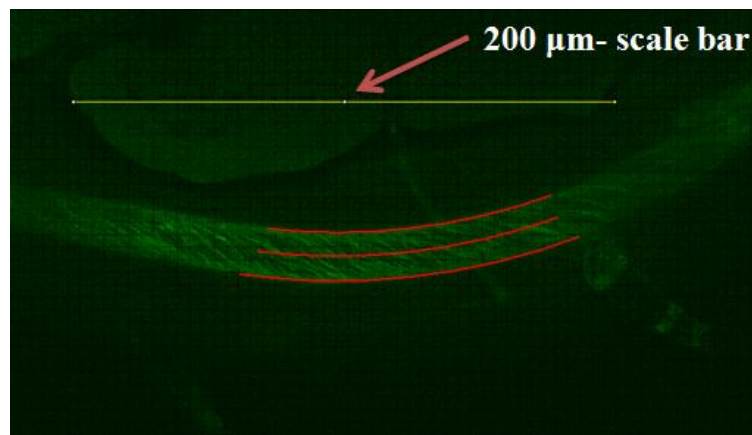


Figure 4-22: Measuring the radius of curvature in each individual cell by means of SolidWorks software.

The radius of curvature of the cell will be the average value of these three radii of curvature. This ensures the accuracy of the radius of curvature measurements.

4.3.5 Effect of gravity on the Cortical Microtubules orientation

One of the very first tests performed on the Arabidopsis root was to verify if gravity (as a natural force) affects the orientation of the Cortical Microtubules or not. Possible influence of gravity on Cortical Microtubules orientation had to be validated before any other mechanical stress were applied so that if there was any gravity induced re-orientation, possible interference or superimposition with mechanical load could be taken into account.

To achieve this, Arabidopsis roots were grown vertically in a normal condition as explained above. After they reached the desired age of 7 to 15 days, Petri dishes were rotated 90 degrees either clockwise or counter clockwise and then visualized after 6 to 7 hours for the two zones of interest in area A, as shown in Figure 4-12: the cell division and cell elongation zone. In both areas, there wasn't any noticeable alteration in the orientation of the Microtubules.

The same experiment was repeated while rotating the Petri dishes 180 degrees relative to the original position as shown in Figure 4-23. Once again, Microtubule orientation was investigated around 6 to 7 hours after rotation was applied.

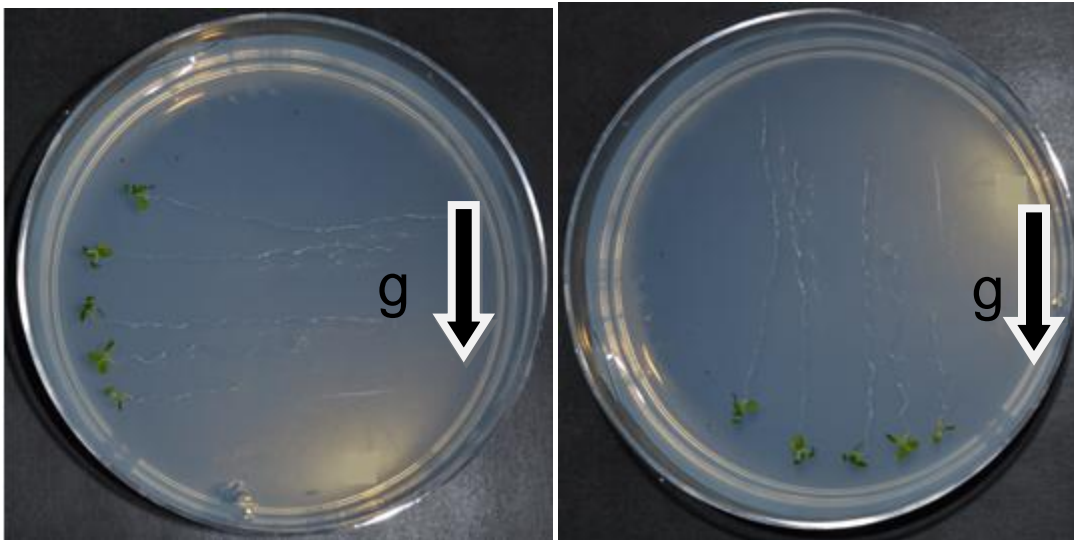


Figure 4-23: Gravity direction alteration of 90 degrees and 180 degrees for a period of six to seven hours

Again, the same results were obtained as there wasn't any tangible change in the Microtubules orientation.

While measuring the average angle of a bundle of Microtubules as explained in Figure 4-21, there is about a ± 5 degrees error margin in the measurement (which is a limitation for all such experimentation). This may partially explain the reason why there isn't a noticeable change in Microtubules orientation. In fact, gravity did not significantly alter Microtubule orientation relative to later results obtained in this research. As S. Matsumoto et al. examined the effects of hyper-gravity (300g) and noticed a significant change in the orientation of epidermal cells, it is probable that hyper-gravity might also affect Microtubules orientation [107]. This needs to be further investigated, but this referenced study did not contradict any results here.

Figure 4-24 illustrates Microtubules orientation in the cell division and cell elongation zones (area A) section of the root. It is obvious that in the cell division zone, Microtubules are perpendicular to the cell main axis while in the cell elongation zone they are angled about 40 to 45 degrees with respect to the main axis; this same result is obtained with or without gravity direction change.

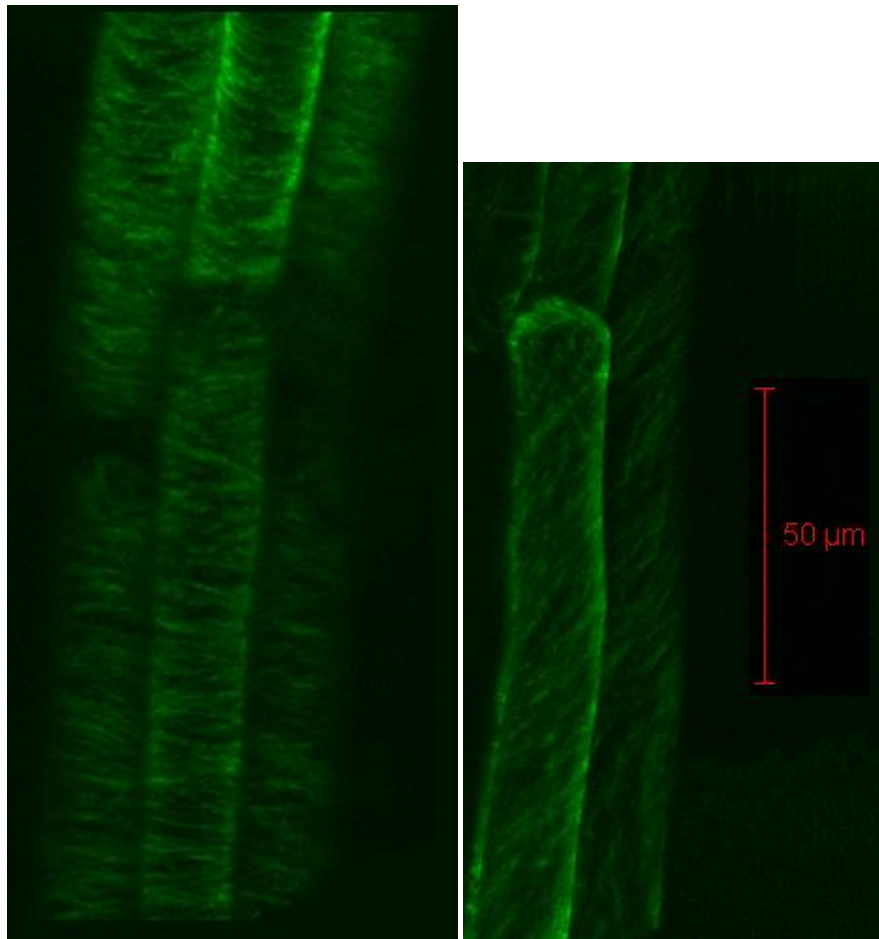


Figure 4-24: Gravity direction changed 90 degrees and 180 degrees to the original direction. *Left-* Microtubules orientation is perpendicular to the main axis in cell division zone *right-* Microtubules orientation is about forty or forty five degrees with respect to the main axis for the cell elongation zone. Such results are identical to the observations with no gravity direction change.

4.4 Observation results

4.4.1 Sample controls with no external mechanical loading

As explained above, Microtubules orientation was first investigated for control samples. Control samples were those samples naturally grown in a vertical position in Petri dishes free of any external loading environment. After studying around a hundred different control samples, there were three different dominant pattern of Microtubules orientation observed in each root. These three different arrangements were observed in Area “A” cell division zone, Area “A” cell elongation zone and areas “B/C” (refer to Figure 4-12).

In part of area A which includes root tip and cell division zone, the prevailing orientation of Microtubules is transverse with respect to the main axis of the cell. This means that Microtubules orientation is perpendicular to the cell growth direction. Figure 4-25 illustrates this.

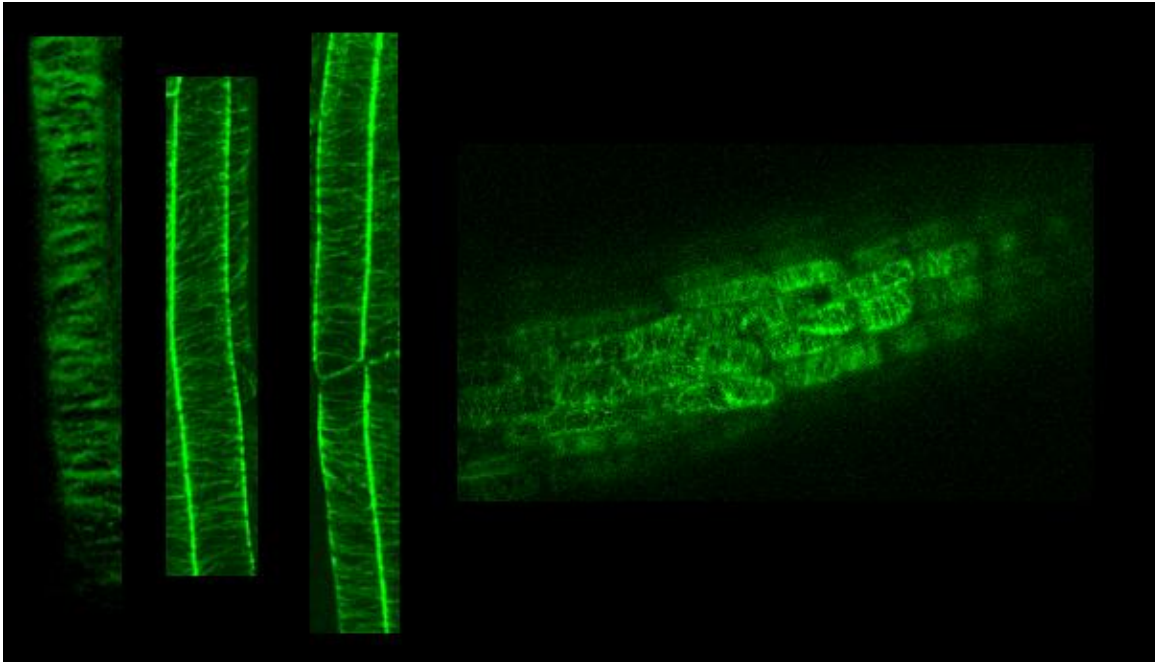


Figure 4-25: Some selected samples indicating transverse arrangement of Microtubules in the root tip and cell division zone.

In the cell elongation zone, the cells' overall length is longer (compared to cell division zone), and since they are fully mature cells, their lengths do not tend to increase any further. In this area, as observation confirmed, the prevailing arrangement direction of Microtubules had an angle of about 45 degrees with respect to the main axis of the root. This angle is in very good agreement with similar experimentation found in literature [108, 109]. Below are some examples from control samples showing the orientation of Microtubules:

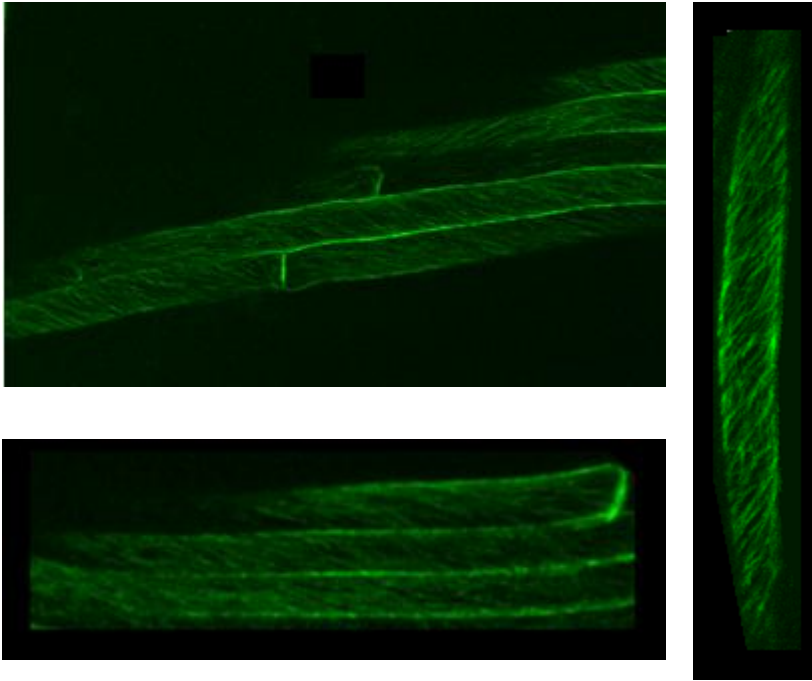


Figure 4-26: Observations in cell elongation zone confirm the existence of a dominant arrangement of Microtubules angled about 45 degrees relative to the cell main axis

However it is essential to mention that these results collected from cell division and cell elongation zone are not necessarily a hundred percent analogous in all cases using the most stringent criteria. Since cell zones slowly transitions from cell division to cell elongation and then maturation zone (when moving along the length of the cell), there isn't a rigid boundary limit defining such zones. Consequently, in the sections where each of these three zones are transitioning from one to another, there are always numbers of cells that have got a combination of Microtubules orientation pattern. For instance, in the area where transitioning from cell division to cell elongation, Microtubules in different neighboring cells could have transverse orientation as well as a 45 degree angle orientation. In the cell division zone, even though it is not very likely,

there have been some other exceptions noticed; an individual cell was observed having both transverse and inclined orientation of Microtubules at the same time in the opposite sides of a cell. Some of these exceptions are noted in Figure 4-27.

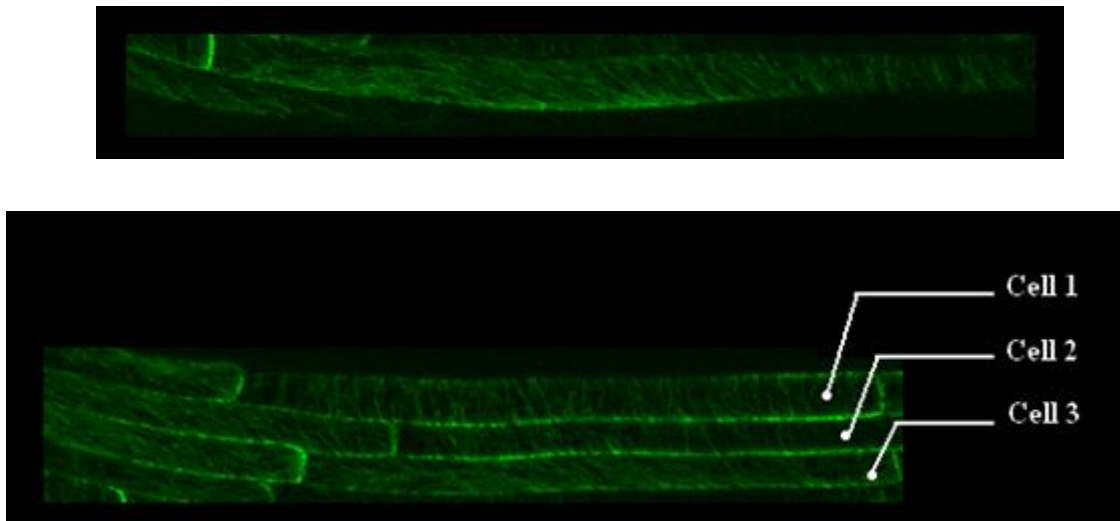


Figure 4-27: *Top*: an individual cell shows different orientation of Microtubules while transitioning from division to elongation zone. *Bottom*: three neighboring cells having different orientation of Microtubules

As illustrated in Figure 4-27, an individual cell while transitioning from division to elongation zone, can have both patterns of transverse and angled orientation for Microtubules. As well, in cells tagged with number 1 to 3, it is shown that cell 1 has a transverse orientation of Microtubules; cell 2 has slightly angled Microtubules orientation and cell 3 has got a combination of orientations for its Microtubules.

When the cell elongation zone is transitioning to the maturation zone in a control sample, it is possible to witness cells having Microtubules aligned around 45 degree in the vicinity of another cell not having a recognizable arrangement of Microtubules.

As mentioned earlier, the maturation zone was the area in which root hairs or lateral roots had started to grow. This zone started around 10 to 15 mm off the root tip. However, in some cases, when Arabidopsis root was slightly growing under the surface of MS-media, the maturation zone starting point could be as far as 15 to 20 mm from the root tip. Thus, if there isn't a root hair or lateral root in the vicinity of cells in this zone, Microtubules angles in this area could still be 45 degrees relative to the cell main axis.

4.4.2 Effect of mechanical bending force on MT orientation

Following the application of bending load, for a subset of samples, Microtubules were studied immediately after the load was first applied (literally minutes after samples were first bent). All samples were studied after 6 to 7 hours of continuous bending load exertion.

Below are some examples of the Microtubules arrangement visualized after 6 to 7 hours after the bending load was first applied. Red lines in the Figures display the dominant pattern of Microtubules measured by ImageJ software.

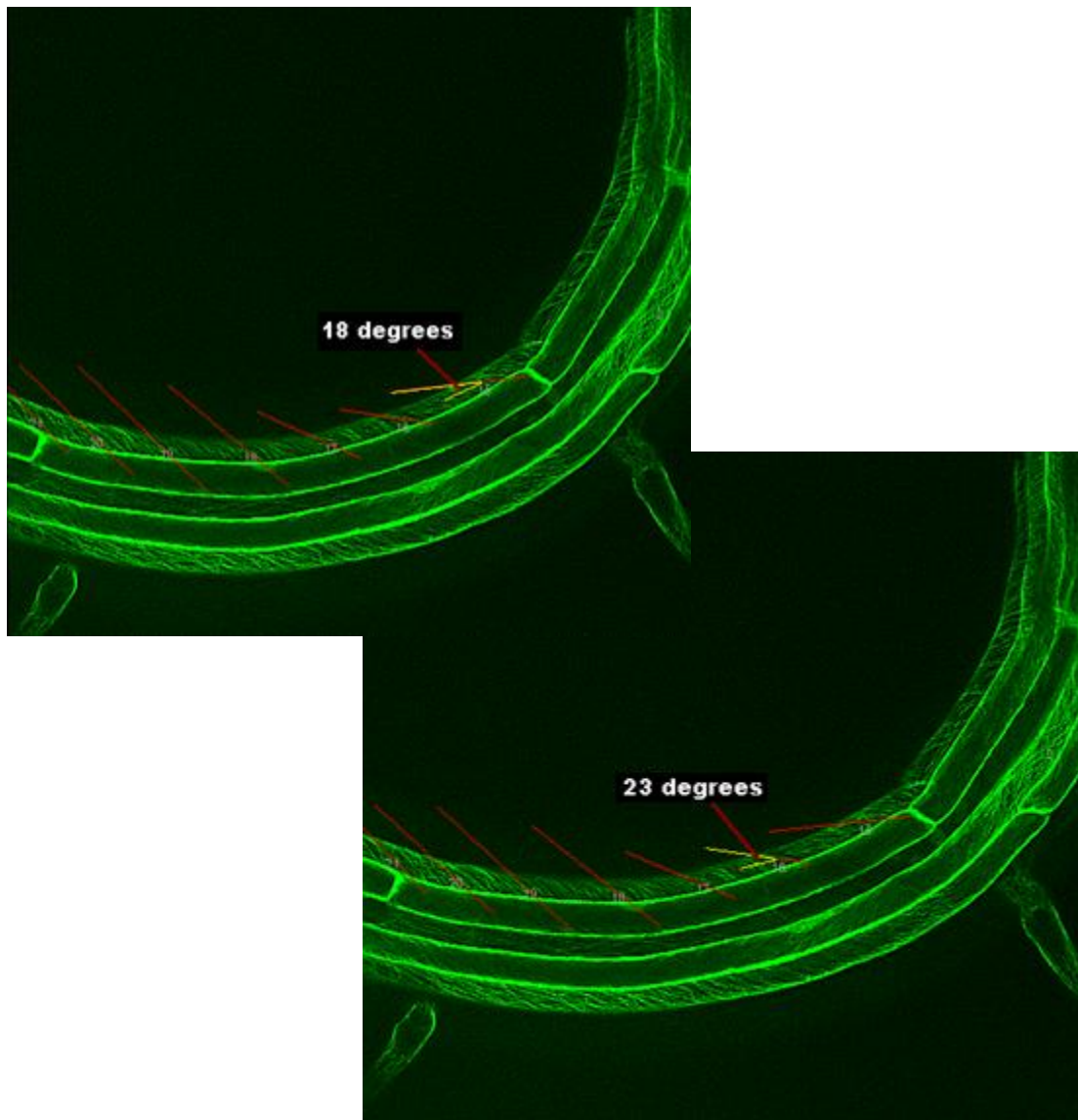


Figure 4-28 ((a) - page 1 of 3): Microtubules orientation along the root cell visualized after 6 to 7 hours after the bending moment was applied to the root.

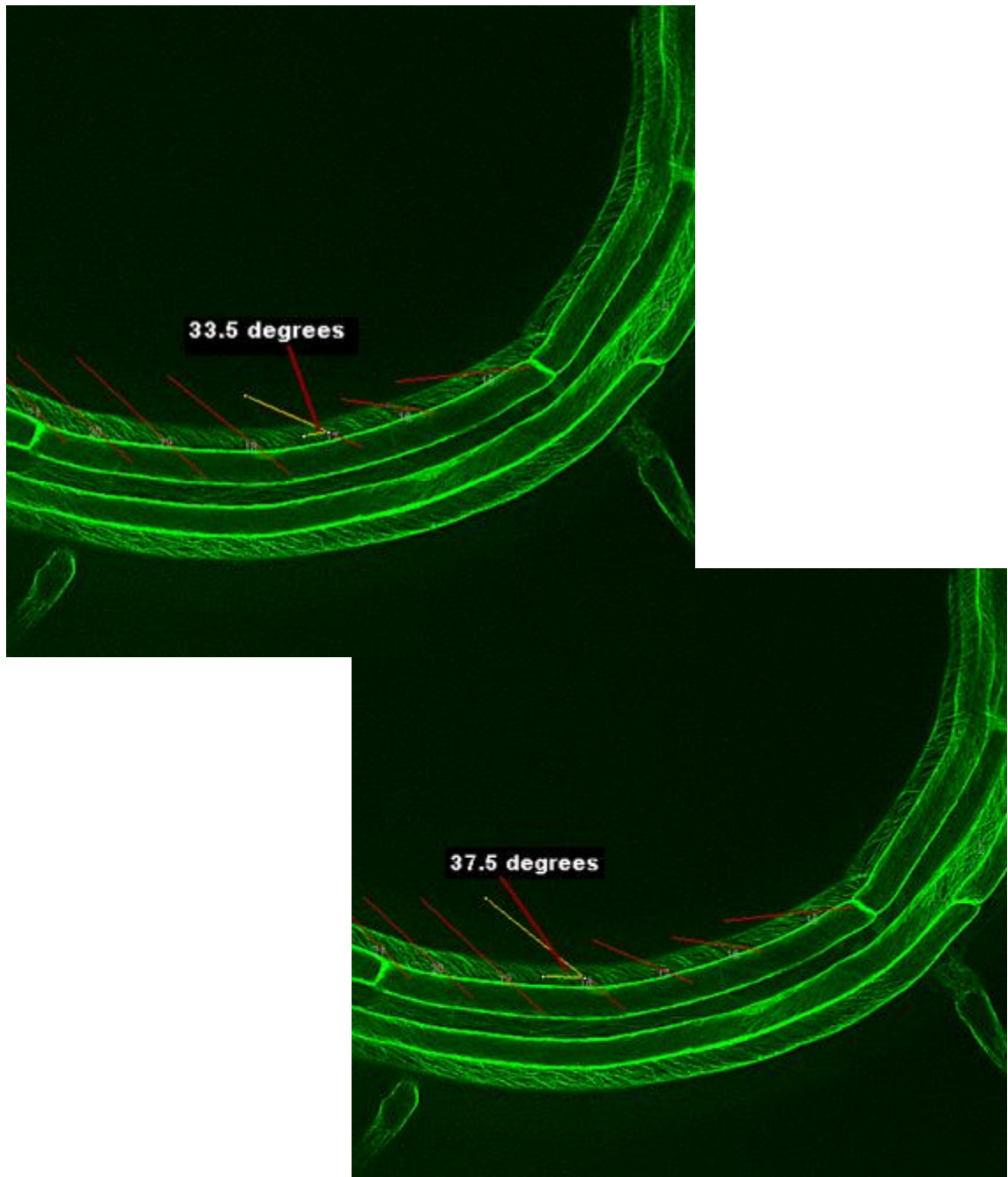


Figure 4-28 ((b) - page 2 of 3): Microtubules orientation along the root cell visualized after 6 to 7 hours after the bending moment was applied to the root.

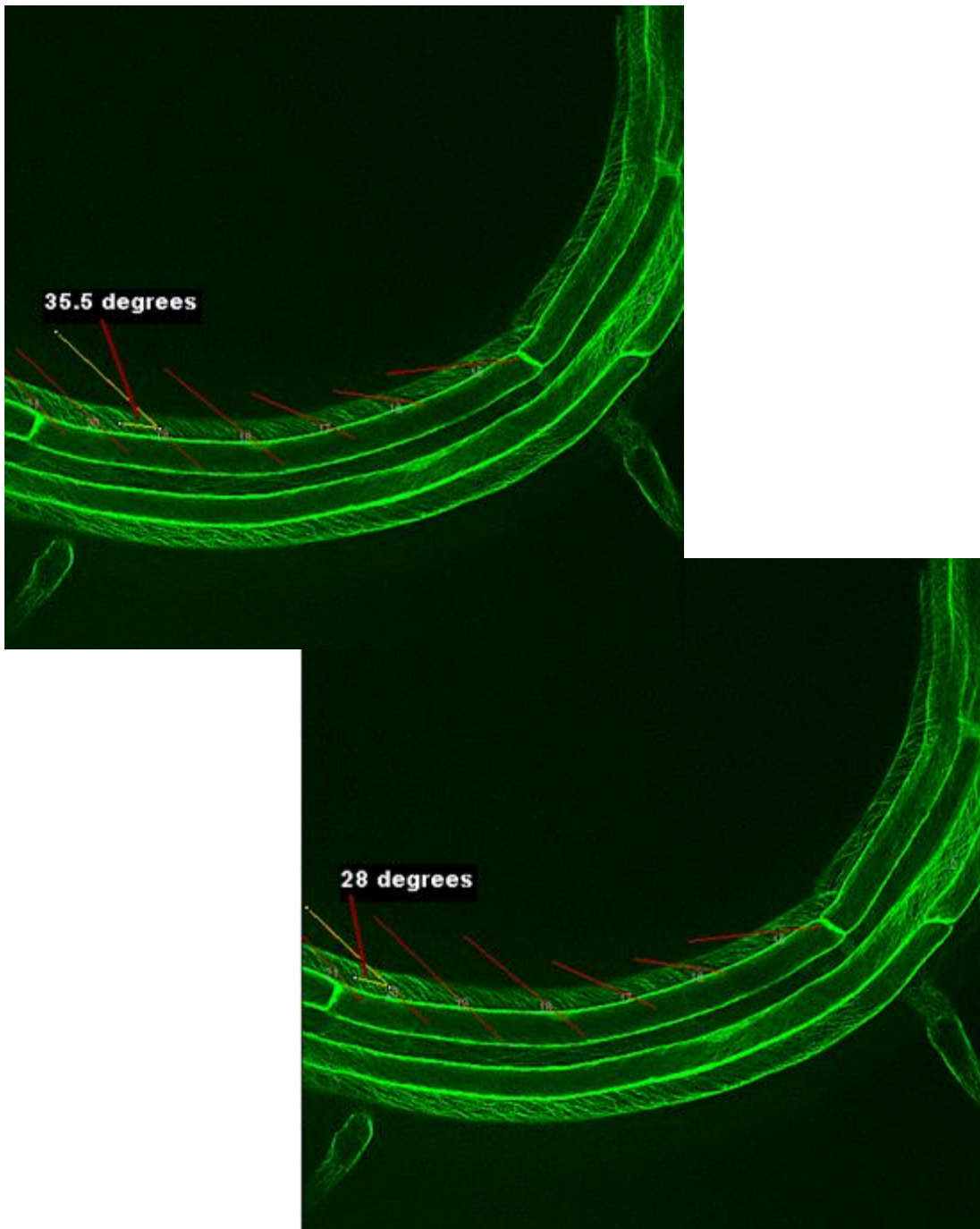


Figure 4-28 ((c) - page 3 of 3): Microtubules orientation along the root cell visualized after 6 to 7 hours after the bending moment was applied to the root.

Below is another series of images taken from a different sample and shows the re-oriented Microtubules tracked directly after 6 to 7 hours of continuous load application:

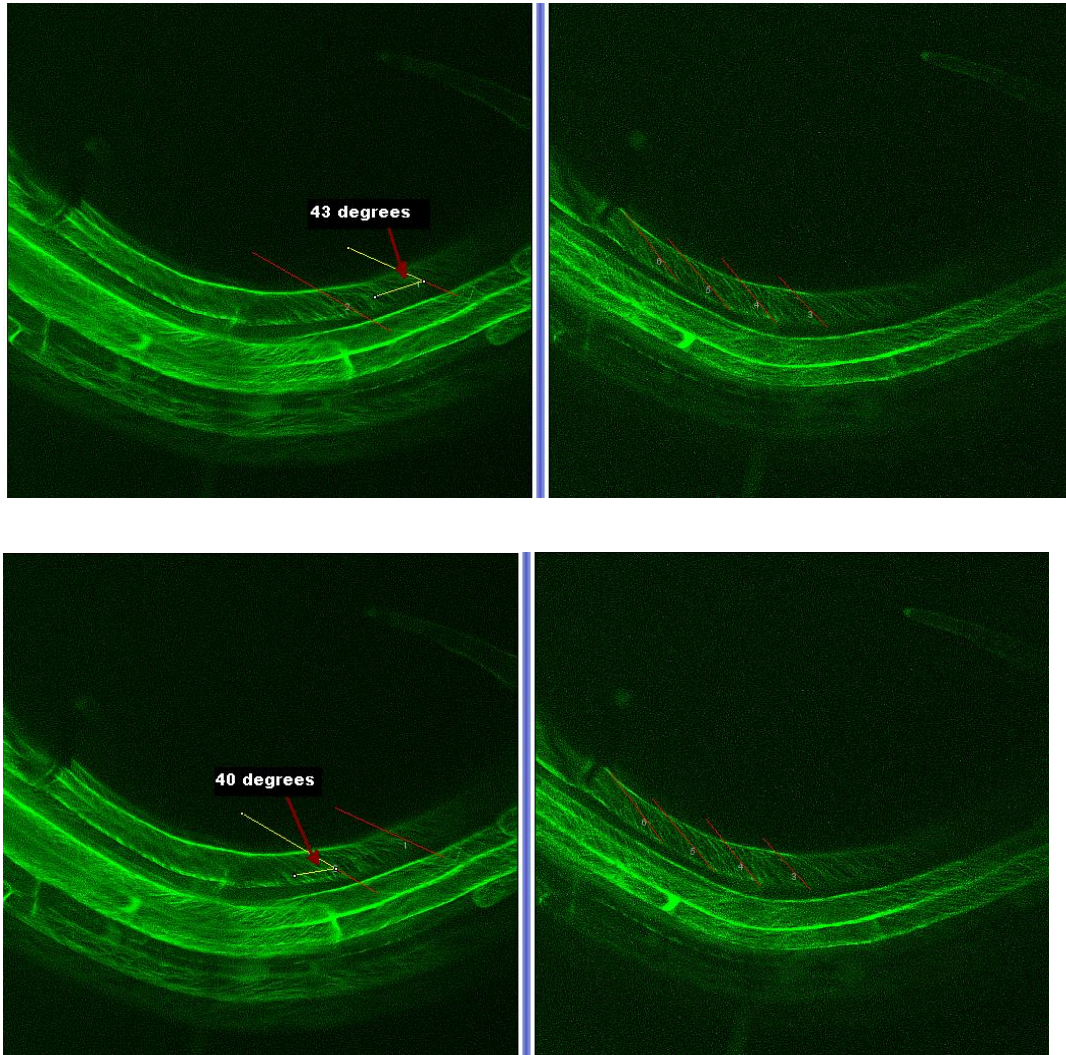


Figure 4-29 ((a) – page 1 of 3): Another sample showing Microtubules orientation along the root cell visualized after 6 to 7 hours after the bending moment was applied to the root.

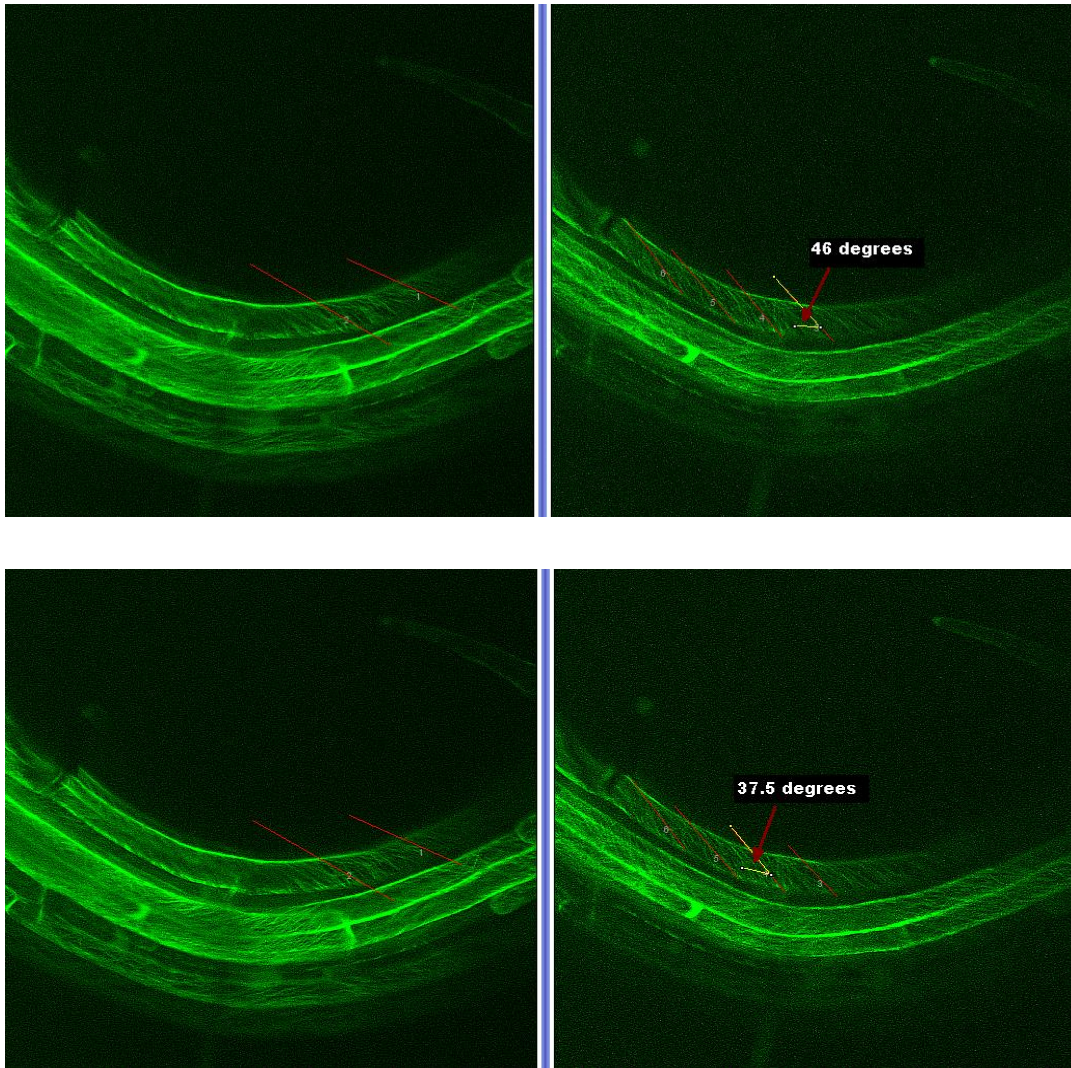


Figure 4-29 ((b) – page 2 of 3): Another sample showing Microtubules orientation along the root cell visualized after 6 to 7 hours after the bending moment was applied to the root.

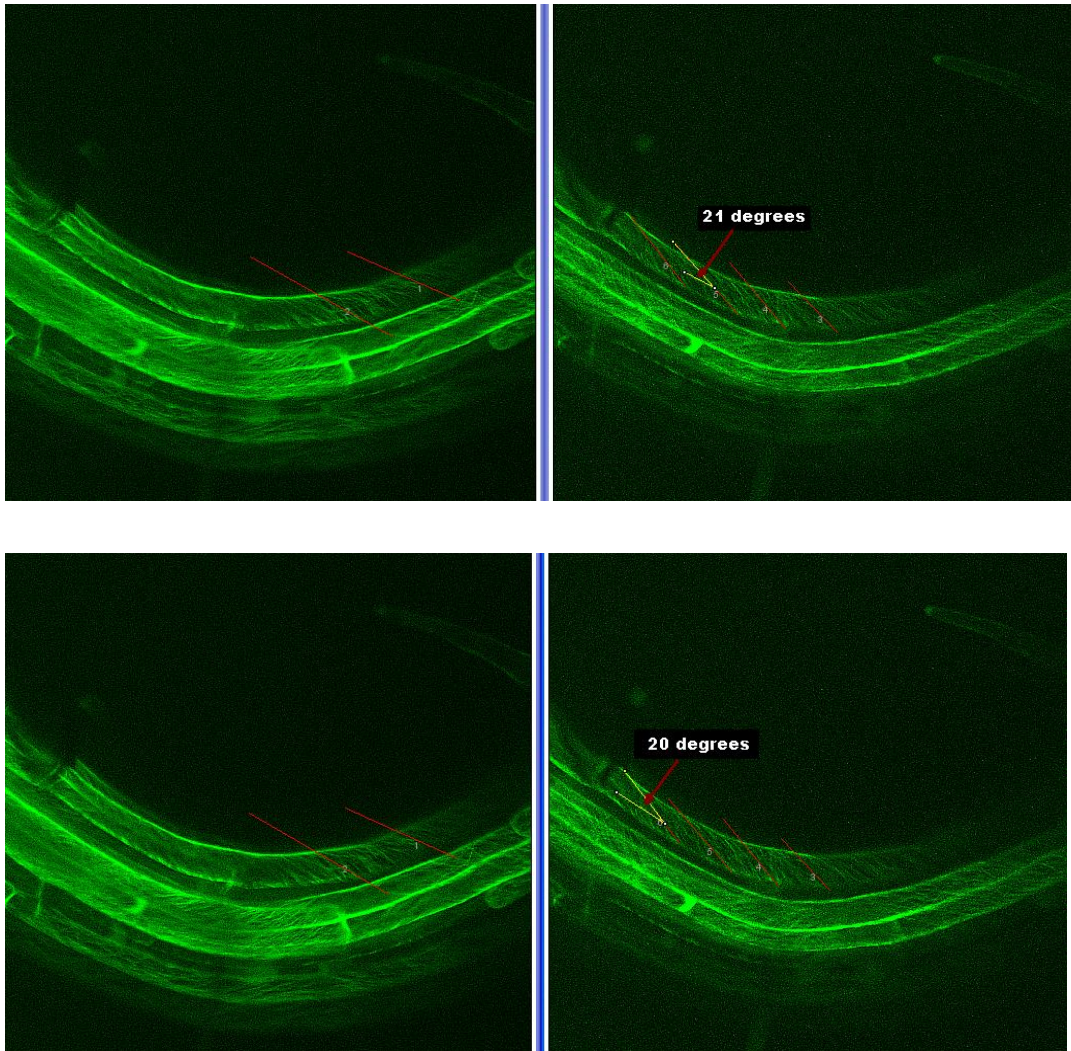


Figure 4-29 ((c) – page 3 of 3): Another sample showing Microtubules orientation along the root cell visualized after 6 to 7 hours after the bending moment was applied to the root.

As shown in Figures 4-28 and 4-29, smaller angles are seen closer to the tail end of the cell (T portion in Figure 4-31) and bigger angles are seen in the middle of the cell (M portion in Figure 4-31).

More figures similar to Figure 4-28 and observations can be found in Appendix B of this thesis.

Another important detail captured in these images is the root hairs undesirable growth in the area of interest. As mentioned before, such root hairs can cause noise in collecting data and even it might be one of the reasons for a disorganized Microtubules arrangement. The following two images in the next figure are taken from the same section of a chosen root:

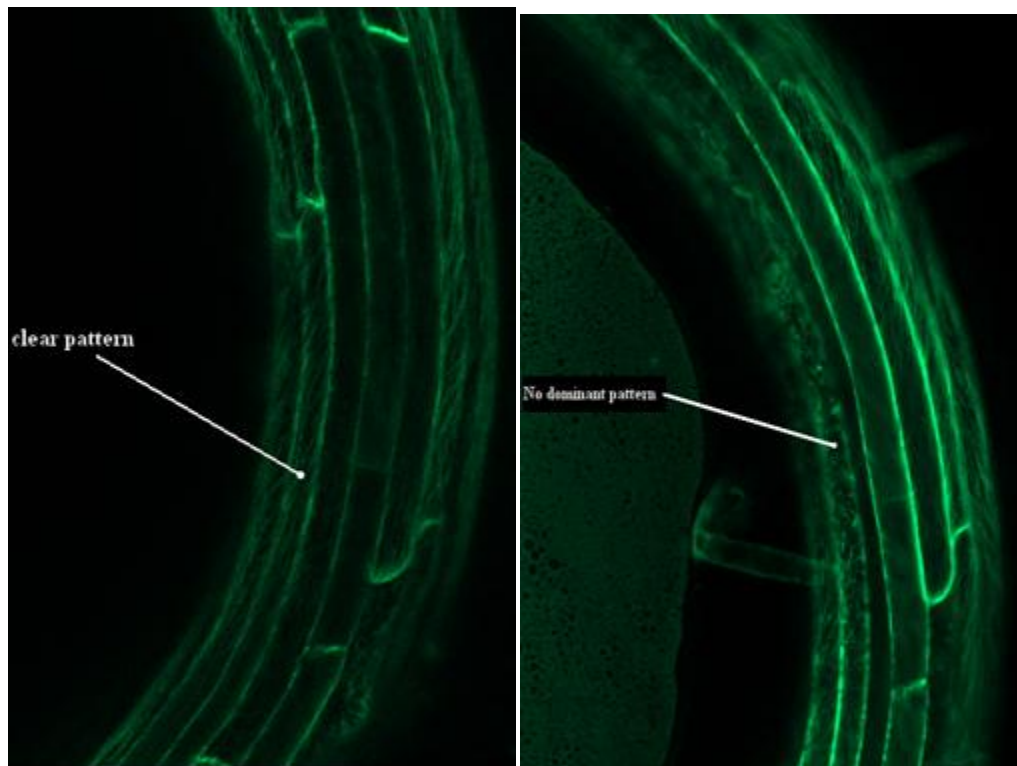


Figure 4-30: Microtubules have lost their arrangement in one of the cells (*right*) after being under the bending load for 7 hours. The *left* image displays more of a typical Microtubule arrangement for when bending load was first applied.

As shown in Figure 4-30, Microtubules in one of the cells had a clear oblique pattern directly after the bending load was first applied (highlighted in the left image) but

after being exposed to the load for around 7 hours, this same cell lost a clear arrangement of its Microtubules (highlighted in the right image). It is hypothesized that such loss of arrangement might be either due to the undesired root hair growth from this cell, or excessive load applied.

For those Microtubules having a clear reorientation pattern, similar observations were performed for many other samples exposed to bending load. Results of such observations are compiled and summarized in the next few figures.

If an individual cell is considered as a long cylinder, two sections of this cell are significant while studying the Microtubules orientation. First is the Middle third of the cell, defined as “M”, and the Tail-end sides (thirds) of the cell, defined as “T” in Figure 4-31.

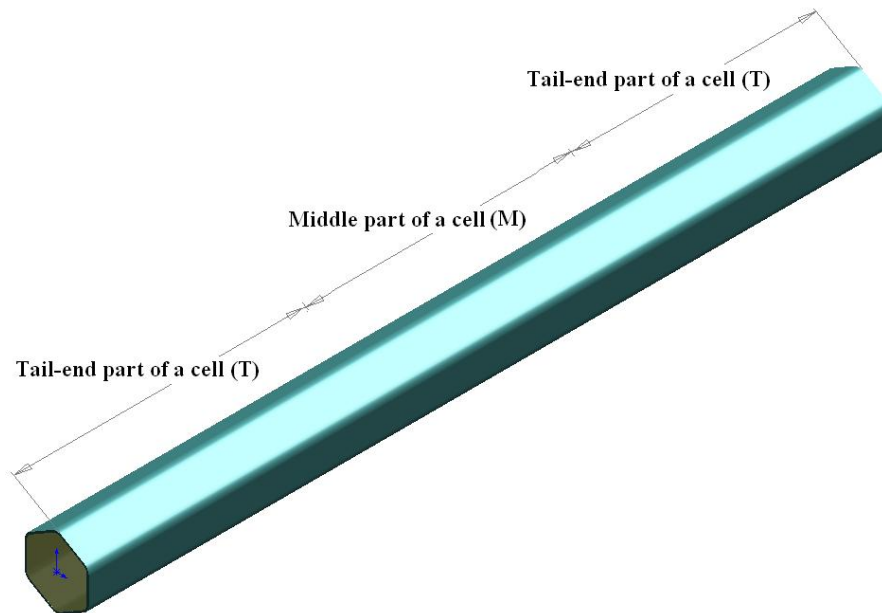


Figure 4-31: Two important sections in tracking Microtubules orientation are Middle part of an individual cell (M) and Tail end sides of the cell (T).

Our investigation showed that in general the Middle portion (M) of a cell tends to have bigger angles of Microtubules with respect to the cell axis after bending load is applied for around six to seven hours; while Tail-end portion (T) of the same cell tends to have a smaller angles of Microtubules direction relative to the main axis of the cell. Again, this may not be the case for each individual cell, but the general trend of the majority of the cells displays such behavior.

Below are histograms showing a summary of the results on the overall length of a cell gathered for control sample and bent samples. The reader should keep in mind that immediately following when cells are first bent, and before Microtubules have a chance to re-orient themselves, Microtubule orientation relative to the main cell axis might be small, as was shown in Figure B-2 (Appendix B). Keeping this in mind, Microtubule re-

orientation for bent samples, as displayed in all following figures (up to the end of this chapter) is quite significant.

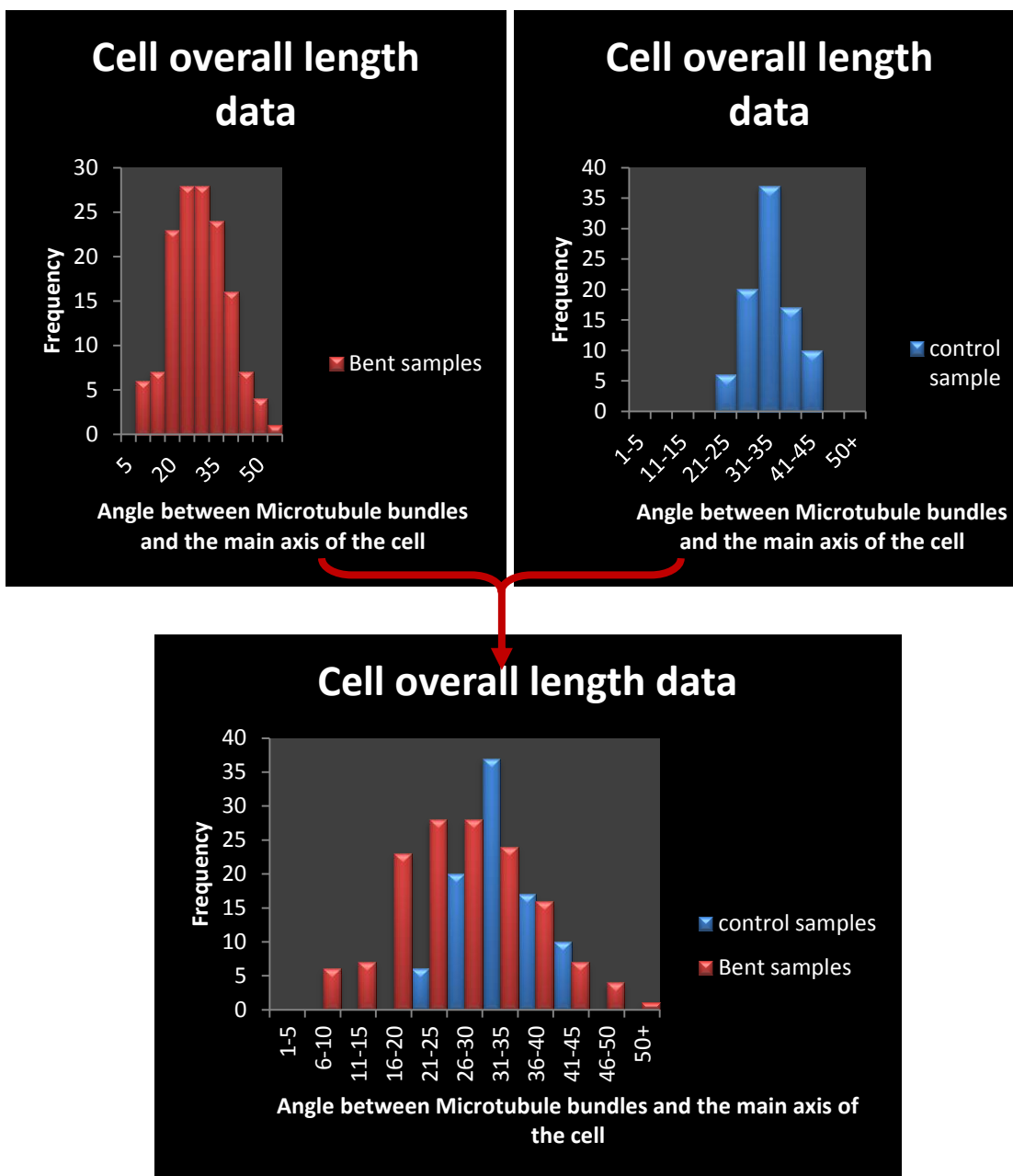


Figure 4-32: Microtubule orientations with respect to the cell's main axis are compared for control samples and bent samples for the overall length of an individual cell

To have a better comparison, based on what is shown in Figure 4-31, let's consider the middle portion "M" and Tail-end portion "T" of a cell. In the "T" section of a cell for a bent sample, Microtubules generally tend to have a smaller angle (relative to the cell main axis) when compared to a control sample; while in "M" section of a cell, Microtubules for a bent sample generally tend to have a larger angle when compared to a control sample. The next figure displays this phenomenon.

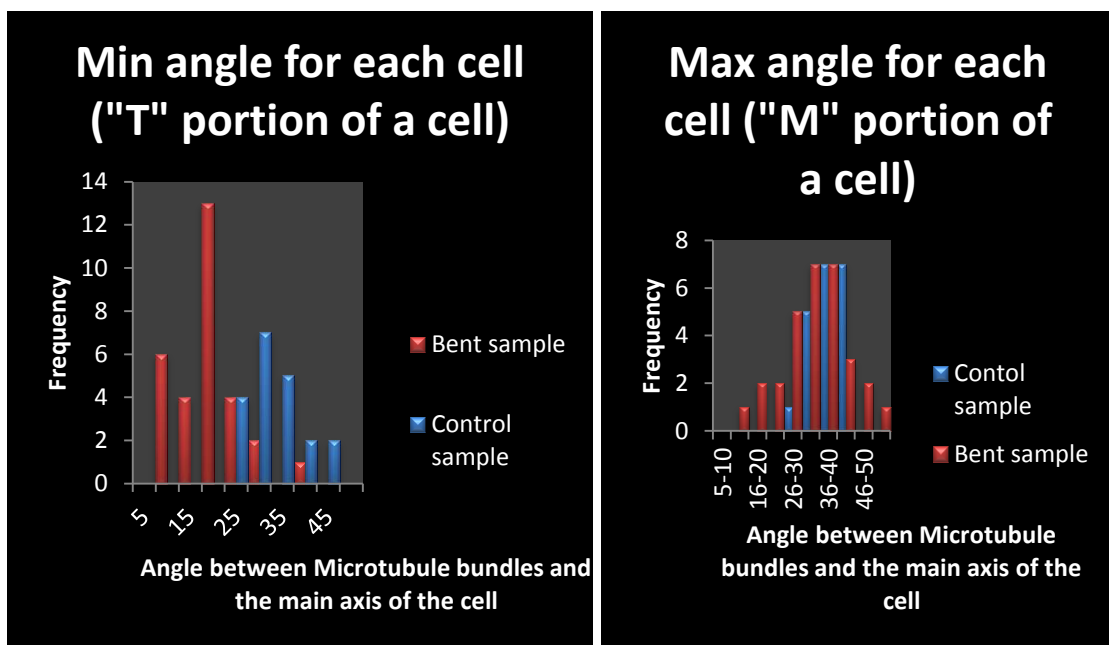


Figure 4-33: Microtubules orientations with respect to the cell's main axis are compared for control samples and bent samples for Middle "M" and Tail-end "T" portion of an individual cell

From the above, and based on what is subsequently shown in Chapter 5 (in Tables 5-3 and 5-5), we can conclude that indeed Microtubules do move to try to orient themselves *closer to* principal stress trajectories when a *large mechanical load* is applied. Chapter 5 will show that principal stress trajectories are generally more transverse (90 degrees in the previous figure) to the cell main axis near the middle of the cell, and part

way between transverse and longitudinal (longitudinal is zero degrees in the previous figure) to the cell main axis near the tail end of cell. Following this, we can see from the previous figure that for both the middle of the cell (with larger more transverse angles) and end of the cell (with smaller more longitudinal angles), Microtubules are orienting themselves closer to principal stress trajectories.

Radius of curvature is also an excellent parameter to measure while investigating Microtubules orientation, and this measurement was obtained as illustrated in Figure 4-22 using the average of three radii of curvature (for the inside, middle and outside of the cell). Since measuring the force or bending load applied to the very delicate and fragile Arabidopsis root is very difficult, measuring radius of curvature of the bent root is best. Figure 4-34 shows the radius of curvature of a cell versus Microtubules average angle in the area of focus. These diagrams are plotted once for the overall length of a cell, then for the Middle “M” portion of a cell and finally for the Tail-end “T” portion of a cell.

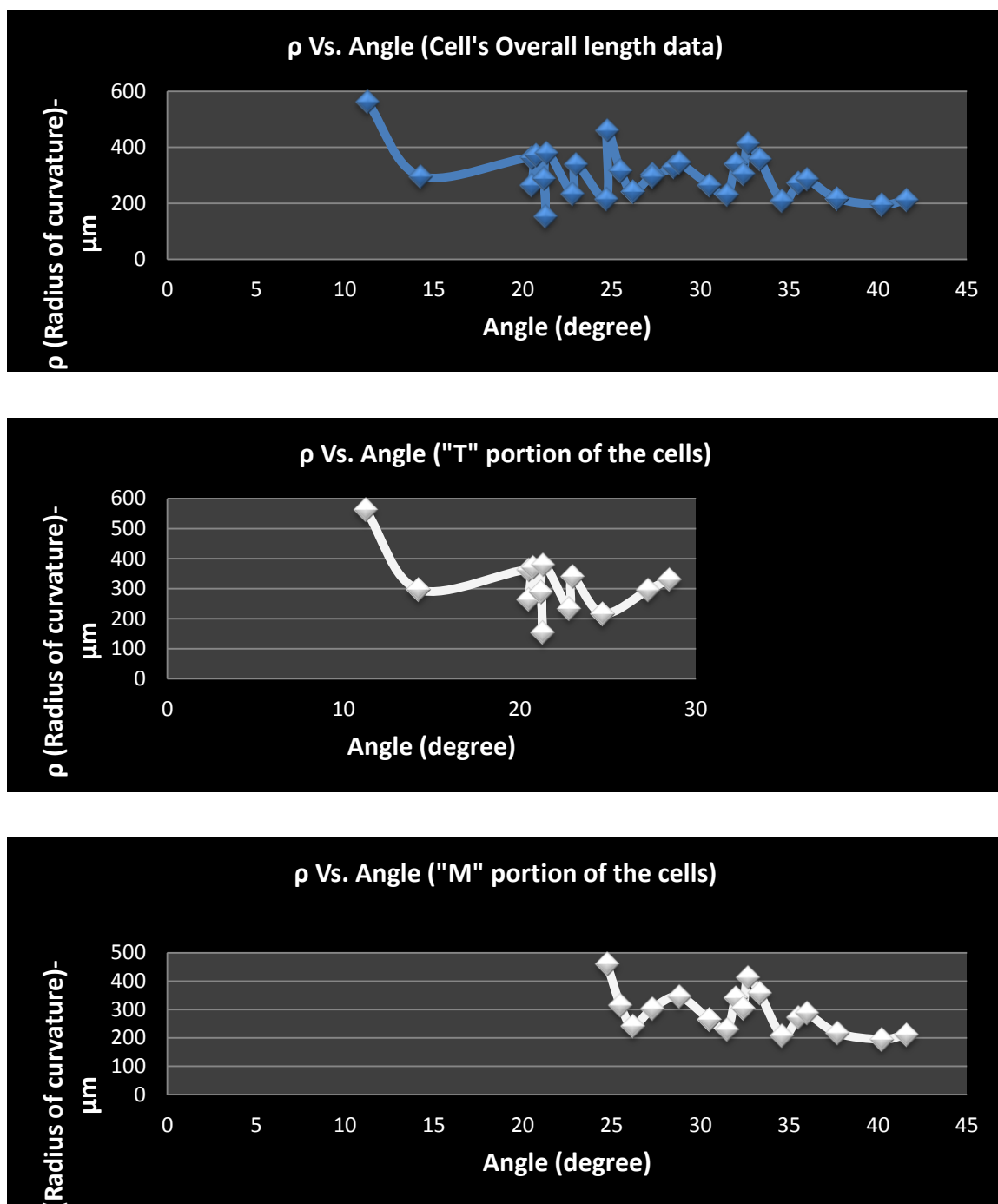


Figure 4-34: Microtubules average angle relative to the main axis of the cell versus the radius of curvature of the same portion of the cell are compared for each individual cell. This comparison is made for the entire length of a cell, and also for Middle "M" and Tail-end "T" portion of a cell.

It is obvious from the data plots in the previous figure that radius of curvature has an inverse relation with the Microtubules orientation. This means that in the Tail-end “T” portion of each cell where radius of curvature is higher, Microtubules hold a smaller angle relative to the cell main axis; and in the Middle “M” portion of a cell where the cell seems to be bent more and having a smaller radius of curvature, Microtubules show a larger angle relative to the cell main axis.

The plots in Figure 4-34 also tend to agree with the statement that Microtubules do move to try to orient themselves *closer to* maximum tensile stress direction when a *large mechanical load* is applied (this is also based on what will be subsequently shown in Chapter 5, in Table 5-3 and 5-5). In Chapter 5 it will be shown that principal stress direction near the middle of the cell are generally more transverse, and such transverse principal stress directions are less the case near the cell ends (where angles are relatively more longitudinal). Correspondingly, Figure 4-34, Microtubule orientations are more transverse to the cell (closer to 90 degrees) near the middle (“M” portions) and less transverse for the end (“T” portions), which tends to suggest Microtubule alignment closer to principal stresses based on what will be shown in Chapter 5.

The effect of Microtubule positional location of a cell in a bent root (located in the inner surface or outer surface of the bent root) was also studied. This is shown in the following figure for the inner and outer surface (of curvature) for the cell.

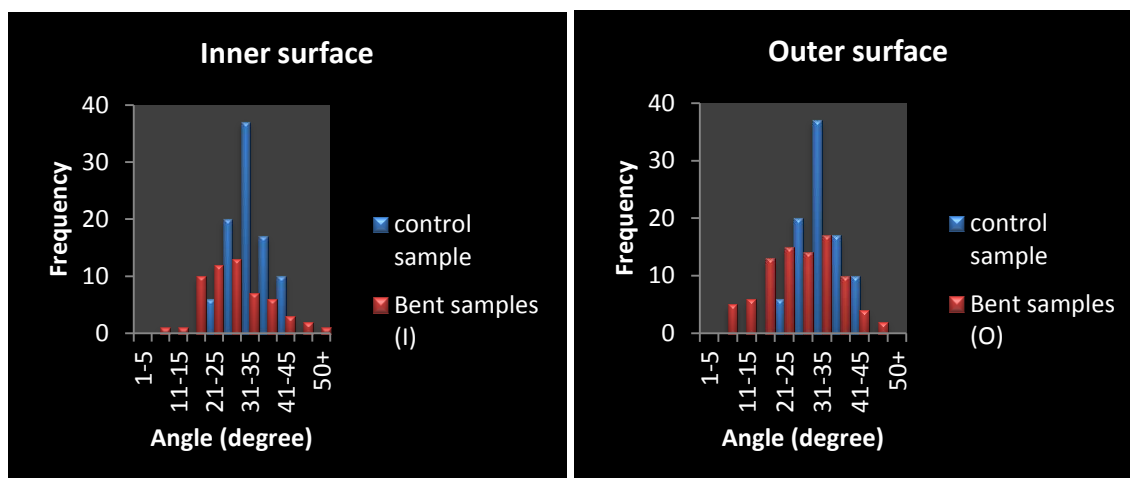


Figure 4-35: The influence of cell's positional location in a bent root (inner surface and outer surface of curvature) is studied.

If we assume a root is like a beam, then the outer surface of a bent root is the area outward from the neutral axis and inner surface will be the inward direction (towards the center of curvature) with respect to the neutral axis of the beam. As illustrated in Figure 4-35, there isn't a significant difference between the Microtubule orientations in the cells located in the outer surface or inner surface of the bent root.

4.5 Experimental Sources of Error

The main sources of error for the experimentation are discussed here. These sources of error were largely mitigated due to carefully carried out experimentation.

One of the main sources of error was the fact that since the experimentation was carried out with biological specimens, none of the specimens were identical, and all had their own somewhat unique micro structure. This introduces some variation into the experimental results.

Another possible source of error was based on the nature of the bending load that was applied. Care had to be taken to make sure that the bending was all in-plane (i.e. with limited torque).

A last source of error has to do with the fact that bending a root can cause growth changes (such as causing root hairs to appear). Specimens with root hairs often had to be discarded because the microtubule pattern was changed drastically in many of these cases. Removing such specimens from the sample set may affect overall results. There is no easy way to mitigate the experimental challenge caused by root hair appearance; when dealing with a living tissue, sometimes not all experimental variables can be controlled as desired as there is always some variability in living tissue behavior.

4.6 Chapter Conclusion

In this chapter, the manner in which microtubules change orientation in response to loading (specifically, bending loading) was the principal focus. In the next chapter (Chapter 5) the experiments carried out in this chapter will be simulated and studied by finite element simulation, and the results of such simulation will be compared against the experiments. It will be shown in Chapter 5 that microtubules orientations (as detailed in the experimental results in the current chapter) are related to the principal stress directions (based on finite element simulations in Chapter 5).

Chapter Five: Microtubule Orientation and Principal Stress Directions

In this chapter, the empirical experiments carried out on Arabidopsis root by applying a bending moment (as discussed in Chapter 4) are analyzed and verified by means of finite element simulation in the Ansys software environment. Firstly in the chapter, challenges and shortcomings in the available data for creating such simulation models will be discussed first, followed by an example demonstrating details of an experiment carried out to determine mechanical properties of the plant tissue. Subsequent to the finite element modeling completed in Ansys, results of such modeling for different geometrical or mechanical properties will be discussed. Finally, these results will be compared to those achieved from physical experimentation (Chapter 4) and the conclusion from such comparison will be presented.

5.1 Some bio-science replication challenges for engineering software

There are various challenges when it comes to simulating a plant tissue in a finite element engineering software like Ansys. The main challenge is that there isn't accurate data available in regards to the material properties (e.g. modulus of elasticity, Poisson's ratio) and also material behavior (e.g. linear or non-linear) of such tissue. These properties tend to vary for different segments of the specimens examined, so any numerical properties presented are estimates. Material properties can also vary widely for different specimens. A full accounting of material properties for each specimen is not currently possible with the available technology, and the available literature does not have any in depth analysis techniques to determine more accurate values of material parameters. Consequently, there are likely some unavoidable inaccuracies for any

simulation of plant response to stress. Verifying that the simulation is behaving in a manner such as to correspond with experimentation is one method that was used to mitigate the effect of such inaccuracies. In the coming decades, more studies will need to be conducted so that more relevant literature can be generated in order to assist with improving the accuracy of model parameters.

In addition to challenges posed by finding suitable material parameters, simulating some real world loading conditions (e.g. the cantilever support type or the force type) as precisely as possible is rather unfeasible and time consuming. A smaller segment of the Arabidopsis root was selected to make it possible to run the simulation in a timely manner, and also because parameters to do a more thorough analysis do not exist in the literature (such as parameters defining cell to cell interaction, Microtubule to cell interaction etc.). In this thesis, a single cell of the Arabidopsis root was simulated with Ansys software. Following is a brief description of one technique utilized to overcome a challenge in determining the mechanical properties (modulus of elasticity) of a plant tissue in cellular level.

5.1.1 Modulus of elasticity of the cell wall

In this section, a creative approach employed by Milani et al [110] to identify modulus of elasticity of the cell wall in an Arabidopsis Shoot Apical Meristem (SAM) is introduced; the author of this thesis was a second author for this work. The paper established a protocol to measure local mechanical properties at the SAM by utilizing Atomic Force Microscopy (AFM).

Atomic force microscopy utilizes a scanning probe microscopy technique which is very high in resolution (nanometer scale). Such AFM is composed of a silicon

cantilever beam with a pyramid shaped probe at its free end that directly touches the plant specimen surface as shown in Figure 5-1.

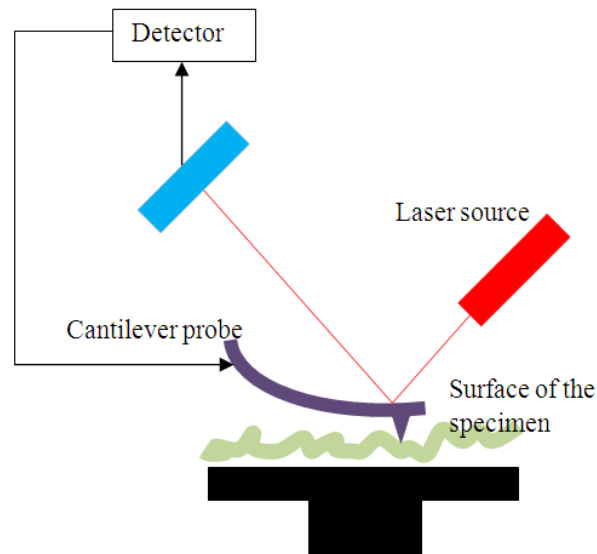


Figure 5-1: Function of Atomic Force Microscopy (AFM)

Once the probe comes in contact with the surface of the sample it deflects and such deflection is sensed and measured by a laser beam. The cantilever is made of piezoelectric material, which enables controlling the displacement of the cantilever (away from the tip) and the laser deflection measurement yields on the amount of bending of the cantilever. By probing the surface in multiple points the force-indentation curve for the surface of the sample can be derived. After reviewing the observations, it is concluded that the applied force (F) is proportional (based on proportionality constant k) to the square of indentation (Δ) which is called a “Pyramidal contact”: $F = k \Delta^2$. Modulus of elasticity was then defined as:

$$E = 0.75 (1 - \nu^2) k / \tan(\theta)$$

Equation 5-1

Where ν is the Poisson ratio, and $\theta = 17.5^\circ$ is the angle of the pyramidal tip of the cantilever beam [110]. Equation 5-1 originates from Hertzian theory of contact and more details about it can be found in “contact mechanics” references.

In Milani’s research (of which the author of this thesis was a part), the force-displacement curve acquired by means of AFM had a parabolic shape as shown in Figure 5-2 [110].

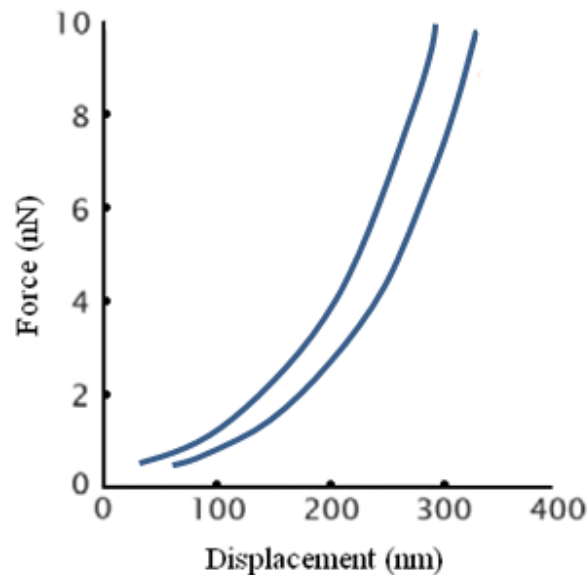


Figure 5-2: Force-displacement curve obtained from the AFM performed on the SAM of an Arabidopsis plant. The axes are in nm and nN. (taken from [110])

The radius of the cantilever tip was around 10–40 nm, while the diameter of the cells are in range of 5–10 μm . The modulus of elasticity (E) of the cell wall can be determined by and employing Equation 5-1. It was assumed the cell wall had linear orthotropic properties with $E_x = E_y = 4 E_z$ while z is the direction normal to the cell

wall. Such an assumption was based on the orientation of cellulose microfibrils, which makes the wall softer in the z direction. This was confirmed by generating the model in Ansys software and arbitrarily choosing E_x , E_y and E_z in a way that the correct corresponding force-displacement values are achieved. The element type selected for such Ansys analysis was a SOLID45 type. SOLID45 is appropriate for 3D modeling of solid materials. This element is determined by 8 nodes and has 3 DOF at each of these nodes. As well, this element has plasticity, large deflection and large strain modeling abilities.

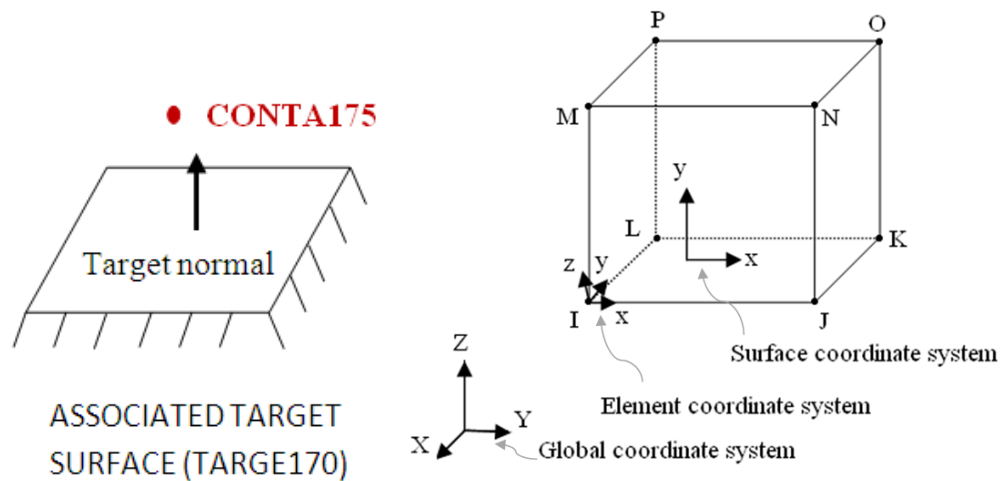


Figure 5-3: Left- TARGE170 and CONTA175 right- SOLID45 geometry and coordinate system

TARGE170 and CONTA175 elements were also utilized to simulate the contact between the AFM cantilever tip and the cell wall surface. The contact elements are (in the simulation) placed on top of the solid element (SOLID45) defining the boundaries of the deformable object. The target surface is defined by target elements (TARGE170) and is paired with its related contact surface (CONTA175). Any translational or rotational

displacement can be imposed on these two elements, which make it possible to model most complex deformations.

Such Ansys simulation analysis has been performed multiple times for different parameters (cell geometry or material) and Figure 5-4 is just a sample representing one of these many simulations.

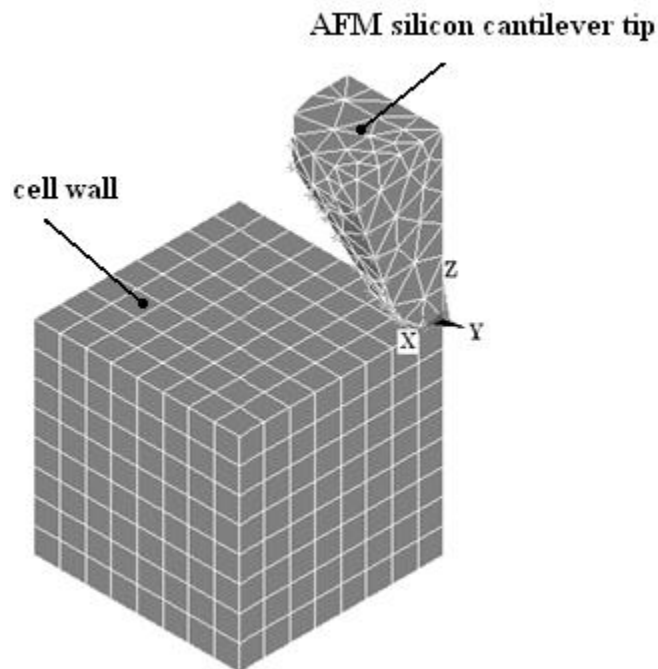


Figure 5-4: One quarter model of the AFM cantilever beam touching the cell wall

As shown in the previous figure, only one quarter of the whole system was modeled in Ansys and symmetrical boundary conditions were then applied to ZX and ZY planes.

The model illustrated in Figure 5-4 had these properties: cell wall size of 150 nm, cell wall rectangular mesh size of 18.75 nm, Poisson's ratio of $\nu = 0.4$ and shear modulus $G_s = 3$ Mpa. By assigning a linear orthotropic material with $E_x = E_y = 4$ MPa and

$E_z = 1$ Mpa, the displacement and stress values for a concentrated force value of 5 nN (on the cantilever) will be as follow: $U_z = -70.997$ nm, $\sigma_x = [-6.698, 2.795]$, $\sigma_y = [-4.276, 1.929]$ and $\sigma_z = [-4.162, 0.644]$ MPa (these values are taken from the simulation in Ansys software).

Such analysis was repeated multiple times for a cell wall size of 250 and 500 nm for a variety of material properties. The results for different sizes of the cell wall were almost analogous, thus confirming that there is no large influence caused by the cell wall boundaries (e.g. stress concentration) affecting the outcome of analysis. Table 5-1 shows one of these force-displacement values.

Table 5-1: Force-Displacement values obtained from a finite element analysis simulating an AFM experiment on a cell wall

Model name:	AFM 31
Material properties:	Linear orthotropic
	$E_{x,y}=4$ MPa, $E_z=1$ MPa $\nu=0.4$, $G_s=3$ MPa
Cell wall size	250 nm
Force (nN)	Displacement (nm)
1	16.606
2	28.929
3	48.283
4	61.654
5	70.938
6	87.833
7	104.613
8	118.806
9	N/A
10	N/A
11	N/A
12	N/A
13	N/A
14	N/A
15	N/A
16	N/A
17	N/A

As observed in Table 5-1, by applying a vertical force greater than 8 nN (which is equivalent of a displacement greater than 118.806nm), the Ansys simulation becomes unstable and does not converge any more.

Figure 5-5 demonstrates the force-displacement results achieved from the finite element analysis performed using Ansys software for a variety of cell wall's modulus of elasticity combinations along X, Y and Z axes. These combinations are shown with labels

as “Isotropic” and “Orthotropic Case 1 to 6” in this figure, whose results are also detailed in Table 5-2.

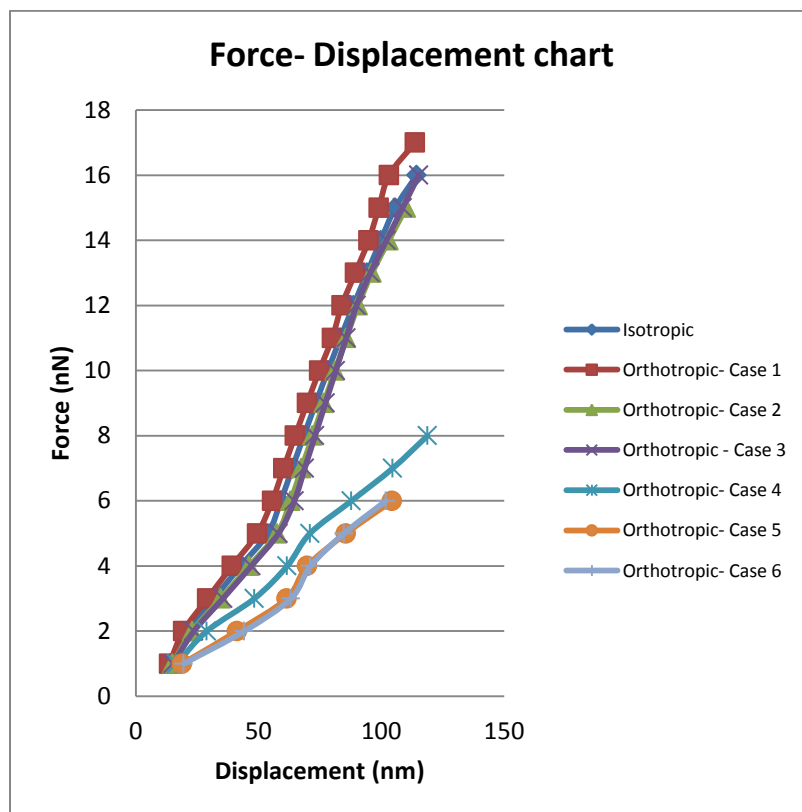


Figure 5-5: Force-displacement outcome of Ansys simulation for the AFM experiment on the plant cell wall with diverse material properties detailed in Table 5-2.

Table 5-2: Material properties of the cell wall for each simulation shown in Figure 5-5

Isotropic:	Linear isotropic, $E=4$ Mpa, $\nu=0.4$, $G_s=3$ Mpa
Orthotropic- Case 1	Linear orthotropic, $E_{x,y}=4$ Mpa, $E_z=3$ Mpa, $\nu=0.4$, $G_s=3$ Mpa
Orthotropic- Case 2	Linear orthotropic, $E_{x,y}=4$ Mpa, $E_z=8$ Mpa, $\nu=0.4$, $G_s=3$ Mpa
Orthotropic- Case 3	Linear orthotropic, $E_{x,y}=4$ Mpa, $E_z=16$ Mpa, $\nu=0.4$, $G_s=3$ Mpa
Orthotropic- Case 4	Linear orthotropic, $E_{x,y}=4$ Mpa, $E_z=1$ Mpa, $\nu=0.4$, $G_s=3$ Mpa
Orthotropic- Case 5	Linear orthotropic, $E_x=4$ Mpa, $E_y=8$ Mpa, $E_z=1$ Mpa, $\nu=0.4$, $G_s=3$ Mpa
Orthotropic- Case 6	Linear orthotropic, $E_x=4$ Mpa, $E_y=16$ Mpa, $E_z=1$ Mpa, $\nu=0.4$, $G_s=3$ Mpa

One of the features in the above analysis performed in Ansys software is that not every simulation with any input entry will converge. For example most of the simulations performed with Poisson's ratio of $\nu=0.3$ did not converge; suggesting that $\nu=0.4$ is possibly closer to the cell's Poisson's ratio in real world. Lack of convergence for $\nu=0.3$ does not imply nonexistence of a solution for this problem; instead it means that with the current assumptions (e.g. material properties and behavior) the program doesn't converge and it might possibly converge by changing the assumptions. As well, some combinations of modulus of elasticity in X, Y and Z direction caused the stress- strain matrix of material to no longer maintain the positive definite condition.

The above results are comparable with the experimental tests results achieved by Milani et al. [110]. In the experimental test, Milani et al. obtained curves with indentation up to around 400nm (Figure 5-2); however the analysis was only considered up to around 100nm indentation because the quadratic behavior of force-displacement curves was observed only up to about 100nm. On the other hand, the finite element modeling performed in Ansys becomes very unstable and stops converging just around same indentation value of 100nm. The reason is not really clear why the program doesn't converge after this point, but likely it is related to some assumptions that the model is based on (like material behavior and properties) which is due to lack of more precise information than what currently exists in the literature. Excessive deformation of some of the elements could possibly be another reason behind non-converging program.

As mentioned earlier the values of $E_x = E_y = 4 E_z$ were selected since they are in better agreement with empirical results and knowing the fact that the natural orientation of cellulose microfibrils causes the cell wall to be softer along the z direction.

Miliani et al. also realized that the outer cell wall was quite stiffer at the apex of the meristem (around 5 MPa), than the side of the meristem (around 1.5 MPa). This means that the meristem surface does not have a “unique single” value as modulus of elasticity, and instead there is a gradient of modulus of elasticity on this surface.

5.2 Arabidopsis root cell deformation simulation in Ansys under the mechanical bending load

To analyze the re-orientation of Microtubules as per the empirical observations explained in Chapter 4, it is essential to simulate Arabidopsis root cell in a finite element software like Ansys, and replicate the same loading system. For this purpose a single

epidermal cell was selected with fraction of two other cells in its vicinity sharing a cell wall as illustrated in Figure 5-6. The rationale for partially modeling the two neighboring cells adjacent to this cell is to diminish the effects of stress concentration ensued from the cantilever's rigid support at one end of the beam, and the concentrated force on the other end. Symmetrical boundary conditions were applied to the YZ plane as shown in this figure.

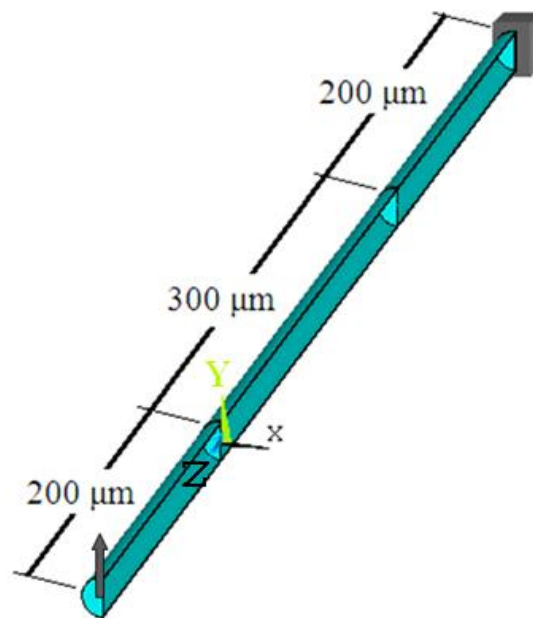


Figure 5-6: Arabidopsis root cell simulated with Ansys software. The diameter of the cell and the wall thickness were considered to be 20 μm and 1 μm respectively.

As mentioned earlier, the whole cross section of the Arabidopsis root was not modeled as modeling all the cell walls' interactions with one another is very tedious and appropriate parameters for this do not exist in the literature. As well, the interaction of other materials (such as the interaction between Microtubules and the cell wall) is not well understood, and appropriate parameters for a model don't exist in the literature.

Another factor is computer simulation time, which for even single cell models is quite long (often few hours).

SOLID185 was utilized for Ansys modeling since it has large deflection and large strain modeling abilities. This element is identified with 8 nodes having 3 DOF at each of these nodes, which is appropriate for 3D modeling. It is necessary to mention that using SHELL element to perform such analysis in Ansys will result in failure of all models in the earlier steps of large deformation simulation; Even though some SHELL elements (e.g. SHELL 181) could tolerate “large strain nonlinear applications”.

Mechanical properties of the cell wall were considered to be linear isotropic with modulus of elasticity of $E = 4 \text{ Mpa}$ and Poisson’s ratio of $\nu=0.4$ (based on work presented at the beginning of this chapter for the Arabidopsis SAM analysis, which is the closest available in the literature for the Arabidopsis RAM analysis outlined in this section).

The turgor pressure of the cell was considered to be 0.1 Mpa being applied in outward direction on all the interior cell walls. Some of the material properties selected for such simulations in this section (like turgor pressure) are based on those found in literature [91, 111, 112]. The analyzed cell had a length of $300 \text{ }\mu\text{m}$, diameter of $20 \text{ }\mu\text{m}$ with the wall thickness of $1 \text{ }\mu\text{m}$. The two neighboring cells for the simulation had $200 \text{ }\mu\text{m}$ length with the same diameter and wall thickness. The mesh type was considered to be a cuboid type all along the cell wall except for the common shared wall between each two cells, which was of tetrahedron type as shown in Figure 5-7.

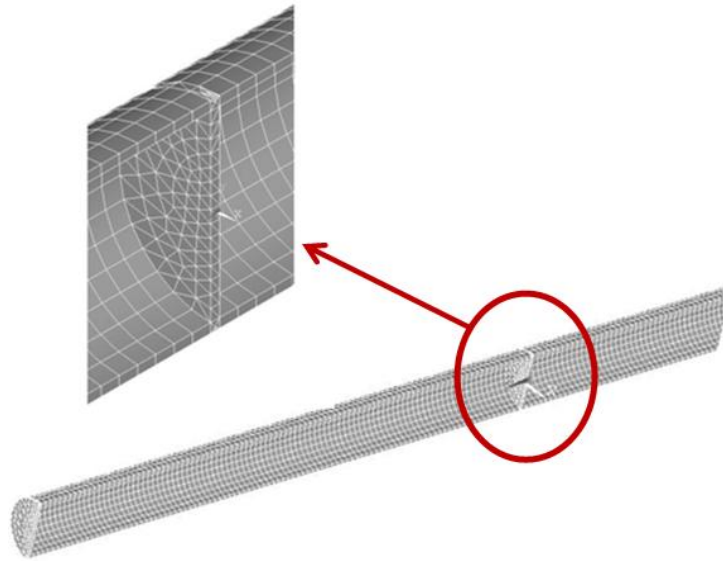


Figure 5-7: Mesh style of the cell walls

Since the Arabidopsis root is experiencing a large bending deformation in the real world, such load in Ansys environment had to be applied to the root cell gradually to avoid any sudden disruption to the model. For this purpose the “Large Displacement Static” option has to be set properly with the number of “substeps” for the nonlinear solution. Once these “substeps” are set properly the status of the “Graphical Solution Tracking” plot will be similar to Figure 5-8. On average iteration numbers required for the problem to converge was around 300 to 400 iterations.

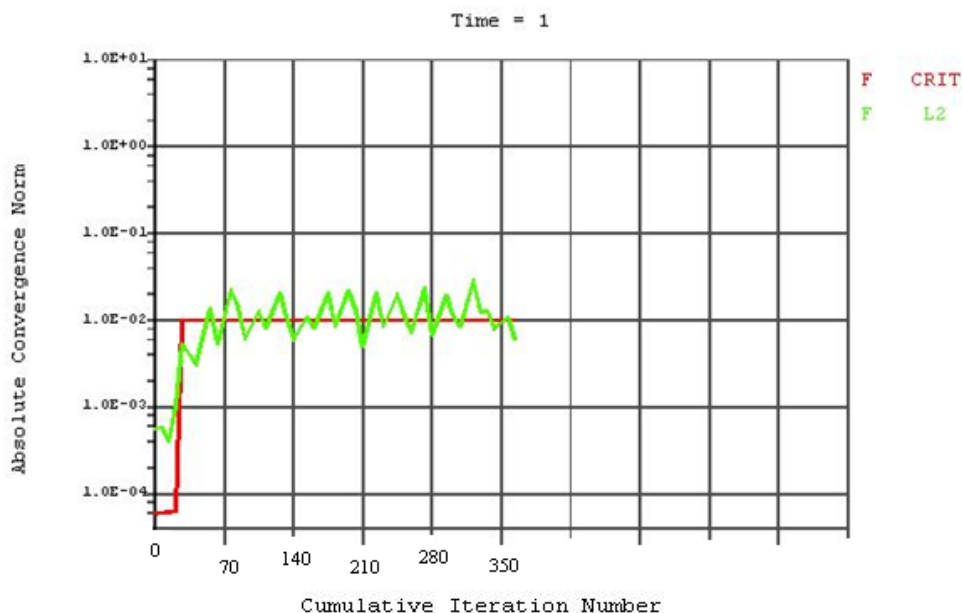


Figure 5-8: Solution convergence tracking in Ansys software. Most of the simulations converged after a couple of hundreds of iterations at most.

The “Time” title of the above chart represents the value of the last calculated iteration which in this case was selected to be 1. Changing this number (i.e. to 10 or 100) will not change the length of the simulation and will just scale it. The x-axis “Cumulative Iteration Number” shows the number of iterations for the program to converge. Ansys’s solver for such non-linear analysis employs an iterative technique (e.g. Newton-Raphson) to find the results. The more non-linear a program is, the larger number of iterations will be required with a lengthier graph in x direction. The y-axis “Absolute Convergence Norm” label implies non-normalized values having relevant units depending on the type of the analysis (in this case force). The “F CRIT” curve is associated to the convergence criteria for the force value. This value is defined as being equal to “VALUE × TOLER”; where “VALUE” is the square root of the sum of the squares of the applied forces, or a

parameter known as “MINREF” (with a default value of 0.001), whichever of the two is larger. The “TOLER” default value is set to 0.5% of the applied loads. The “F L2” curve specifies the “L2 Vector Norm” of the applied forces. L2 Vector Norm is the square root of the sum of the squares of the “force imbalance” for all degree of freedoms. In simpler words, it is the square root of the sum of the squares of the difference between the internal forces at a specific point and the external forces in that point.

Figure 5-9 illustrates the model created in Ansys with the abovementioned specifications (e.g. material properties) having a displacement value of $U_y = 150 \mu\text{m}$ and $U_z = -100 \mu\text{m}$.

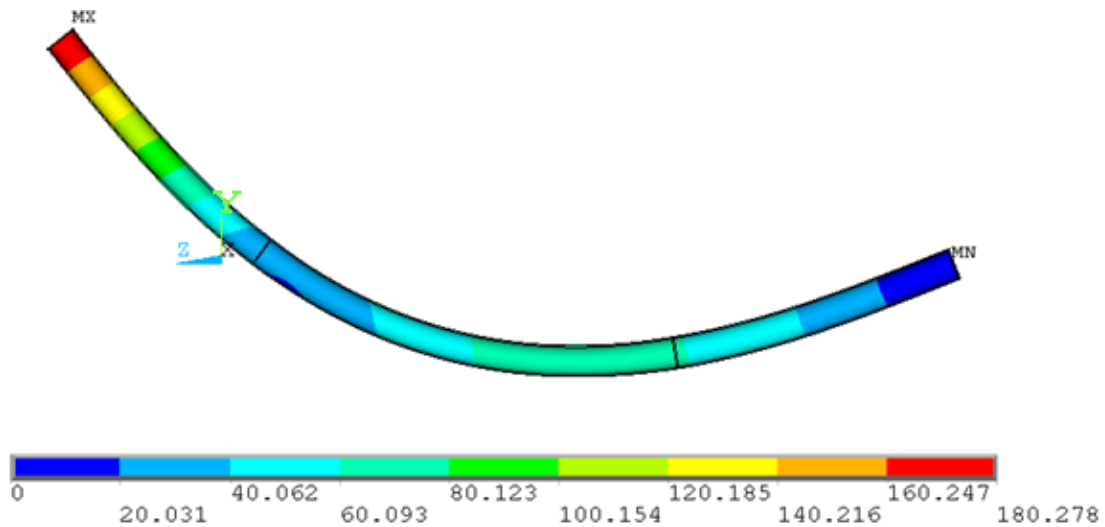


Figure 5-9: Displacement vector sum (color coded) of a cell modeled in Ansys having displacement magnitude of $U_y = 150 \mu\text{m}$ and $U_z = -100 \mu\text{m}$.

5.2.1 Principal directions in the simulated *Arabidopsis* root cell

In this section, the results of stress analysis of the simulation performed in previous section (5.2) will be studied. Three different sections of the root cell were of main interest: sections A, B and C as shown in Figure 5-10.

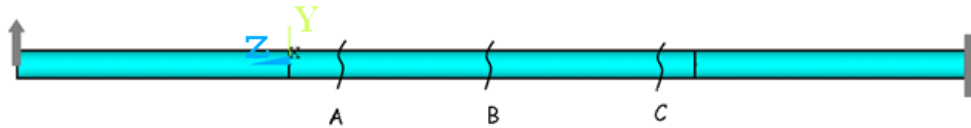


Figure 5-10: Sections A, B and C of the simulated cell being studied and compared to one another.

For each of these sections, the maximum value of the 1st principal stress (σ_1) was obtained from the stress analysis performed in Ansys, and the associated principal direction was achieved based on the Equation 3-3. There is a slight transformation of coordinate axes so this equation will be usable. By transforming the *local* coordinate system at each node from (x,y,z) to (y,z,x) this equation will be revised as follow:

$$\theta'_p = \frac{1}{2}(\text{tg}^{-1}[2\tau_{yz}/(\sigma_y - \sigma_z)]) \quad \text{Equation 5-2}$$

Note that θ'_p is the angle that the principal direction makes with the *local* Y-axis at each node, as shown in Figure 5-11. The Y-axis shown in Figures 5-6, 5-9 and 5-10 is *global* Y axis and should not be confused with the *local* coordinate system. Angle θ''_p will be defined as $\theta''_p = 90 \pm \theta'_p$ and is the angle that principal direction makes with the *local* Z-axis. The Z-axis shown in Figures 5-6, 5-9 and 5-10 is the *global* Z axis and should not be confused with the *local* coordinate system:

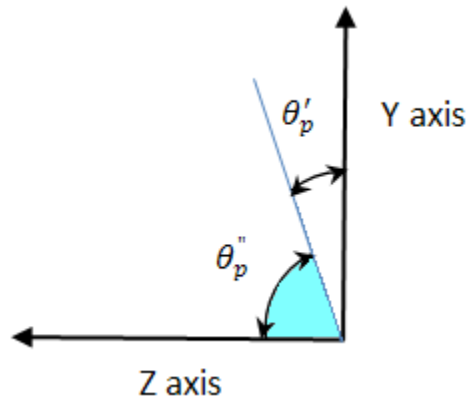


Figure 5-11: Principal stress direction in the transformed *local* coordinate system of each node

By extracting the maximum values of principal stress (σ_1) (which is tensile) of the nodes in section A, B and C of Figure 5-10 and Figure 5-12 and calculating θ'_p from Equation 5-2, these following values will be achieved:

$$\theta'_p|_A = 42.260, \theta'_p|_B = -11.6858 \text{ and } \theta'_p|_C = 23.01 \text{ degrees}$$

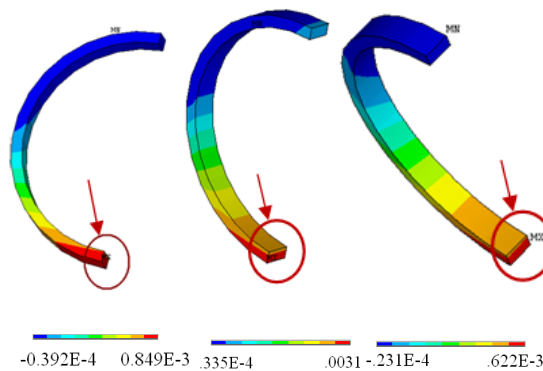


Figure 5-12: Maximum value of the principal stress (tensile) in sections A, B and C (left to right) detailed in Table 5-3

Details of the Ansys analysis outcome are as follows:

Table 5-3: Nodal stress values along with principal stress direction in three different cross sections of the root cell ($U_y=150 \mu\text{m}$ and $U_z=-100 \mu\text{m}$)

	Max. principal stress σ_1 (Mpa) (tensile)	NODE Number	σ_y (Mpa)	σ_z (Mpa)	τ_{yz} (Mpa)	θ_p' (degree)	θ_p'' (degree)
Section A	0.84490	8187	0.47703	0.39938	0.40469	42.26	47.74
Section B	3.0996	4757	0.15745	2.9737	0.60852	-11.69	78.31
Section C	0.61076	11531	0.10261	0.51902	-0.21568	23.01	66.99

The compressive principal stresses as well as maximum shear stresses directions can be calculated from Table 5-3 knowing that their planes form 90 and 45 degree angles with the tensile stresses planes.

Such analysis was performed another time for same cross sections A to C, but this time for the principal directions of the “average” values of the stresses at the nodes in each of these cross sections. As shown in Figure 5-13, the nodes used for averaging are located on the outer circumferential border of the root cross section.

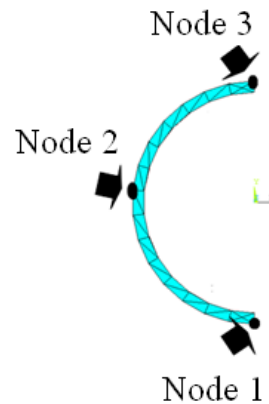


Figure 5-13: Average values to find principal stress directions were calculated based on the nodes located on the perimeter of each cross section in the root cell

Results of such analysis are summarized in Table 5-4 below.

Table 5-4: Principal stress directions of the *average* value of stress ($U_y=150 \mu\text{m}$ and $U_z=-100 \mu\text{m}$)

	$\sigma_{y_{avg}}$ (Mpa)	$\sigma_{z_{avg}}$ (Mpa)	$\tau_{yz_{avg}}$ (Mpa)	$\theta'_{p_{avg}}$ (degree)	$\theta''_{p_{avg}}$ (degree)
Section A	-0.06294	-0.05650	-0.05754	43.40	46.6
Section B	0.03175	-0.07720	-0.15886	-35.54	54.46
Section C	0.03479	-0.12975	-0.011052	-3.83	76.17

Values of $\sigma_{y_{avg}}$, $\sigma_{z_{avg}}$ and $\tau_{yz_{avg}}$ components in Table 5-4 are calculated based on the associated average values of these components in Node 1 to 3 as illustrated in Figure 5-13. For example $\sigma_{y_{avg}} = \frac{1}{3}(\sigma_{y_{Node1}} + \sigma_{y_{Node2}} + \sigma_{y_{Node3}})$. Increasing the number of

nodes in each cross section to have a better estimate of the average values of stress components did not considerably affect the results in Table 5-4.

The same analysis was replicated again for different bending loads. As mentioned before, such bending was applied by displacement load and the results were consistent with the above simulation outcome. This is summarized in Table 5-5 and Table 5-6 for displacement values of $\Delta y = 170 \mu\text{m}$, $\Delta z = -140 \mu\text{m}$ and $\Delta y = 170 \mu\text{m}$, $\Delta z = -170 \mu\text{m}$ respectively. Table 5-5 is analogous to Table 5-3, where one nodal value of stress was examined, and Table 5-6 is analogous to Table 5-4 where an average of three nodes were used at each cross section to evaluate average stress.

Table 5-5: Stress components and principal stress value and direction in three different cross sections of the root cell for two different models with two different displacements

$\Delta y=170$ $\Delta z=-140 \mu\text{m}$	Max. principal stress σ_1 (Mpa) (tensile)	σ_y (Mpa)	σ_z (Mpa)	τ_{yz} (Mpa)	θ'_p (degree)	θ''_p (degree)
Section A	4.2644	1.8720	2.3854	2.1195	-41.55	48.45
Section B	4.0515	-0.07519	4.0445	0.16229	-2.25	87.75
Section C	1.1126	0.11715	1.0317	-0.28359	15.90	74.1

$\Delta y=170$ $\Delta z=-170 \mu\text{m}$	Max. principal stress σ_1 (Mpa) (tensile)	σ_y (Mpa)	σ_z (Mpa)	τ_{yz} (Mpa)	θ'_p (degree)	θ''_p (degree)
Section A	3.3470E	1.8753	1.4312	1.6787	41.23	48.77
Section B	4.4143	-0.07658	4.3930	0.30622	-3.90	86.1
Section C	3.2332	0.14822	3.0843	-0.67607	12.36	77.64

Table 5-6: Principal stress directions of the *average* value of stress evaluated in three different cross sections of the root cell for two different models with two different displacements

$\Delta y=170$ $\Delta z=-140 \mu\text{m}$	$\sigma_{y_{avg}}$ (Mpa)	$\sigma_{z_{avg}}$ (Mpa)	$\tau_{yz_{avg}}$ (Mpa)	$\theta'_{p_{avg}}$ (degree)	$\theta''_{p_{avg}}$ (degree)
Section A	-0.11069	0.04422	-0.89910	24.63	65.37
Section B	0.28025	-0.07691	-0.20061	-24.16	65.84
Section C	0.05310	-0.17298	-0.04829	-11.57	78.43

$\Delta y=170$ $\Delta z=-170 \mu\text{m}$	$\sigma_{y_{avg}}$ (Mpa)	$\sigma_{z_{avg}}$ (Mpa)	$\tau_{yz_{avg}}$ (Mpa)	$\theta'_{p_{avg}}$ (degree)	$\theta''_{p_{avg}}$ (degree)
Section A	-0.07499	0.03164	-0.08543	29.02	60.98
Section B	0.31566	9.1333e-04	-0.19959	-25.87	64.13
Section C	0.04582	-0.11056	-0.03837	-13.07	76.93

Adjusting some parameters such as the mesh type or material properties of the cell (e.g. normal or shear modulus) will not significantly affect the results, and the general trend of the outcomes is analogous to those presented in Table 5-3 to Table 5-6.

5.3 Chapter Conclusion

Comparing the results of such analysis with those achieved from the experiment and as detailed in Chapter 4 of this thesis confirms that the Microtubule direction is certainly influenced by the maximum value of the principal stress (tensile). In Figure 4-33 and 4-34 from Chapter 4, the tendency of Microtubules near the middle of the cell to orient themselves more transversely to the cell main axis relative to Microtubules near the ends of the cell (which were oriented less transversely) is shown from experimentation. What is been shown here (and explained in detail in the next few paragraphs) is that maximum principal stress direction (tensile), which Microtubules tend to align to, is also more transverse near the middle of the cell than at the ends of the cell. Since both Microtubule orientation and maximum principal stress direction are more transverse near the middle of the cell, the experimentation (physical and numerical simulation) confirm that Microtubules move to try to orient themselves closer to principal stress trajectories when a *large mechanical load* is applied. This principal stress is based on a maximum value, which is the maximum in the node, among those in each of the selected cross sections (A, B and C) of the root cell; this root cell is located in the external layer of each of the cross sections as illustrated in Figure 5-12. As detailed in Table 5-3 and Table 5-5, by calculating the direction of the maximum principal stress, it is demonstrated that in section B the maximum principal stress (tensile) is more transverse to the cell main axis (corresponding to an angle closer to zero degrees in Tables 5-3 and 5-5), while in sections A and C the maximum principal stress (tensile) is less transverse to the cell main axis (corresponding to an angle larger than zero degrees in Tables 5-3 and 5-5). This means that in section B of the root cell, the maximum principal

stress (tensile) direction is closer to vertical axis (Y), and in contrast in sections A and C, the maximum principal stress (tensile) direction is comparatively closer to horizontal axis (Z) (refer to Figure 5-11).

As one can notice in Table 5-4 and Table 5-6, which display the results for principal directions for *average* stresses calculated in each cross section of the root cell, principal stress directions do not correspond to the patterns of Microtubules arrangement. This suggests that the principal direction of the *average* stresses cannot explain Microtubules arrangement in the Arabidopsis root cell, the *maximum* principal stress is instead the determining factor

These are very appealing results steering us closer to understanding the main cause of Microtubules re-orientation, which corresponds to most of the former similar research works conducted in this field.

There were two major achievements in the research presented in this thesis. The first one is the fact that mechanical loads do influence the micro-structure of a plant cell by altering the arrangements of Microtubule orientation. Specifically, Microtubules move to try to orient themselves closer to principal stress trajectories when a large mechanical load is applied. The originality in this research is that such kind of research experiment (studying effects of external bending moment on the Microtubules orientation) hasn't been performed on Arabidopsis root previously. The second achievement of the thesis research is based on the fact that Microtubules orientations tend to move closer to the direction of maximum principal stresses in the root cell. It's worthwhile to mention that the mechanism behind such reorientations directed by mechanical forces at sub-cellular level is still not very well recognized in the literature.

Chapter Six: Conclusions and Recommendations

The core of this thesis began in Chapter 2 with a literature review of Wolff's law, Michell theory and expanded concept of Wolff's theorem in plants; this expanded concept involved the role of mechanical forces affecting the reorganization of microtubules in micro-structure of plant cell. The subsequent chapter (Chapter 3) focused on generating engineering frame structures based on Wolff's and Michell's theories. The strength of such structures was analyzed based on the condition and constraints provided. In Chapter 4, some biological terms were first introduced. Afterwards, the materials and methods employed in performing the empirical test on the Arabidopsis root were detailed, followed by the data collection and analysis of the achieved results. Such experimental observations detailed in Chapter 4 were then validated in Chapter 5 by means of finite element simulation in Ansys software.

In conclusion, the main goals of this thesis were achieved. It was shown that mechanical forces definitely affect the microstructure of a plant segment (Arabidopsis root) by changing the microtubules arrangement. This confirms that Wolff's theory has the potential to be applied to plants in addition to bone tissue (which is the focus of the theory). As well, an enhanced structural performance is obtained if Wolff's theory is employed to generate frame structures rather than Michell's theory (as was shown in Chapter 3). The above mentioned results are further outlined in the following section of this thesis.

6.1 Objectives achieved

From all of the aspects highlighted in this research, there were novel objectives that were achieved for the study carried out. These objectives were first summarized in Section 1.1 of the thesis, and will be detailed here.

One of the key objectives was to enhance understanding regarding the Arabidopsis root cell's micro-structural reaction to mechanical forces. In this research, when talking about plants' micro-structural reaction, this refers to the reorientation of microtubules in Arabidopsis root cells (the key structure of study). This task was carried out by means of the empirical tests implemented on the Arabidopsis root. Undertaking tests included changing the gravity direction, and also applying an external bending load to the root to bend the cells and then visualize and record the alterations in microtubule arrangement in certain times by means of a confocal microscope. Details of such empirical tests, visualization and processing of the outcome along with the challenges involved in performing such observations are well detailed in Chapter 4 of the thesis. The main conclusion was that the answer to the question of "do microtubules sense and respond to the mechanical forces?" is "yes". Microtubules in Arabidopsis root cells do sense the mechanical forces and their orientation changes once the external mechanical force was applied; however there was no significant change in the microtubules orientation when the gravity direction was altered (which is consistent with the literature).

Another objective was to expand the application of Wolff's theory from bone micro-structure to plants (Arabidopsis root) micro-structure, and to verify this expanded application. This goal was obtained when the empirical tests (detailed in Chapter 4) were

further analyzed in finite element software. The results of such simulation in Ansys software (detailed in Chapter 5) proved that once the bending force is applied, the dominant orientation of the microtubules is altered to align more closely to the direction of the maximum principal tension stress.

It is essential to mention that the orientation of microtubules in the Arabidopsis root in the newly born cells (free of any external stresses) is along the principal stress direction, aligned with hoop stress in a thin wall cylinder. This was also confirmed by a simple simulation carried out in Ansys. Microtubules in these young cells are orthogonal to the main longitudinal axis of the cell. However, once the cells are fully grown and mature, the microtubules are no longer perpendicular to the longitudinal axis of the cell. Instead, they form a 45 degree angle with the main axis of the cell. This means that maximum principal tension stress direction is influencing microtubule orientation for the growing cells in development, but not for mature cells (for the case of no external load). This can be partly explained by knowing the fact that maximum shear stress makes a 45 degree angle with the main axis of the cell, and microtubules, for some unknown reason, seem to prefer aligning to maximum shear stress direction instead of aligning to maximum normal stress. It is not completely understood in the literature why the orientation of microtubules have such a preference once the root cells grow longer (as they become more mature). Also, the mechanism behind the noted reorientation for the case of applied external load is not very well recognized in the literature.

The third and final main objective of the thesis was to apply the theorized phenomena governing a natural tissue's micro-structure (as a self-optimizing agent) in designing engineering frame structures. As mentioned before, structural optimization is

often accompanied by time and cost savings for engineering projects. The third objective was realized by modeling engineering frame structures based on the two major theories, Wolff and Michell, and comparing the strength of each model to the other. Michell's theory is merely mathematically oriented, while Wolff's is based on observations from nature (bone micro-structure) merged with some engineering calculations. Features of such strength comparison made between the two models are well described in Chapter 3 of the thesis.

The models produced from the two theories outlined had similar geometry (analogous to a cantilever beam), aspect ratio, total mass and also similar mass distribution (per unit area). The results showed that the frame structures modeled based on Wolff's theory had higher yield strength capabilities than those modeled based on Michell's theory, meaning that Wolff's theory was found to be better for guiding potential engineering design.

6.2 Assumptions and Limitations

There are assumptions and limitations for the work outlined in this thesis and these are explained here in greater detail. These assumptions and limitations are principally related to the fact that biological materials are not ideal engineering materials and thus treating them from an engineering point of view requires certain simplifications.

The first assumption is that biological material modeled as engineering material has consistent material properties (for example, in terms of yield strength, Poisson's ratio etc.). This is, of course, not the case with real biological materials, but this assumption needed to be made in order for mathematical analysis (Chapter 3) and simulation (Chapter 5) to be carried out in a manner relevant to the thesis. A great deal of future

work would need to be conducted (likely over many decades) before an assumption like this could be discarded for future studies. Such studies would have to detail for many samples material properties and how they vary over a sample specimen.

Another major assumption of the work is that simulation results at the micro scale can be extended to the macro scale; this assumption is well grounded because the microtubules, which were the focus of the simulation, are well documented to be the chief stress resistant structure for the specimens studied. The simulation carried out in Chapter 5 needed to be conducted at the micro scale because intercellular interaction is not well enough documented in the literature to permit a macro scale simulation (as such a simulation would need to take into account how mechanical stress is transferred from one neighboring cell to another). There are other parameters that would also need to be obtained to do a full macro-scale simulation (and these also do not exist in the literature), such as the material properties and interactions between cells. A macro level simulation taking into account all relevant parameters is likely only going to be possible well into the future after much more thorough analysis of plant material is undertaken.

6.3 Future work and recommendations

There are numerous potential avenues in developing different aspects of this research. For instance, this research could be undertaken with other types of loading regimes like laser ablation of cells, gravity with elevated magnitude, tension, torque or hydrostatic pressure applied on the cells, or even a combination of such loads could be applied on the plant. The results of such analysis would certainly fortify a better understanding of mechanical stresses affecting microstructure of a plant. For a fragile object like Arabidopsis root to be visualized on an unstable and slippery surface like agar

(a necessary medium when growing the plant), developing appropriate tools to apply mechanical stresses such as tension and torsion would be beneficial and often necessary.

Employing another type of plant with bigger physical size would also be very beneficial, since the Arabidopsis root is an extremely delicate and difficult to handle object. To the writers' knowledge, there isn't yet another type of mutant plant with noticeably bigger cell size (or organ's size) whose microtubules are visible and traceable under microscope. This should motivate the biological and/or engineering researchers to develop other plant alternatives with GFP (for microtubule visualization).

Another recommendation is related to simulations carried out in finite element software. Such simulations could be carried out for the entire root cross section rather than a single cell. However, since material properties and behavior of the plant cell is not very well recognized at present, this is a very difficult undertaking. A plant cell is complex with many different structures that can affect a cell's response to external loading; and not only do each of these structures have to be modelled, but their interaction with one another has to be modeled as well. Parameters needed for such modeling are often non-existent in the literature. Perhaps employing other non-linear materials (e.g. visco-elasto-plastic) with different properties (e.g. shear or normal modulus, Poisson's ratio) might offer an avenue for exploration.

Another area of focus for the future work is making a more comprehensive comparison between the frame structures generated based on Michell theory and Wolff's theory. For example, using a superimposed loading (rather than a single concentrated force) as well as a different geometry of the cantilever beam could be employed, and the

performance outcome could be compared for various material properties (e.g. non-linear or non-isotropic).

Another aspect of focus for future work over the long term is that the effects of mechanical forces on plants microstructure could be applied to animals as well. For example, this can be studied by changing the stress pattern applied to an animal by altering the daily activities and then visualizing the stress trajectories in the femur bone. This would provide further application of Wolff's theory.

In coming up with the last recommendation, it is worthwhile to remember that the mechanism behind microtubules reorientation is not thoroughly understood to date; however, by investigating more in this field, one can potentially determine the parameters influencing microtubules reorientation and/or the logic of such a mechanism, which undoubtedly will allow for a better model of such a phenomenon.

References:

- [1]- R. Chiong (Ed.), “Nature-Inspired Algorithms for Optimization”, Series: Studies in Computational Intelligence, Vol. 193, 2009.
- [2]- J. G. Skedrosa et al., “Mathematical analysis of trabecular ‘trajectories’ in apparent trajectorial structures: The unfortunate historical emphasis on the human proximal femur”, *Journal of Theoretical Biology* 244, pp. 15–45, 2007.
- [3]- JC Koch, “The laws of bone architecture”, *The American Journal of Anatomy*, Vol. 21, No. 2, 1917.
- [4]- P. Fernandes, H. Rodrigues and C. Jacobs, "A model of bone adaptation using a global optimization criterion based on the trajectorial theory of Wolff", *Computer methods in Biomechanics and Biomedical Engineering*, Vol. 2, pp. 125-138, 1999.
- [5]- M.H. Luxner, A. Woesz, J. Stampfl, P. Fratzl, H.E. Pettermann, "A finite element study on the effects of disorder in cellular structures", *Journal of Acta Biomaterialia* 5, pp. 381–390, 2009.
- [6]- W.A.M. Brekelmans, H.W. Poort & T.J.J.H. Slooff, "A new method to analyze the mechanical behavior of skeletal parts", *Acta Orthop Scand.* 43, pp. 301-17, 1972.
- [7]- J.E.A. Bertram and S.M. Swartz, "The 'Law of Bone Transformation': A Case of Crying Wolff?", *Biol. Rev.* 66, pp. 245-273, 1991.
- [8]- Z. Xinghua, G. He, G. Bingzhao, “The application of topology optimization on the quantitative description of the external shape of bone structure”, *Journal of Biomechanics* 38, pp 1612–1620, 2005.
- [9]- MK Bahari, F Farahmand, G. Rouhi, MR Movahhedy, “Prediction of shape and internal structure of the proximal femur using a modified level set method for structural topology optimization”, *Computer Methods in Biomechanics and Biomedical Engineering Journal* 15(8), pp 835-44, 2011..
- [10]- D.P. Fyhrie and D.R. Carter, "A Unifying Principle Relating Stress to Trabecular Bone Morphology", *Journal of Orthopaedic Research* 4, pp. 304-311, 1986.
- [11]- B. Chen et al., “A strain energy criterion for trabecular bone adaptation”, *IEEE digital library, 3rd International Conference on Bioinformatics and Biomedical Engineering*, 2009.
- [12]- C. Mattheck, “Biomechanics and Structural Optimization”, http://141.52.27.55/fzk/groups/imf-2/documents/internetdokument/id_052585.pdf
- [13]- M.G. Mullender and R. Huiskes, “Proposal for the Regulatory Mechanism of Wolff's Law”, *Journal of Orthopaedic Research* 13, pp 503-512, 1995.

- [14]- R. Huiskes, Ronald Ruimerman, G. H. van Lenthe and Jan D. Janssen, "Effects of mechanical forces on maintenance and adaptation of form in trabecular bone", *Nature* Vol 405, pp 704-706, June 2000.
- [15]- R. Huiskes, "If bone is the answer, then what is the question?", *Journal of Anatomy* 197, pp 145-156, 2000.
- [16]- A. Prakash Apte, "Topology Optimization Using Hyper Radial Basis Function Network, Phd thesis, The University of Texas at Arlington, 2009.
- [17]- I.G. Janga, I.Y. Kim, "Computational study of Wolff's law with trabecular architecture in the human proximal femur using topology optimization", *Journal of Biomechanics* 41, PP. 2353–2361, 2008.
- [18]- GN. Vanderplaats, "Structural optimization for statics, dynamics and beyond", *Journal of the Brazilian Society of Mechanical Sciences and Engineering* 28, pp 316-322, 2006.
- [19]- O. Sigmund, "Topology optimization: a tool for the tailoring of structures and Materials", *Philosophical Transactions of the Royal Society* 358, pp 211-227, 2000.
- [20]- G.I.N. Rozvany, "A critical review of established methods of structural topology optimization", *Struct. Multidisc. Optim.* 37, pp 217–237, 2009.
- [21]- J.M. Rossi and S. Wendling-Mansuy, "A topology optimization based model of bone adaptation", *Journal of Computer Methods in Biomechanics and Biomedical Engineering*, Vol. 10, No. 6, pp. 419–427, 2007.
- [22]- I.G. Jang & I.Y. Kim, "Analogy of Strain Energy Density Based Bone-remodeling Algorithm and Structural Topology Optimization", *Journal of Biomechanical Engineering*, Vol. 131, 2009.
- [23]- G.I.N. Rozvany, "Partial relaxation of the orthogonality requirement for classical Michell trusses", *Structural Optimization* 13, pp 271-274, 1997.
- [24]- P. Dewhurst, "Analytical solutions and numerical procedures for minimum-weight Michell structures", *Journal of the Mechanics and Physics of Solids* 49, pp 445 – 467, 2001.
- [25]- 4- G.A. Hegemier, W. Prager, "On Michell trusses", *Int. J. Mech. Sci.* 11, pp 209–215, 1969.
- [26]- A.S. L Chan et al., "The Design of Michell Optimum Structures", The College of Aeronautics Cranfield, 1960.
- [27]- R.N. Iyengar, K.S. Jagadish, "Recent Advances in Structural Engineering", Universities Press, 2005.

- [28]- G.I.N. Rozvany and W. Prager, "A new class of structural optimization problems: optimal archgrids", *Computer methods in applied mechanics and engineering* 19, pp 127-150, 1979.
- [29]- William Prager, "A note on discretized Michell structures", *Computer methods in applied mechanics and engineering* 3, pp 349-355, 1974.
- [30]- G.I.N. Rozvany, "On the validity structures of Prager's example of nonunique Michell", *Structural Optimization* 13, pp. 191-194, Springer-Verlag 1996.
- [31]- G.I.N. Rozvany, "Some shortcomings in Michell's truss theory", *Structural Optimization Journal* 13, PP 203-204, 1997.
- [32]- J. Kepler, "Structural optimization as a design and styling tool - with emphasis on truss structures", published online <http://www.c-i-d.dk/pdf/s-d-001.pdf>
- [33]- J. Eyckmans, T. Boudou, X. Yu and C.S. Chen, "A Hitchhiker's Guide to Mechanobiology", *Developmental Cell* 21, 2011.
- [34]- G.T. Charras and M.A. Horton, "Single Cell Mechanotransduction and Its Modulation Analyzed by Atomic Force Microscope Indentation", *Biophysical Journal*, Vol. 82, PP. 2970–2981, 2002.
- [35]- C.B. Khatiwala, S.R. Peyton and A.J. Putnam, "Intrinsic mechanical properties of the extracellular matrix affect the behavior of pre-osteoblastic MC3T3-E1 cells", *AJP-Cell Physiol* Vol. 290, PP. 1640-1650, 2006.
- [36]- H. Shibaoka, "Plant hormone-induced changes in the orientation of cortical microtubules: Alterations in the cross-linking between microtubules and the plasma membrane", *Annu. Rev. Plant Physiol. Plant Mol. Biol.* 45, PP. 527–544, 1994.
- [37]- P. Nick, R. Bergfeld, E. Schaifer, and P. Schopfer, "Unilateral reorientation of microtubules at the outer epidermal wall during photo- and gravitropic curvature of maize coleoptiles and sunflower hypocotyls", *Planta Journal* 181, PP. 162-168, 1990.
- [38]- C. Oakley and D. M. Brunette, "The sequence of alignment of microtubules, focal contacts and actin filaments in fibroblasts spreading on smooth and grooved titanium substrata", *Journal of Cell Science* 106, PP. 343-354, 1993.
- [39]- A. Geitmann, R. Palanivelu, "Fertilization Requires Communication: Signal Generation and Perception during Pollen Tube Guidance", *Floriculture and Ornamental Biotechnology* 1 (2), PP. 77-89, 2007.
- [40]- R.L. Cyr, "Microtubules in Plant Morphogenesis: Role of the Cortical Array", *Annual Reviews Cell Biology* 10, pp 153-80, 1994.
- [41]- A.R. Paredez, S. Persson, D.W. Ehrhardt, and C.R. Somerville, "Genetic Evidence That Cellulose Synthase Activity Influences Microtubule Cortical Array Organization", *Plant Physiology*, Vol. 147, pp. 1723–1734, 2008.

- [42]- C. Wasternack, "Jasmonates: An Update on Biosynthesis, Signal Transduction and Action in Plant Stress Response, Growth and Development", *Annals of Botany* 100, PP. 681–697, 2007.
- [43]- R. E. Williamson, "Alignment of Cortical Microtubules by Anisotropic Wall Stresses", *Aust. J. Plant Physiol.* 17, pp 601-13, 1990.
- [44]- T.I. Baskin, "Anisotropic Expansion of the Plant Cell Wall", *Annu. Rev. Cell Dev. Biol.* 21, pp. 203–22, 2005.
- [45]- A. Bichet et al., "BOTERO1 is required for normal orientation of cortical microtubules and anisotropic cell expansion in Arabidopsis", *The Plant Journal*, 25, pp 137-148, 2001.
- [46]- P. Schopfer, "Biomechanics of Plant Growth", *American Journal of Botany* 93 (10), PP. 1415–1425, 2006.
- [47]- J.F. Bolduc, L.J. Lewis, C.E. Aubin, A. Geitmann, "Finite-element analysis of geometrical factors in micro-indentation of pollen tubes", *Biomechan Model Mechanobiol* 5, PP. 227–236, 2006.
- [48]- J.V. Small, B. Geiger, I. Kaverina and A. Bershadsky, "How do microtubules guide migrating cells?", *Nature reviews, Molecular Biology*, Vol. 3, 2002.
- [49]- A. Geitmann and J.K.E. Ortega, "Mechanics and modeling of plant cell growth", *Trends in Plant Science* Vol.14, No.9, 2009.
- [50]- P.W. Barlow and J.S. Parker, "Microtubular cytoskeleton and root morphogenesis", *Plant and Soil* 187, PP. 23-36, 1996.
- [51]- Z. Zhang, H. Friedman, S. Meir, I. Rosenberger, A.H. Halevy, S. Philosoph-Hadas, "Microtubule reorientation in shoots precedes bending during the gravitropic response of cut snapdragon spikes", *Journal of Plant Physiology* 165, PP. 289—296, 2008.
- [52]- S. Jesuthasan and P.B. Green, "On the Mechanism of Decussate Phyllotaxis: Biophysical Studies on the Tunicalayer of *Vinca Major*", *Amer. J. Bot.* 76 (8), PP. 1152-1166, 1989.
- [53]- P.B. Green, R.O. Erickson, and P.A. Richmond, "On the Physical Basis of Cell Morphogenesis", *Annals of the New York Academy of Sciences*, Vol. 175, PP. 712–731, 1970.
- [54]- F. Corson, M. Adda-Bedia, A. Boudaoud, "In silico leaf venation networks: growth and reorganization driven by mechanical forces", *J Theor Biol.* 259 (3), PP. 440-8, 2009.
- [55]- Y. Nakagawa, T. Katagiri, K. Shinozaki, Z. Qi, H. Tatsumi, T. Furuichi, A. Kishigami, M. Sokabee, I. Kojimad, S. Sato, T. Kato, S. Tabata, K. Iida, A. Terashima, M. Nakano, M. Ikeda, T. Yamanaka, and H. Iida, "Arabidopsis plasma membrane protein crucial for Ca²⁺ influx and touch sensing in roots", *PNAS*, vol. 104, no. 9, PP. 3639–3644, 2007.

- [56]- K. Zandomeni and P. Schopfer, "Mechanosensory microtubule reorientation in the epidermis of maize coleoptiles subjected to bending stress", *Protoplasma* 182, PP. 96- 101, 1994.
- [57]- O. Hamant and J. Traas, "The mechanics behind plant development", *New Phytologist Journal* 185, pp 369–385, 2010.
- [58]- Y. Chebli, A. Geitmann, "Mechanical Principles Governing Pollen Tube Growth", *Functional Plant Science and Biotechnology* 1 (2), PP. 232-245, 2007.
- [59]- J. Lucas and S.L. Shaw, "Cortical microtubule arrays in the Arabidopsis seedling", *Current Opinion in Plant Biology* 11, pp 94–98, 2008.
- [60]- Z. Hejnowicz, "Autonomous changes in the orientation of cortical microtubules underlying the helicoidal cell wall of the sunflower hypocotyl epidermis: spatial variation translated into temporal changes", *Protoplasma* 225, 2005, pp 243–256.
- [61]- Z. hejnowicz. A. Burian, I. Dobrowloska, E. Kolano, "Orientational Variability of Parallel Arrays of Cortical Microtubules Under the Outer Cell Wall of the Helianthus Hypocotyl Epidermis", *Polish Botanical Society Journals*, Vol. 75, No 3, PP. 201-206, 2006.
- [62]- Z. Hejnowicz, A. Rusin, and T. Rusin, "Tensile Tissue Stress Affects the Orientation of Cortical Microtubules in the Epidermis of Sunflower Hypocotyl", *Journal of Plant Growth Regul* 19, PP. 31–44, 2000.
- [63]- D. Kwiatkowska, "Structural Integration at the Shoot Apical Meristem: Models, Measurements, and Experiments", *American Journal of Botany* 91 (9), PP. 1277–1293, 2004.
- [64]- J. Dumais, "Can mechanics control pattern formation in plants?", *Current Opinion in Plant Biology* 10, pp 58–62, 2007.
- [65]- R. L. Duncan, "Transduction of mechanical strain in bone", *ASGSB Bulletin* 8 (2), PP. 49-62, 1995.
- [66]- E.H. Burger and J.Klein-Nulend, "Mechanotransduction in bone—role of the lacunocanalicular network", *The FASEB Journal*, Vol. 13, 1999.
- [67]- M. Saiki et al., "Cellular basis for the automorphic curvature of rice coleoptiles on a three-dimensional clinostat: possible involvement of reorientation of cortical microtubules", *J Plant Res* 118:199–205, 2005.
- [68]- R. Ranjeva et al., "Plant graviperception and gravitropism: a newcomer's view", *The FASEB Journal*, Vol. 13 Supplement 1999, pp 136-141.
- [69]- A.R. Hardham, D. Takemoto and R.G White, "Rapid and dynamic subcellular reorganization following mechanical stimulation of Arabidopsis epidermal cells mimics responses to fungal and oomycete attack", *BMC Plant Biology* 8:63, 2008.

- [70]- J. Elsner, "Effect of steady torque twisting on the orientation of cortical microtubules in the epidermis of the sunflower hypocotyls", *Plant Biology* 10 pp 422–432, 2008.
- [71]- R. Himmelspach et al., "Gravity-induced reorientation of cortical microtubules observed in vivo", *The Plant Journal* 18 (4), pp 449- 453, 1999.
- [72]- D. D. Fisher, R. J. Cyr, "Mechanical Forces in Plant Growth and Development", *Gravitational and Space Biology Bulletin* 13(2), pp 67-74, June 2000.
- [73]- P.M. Lintilhac, "Differentiation, Organogenesis, and the Tectonics of Cell Wall Orientation. III. Theoretical Considerations of Cell Wall Mechanics", *Amer. J. Bot.* 61(3), pp 230-237, 1974.
- [74]- O. Hamant, M. G. Heisler, H. Jonsson, P. Krupinski, M. Uyttewaal, P. Bokov, F. Corson, P. Sahlin, A. Boudaoud, E. M. Meyerowitz, Y. Couder and J. Traas1, "Developmental Patterning by Mechanical Signals in Arabidopsis", *Science* 322, Dec. 2008.
- [75]- M. Uyttewaal, J. Traas and O. Hamant, "Integrating physical stress, growth, and development", *Current Opinion in Plant Biology* 13, pp 46–52, 2010.
- [76]- J. Dumais, "Plant Morphogenesis: A Role for Mechanical Signals", *Current Biology* Vol 19 No 5.
- [77]- Jing Zhou et al., Bochun, "Responses of Chrysanthemum Cells to Mechanical Stimulation Require Intact Microtubules and Plasma Membrane–Cell Wall Adhesion", *J Plant Growth Regul* 26, pp 55–68, 2007.
- [78]- C.L. Wymer, "Plant Cell Growth Responds to External Forces and the Response Requires Intact Microtubules", *Plant Physiology* 110, pp 425-430, 1996.
- [79]- J. Hush , R. Overall, "Electrical and mechanical fields orient cortical microtubules in higher plant tissues", *Cell Biology International Reports* 15, p 551-60, 1991.
- [80]- AL. Cleary, AR. Hardham, "Pressure induced reorientation of cortical microtubules in epidermal cells of *Lolium rigidum* leaves", *Plant and Cell Physiology* 34, p 1003-8, 1993.
- [81]- K. Fischer and P. Schopfer, "Interaction of auxin, light, and mechanical stress in orienting microtubules in relation to tropic curvature in the epidermis of maize coleoptiles", *Protoplasma Journal* 196, pp 108-116, 1997.
- [82]- J.M. Hush, C.R. Hawes and R.L. Overall, "Interphase microtubule re-orientation predicts a new cell polarity in wounded pea roots", *Journal of Cell Science* 96, pp 47-61, 1990.
- [83]- D.R. Carter, D.P. Fyhrie and R.T. Whales, "Trabecular Bone Density and Loading History: Regulation of Connective Tissue Biology by Mechanical Energy", *J Biomech.* 20 (8), PP. 785-94, 1987.

- [84]- Stephen C. Cowin, "Bone Mechanics HANDBOOK", second edition edited, CRC Press, 2001.
- [85]- J.S. Rao, "Dynamics of Plates", CRC Press, 1999.
- [86]- M. Gholamirad & M. Epstein, "A theoretical approach of obtaining principal stress trajectories", International Conference on Mechanical Engineering (ISME2010), Tehran, Iran, May 2010.
- [87]- A.G.M. Michell, "The limit of economy of material in frame structures", Philosophical Magazine Series 6, Vol 8, 1904.
- [88]- W.S., Hemp, "Theory of structural design", College of Aeronautics in Cranfield, Bedfordshire, 1958.
- [89]- M. Gholamirad & M. Epstein, "Bone remodeling as a problem in optimal structural design", Proceedings of The Canadian Society for Mechanical Engineering (CSME FORUM), Victoria, BC, Canada, June 2010.
- [90]- M. Gholamirad & M. Epstein, "Performance comparison of frame structures: discrete Michell or Wolff?", Proceedings of the ASME International Mechanical Engineering Congress & Exposition IMECE2010, Vancouver, BC, Canada, Nov. 2010.
- [91]- K.J. Niklas, "Plant Biomechanics- An Engineering Approach to Plant Form and Function", The University of Chicago Press, 1992.
- [92]- C. Mattheck, "Biomechanics and Structural Optimization", Forschungszentrum Karlsruhe in der Helmholtz-gemeinschaft.
- [93]- T.I. Baskin, "Microtubules, Microfibrils, and Growth Anisotropy", Plant Physiology Journal, 5th edition, Essay 15.2, 2006.
- [94]- A. Desai and T.J. Mitchison, "Microtubule polymerization dynamic", Annual Rev. Cell Dev. Biology 13, pp 83–117, 1997.
- [95]- T.I. Baskin, G.T.S. Beemster, J.E. Judy-March and F. Marga, "Disorganization of Cortical Microtubules Stimulates Tangential Expansion and Reduces the Uniformity of Cellulose Microfibril Alignment among Cells in the Root of Arabidopsis", Plant Physiology, Vol. 135, pp. 2279–2290, 2004.
- [96]- F. Corson, O. Hamant, S. Bohn, J. Traas, A. Boudaoud and Y. Couder, "Turning a plant tissue into a living cell froth through isotropic growth", PNAS vol. 106, no. 21, PP. 8453–8458, 2009.
- [97]- D.B. Szymanski and D.J. Cosgrove, "Dynamic Coordination of Cytoskeletal and Cell Wall Systems during Plant Cell Morphogenesis", Current Biology 19, R800–R811, 2009.

- [98]- G. Tian, D. Smith, S. Gluck and T.I. Baskin, "Higher Plant Cortical Microtubule Array Analyzed In Vitro in the Presence of the Cell Wall", *Cell Motility and the Cytoskeleton* 57, PP. 26–36, 2004.
- [99]- D. M. Orcutt, E. T. Nilsen, "The Physiology of Plants Under Stress: Soil and biotic factors", pp 195, John Wiley Inc., 2000.
- [100]- K. Sugimoto¹, R.E. Williamson and G.O. Wasteneys, "New Techniques Enable Comparative Analysis of Microtubule Orientation, Wall Texture, and Growth Rate in Intact Roots of Arabidopsis", *Plant Physiology*, Vol. 124, pp. 1493–1506, 2000.
- [101]- J. Marc, C. L. Granger, J. Brincat, D.D. Fisher, T. Kao, A.G. McCubbin, R.J. Cyr, "A GFP–MAP4 Reporter Gene for Visualizing Cortical Microtubule Rearrangements in Living Epidermal Cells", *The Plant Cell*, Vol. 10, PP. 1927–1939, 1998.
- [102]- J.M. Hush, C.R. Hawes and R.L. Overall, "Interphase microtubule re-orientation predicts a new cell polarity in wounded pea roots", *Journal of Cell Science* 96, pp 47-61, 1990.
- [103]- N.J. Holdaway, R.G. White and R.L. Overall, "Is the recovery of microtubule orientation in pea roots dependent on the cell wall?", *Cell Biology International*, Vol. 19, No. 11, 1995.
- [104]- Y. Wang, B. Wang, S. Gilroy, E.W. Chehab, J. Braam, "CML24 is Involved in Root Mechanoresponses and Cortical Microtubule Orientation in Arabidopsis", *J Plant Growth Regul*, 2011.
- [105]- F.A. Ditengou, W.D. Teale, P. Kochersperger, K.A. Flittner, I. Kneuper, E. Graaff, H. Nziengui, F. Pinosa, X. Li, R. Nitschke, T. Laux and K. Palme, "Mechanical induction of lateral root initiation in Arabidopsis thaliana", *PNAS Journal*, vol. 105, no. 48, 2008.
- [106]- Uyttewaal M, Burian A, Alim K, Landrein B, Borowska-Wykręć D, Dedieu A, Peaucelle A, Ludynia M, Traas J, Boudaoud A, Kwiatkowska D, Hamant O. , "A katanin-dependent microtubule response to mechanical stress enhances growth gradients between neighboring cells in Arabidopsis", *CELL* in press, 2012.
- [107]- S. Matsumoto, S. Kumasaki, K. Soga, K. Wakabayashi, T. Hashimoto and Takayuki Hoson, "Gravity-Induced Modifications to Development in Hypocotyls of Arabidopsis Tubulin Mutants", *Plant Physiology*, Vol. 152, pp. 918–926, 2010.
- [108]- A. Geitmann, "Mechanical modeling and structural analysis of the primary plant cell wall", *Current Opinion in Plant Biology* 13, PP. 693–699, 2010.
- [109]- J. Chan, M. Eder, E.F. Crowell, J. Hampson, G. Calder and C. Lloyd, "Microtubules and CESA tracks at the inner epidermal wall align independently of those on the outer wall of light-grown Arabidopsis hypocotyls", *Journal of Cell Science* 124, PP. 1088-1094, 2011.
- [110]- P. Milani, M. Gholamirad, J. Traas, A. Arnéodo, A. Boudaoud, F. Argoul, O. Hamant, "In vivo analysis of local wall stiffness at the shoot apical meristem in Arabidopsis using atomic force microscopy", *The Plant Journal*, Sep;67(6):1116-23, 2011.

[111]- E. Steudle, U. Zimmermann and U. Lüttge, “Effect of Turgor Pressure and Cell Size on the Wall Elasticity of Plant Cells”, *Plant Physiol.* 59, PP. 285-289, 1977.

[112]- J.H. Kroeger, R. Zerzour, A. Geitmann, “Regulator or Driving Force? The Role of Turgor Pressure in Oscillatory Plant Cell Growth”, *PLoS ONE Journal*, Volume 6, Issue 4, 2011.

Appendix A: Matlab Programs Details

Matlab program set #1:

```

% A cantilever beam with transverse load "F" at the end is modeled to
% define the stress trajectories curves (Similar to the Figure 3.9 in
this thesis)
% ***** Compression Curves *****

clc
clear
% h= Half-depth of the beam in Y direction (2h=Total depth along Y
axis), mm
% L= Total length of the beam in X direction, mm
% S= Step length on trajectory Curve, mm. The finer S is the more
smooth
% the curve will be.
% N= Number of Iteration; Increase it when you have longer beam
N=100;
L=input('what is the length of the cantilever, L, in x direction,
L=');
h=input('what is the half-depth of the cantilever, h, in y direction,
h=');
% example h=40; L=180;
y1(1)=0; S=.5; Y1(1)=0;
ctrD=1;
for II=0:10:L % If you want to see an individual trajectory, then you
can run the program from NEXT line. Simply replace 'II' in EACH step
from 0 to L
    cn=1; x1(1)=II; X1(1)=II;
    for i=2:N
        a1=atan((-x1(cn)*y1(cn)-sqrt((h^2-
y1(cn)^2)+x1(cn)^2*y1(cn)^2))/(h^2-y1(cn)^2));
        A1=atan((-X1(cn)*Y1(cn)-sqrt((h^2-
Y1(cn)^2)+X1(cn)^2*Y1(cn)^2))/(h^2-Y1(cn)^2));
        x1(i)=x1(cn)+S*cos(a1);
        X1(i)=X1(cn)-S*cos(A1);
        y1(i)=y1(cn)+S*sin(a1);
        Y1(i)=Y1(cn)-S*sin(A1);
        cn=cn+1;
    end

    C1=0;
    for i=1:N
        if x1(i)<=L
            p(i)=x1(i);
            q(i)=y1(i);
        end
        if X1(i)>=0
            P(i)=X1(i);
            Q(i)=Y1(i);
        end
    end
end

```

```

        C1=C1+1;
    end
end

C2=1;
for i=C1:-1:1
    P2(i)=P(C2);
    Q2(i)=Q(C2);
    C2=C2+1;
end
A=transpose([P2 p;Q2 q]);

A(:,3)=0;
clear A2
V=1;
for i=1:size(A)
    A2(V,1)=A(i,1);
    A2(V,2)=A(i,2);
    V=V+1;
end
A2(V-1,3)=0;
for i=1:V-1
    plot(A2(i,1),A2(i,2))
    hold on
end
axis equal

F_No_D=int2str(ctrD);
save(F_No_D, 'A2', '-ascii', '-double')
ctrD=ctrD+1;
end

% ***** Tensile Curves *****

clc
clear
% h= Half-depth of the beam in Y direction (2h=Total depth along Y
axis), mm
% L= Total length of the beam in X direction, mm
% S= Step length on trajectory Curve, mm. The finer S is the more
smooth
% the curve will be.
% N= Number of Iteration; Increase it when you have longer beam
N=100;
L=input('what is the length of the cantilever, L, in x direction,
L=');
h=input('what is the half-depth of the cantilever, h, in y direction,
h=');
y2(1)=0;S=.5; Y2(1)=0;
ctrU=1;
for II=0:10:L % If you want to see an individual trajectory, then you
can run the program from NEXT line. Simply replace 'II' in EACH step
from 0 to L
    cn=1; x2(1)=II; X2(1)=II;

```

```

    for i=2:N
        a2=atan((-x2(cn)*y2(cn)+sqrt((h^2-
y2(cn)^2)+x2(cn)^2*y2(cn)^2))/(h^2-y2(cn)^2));
        A2=atan((-X2(cn)*Y2(cn)+sqrt((h^2-
Y2(cn)^2)+X2(cn)^2*Y2(cn)^2))/(h^2-Y2(cn)^2));
        x2(i)=x2(cn)+S*cos(a2);
        X2(i)=X2(cn)-S*cos(A2);
        y2(i)=y2(cn)+S*sin(a2);
        Y2(i)=Y2(cn)-S*sin(A2);
        cn=cn+1;

    end

    C1=0;
    for i=1:N
        if x2(i)<=L
            p(i)=x2(i);
            q(i)=y2(i);
        end
        if X2(i)>=0
            P(i)=X2(i);
            Q(i)=Y2(i);
            C1=C1+1;
        end
    end

    C2=1;
    for i=C1:-1:1
        P2(i)=P(C2);
        Q2(i)=Q(C2);
        C2=C2+1;
    end
    A=transpose([P2 p;Q2 q]);

    A(:,3)=0;

    clear A2
    V=1;
    for i=1:size(A)% change it according to your A matrix
        A2(V,1)=A(i,1);
        A2(V,2)=A(i,2);
        V=V+1;
    end
    A2(V-1,3)=0;
    for i=1:V-1
        plot(A2(i,1),A2(i,2))
        hold on
    end
    axis equal

    F_No_U=int2str(ctrU);
    save(F_No_U,'A2','-ascii','-double')
    ctrU=ctrU+1;
end

```

These previously shown programs in Appendix A are saved with the name “CantileverBeam-StressTrajectory-DOWN-ALL-2.m” and “CantileverBeam-StressTrajectory-UP-ALL-2.m”, respectively.

Matlab program #2:

```

% This program is written to sort Node Numbers and corresponding Node's
% Outputs (e.g. principal stress) from Ansys software
% Refer to image "Figure (3.16)"
clear
clc
fprintf('According to "NodeSortingGuide.jpeg":  ')
XL=input('Enter Xl='); % XL= Total length of beam in X direction, mm
YL=input('Enter Yl='); % YL= Total length of beam in Y direction, mm
YL=2c
% DX=Delta X & DY=Delta Y:
DX=input('Enter Delta x, DX=');
DY=input('Enter Delta y, DY=');
% m & n are number of division along X and Y axes:
m=XL/DX+1;
n=YL/DY+1;
% Matrix M is the matrix whose components are coordinates of the
meshgrid
% and the size of the matrix is "P*3" (P rows and 3 Columns). 1st
column is
% NEW node numbers
P=m*n;
% Here we define matrix M:
x=0;y=0;
for i=1:P
    M(i,1)=i;
    M(i,2)=x;
    M(i,3)=y;
    x=x+DX;
    if x>XL
        x=0;
        y=y+DY;
    end
end
end

% Here we load a '.txt' file which has XYZ components of Nodes:
U=load('Box5-Node-XYZ-2.txt');
% Now we only choose those Rows of U matrix which have Z=0 (Nodes on XY
plane) & we call it U2:
ctr=1;
for i=1:size(U)
    if U(i,4)==0
        U2(ctr,1)=U(i,1);
        U2(ctr,2)=U(i,2);
        U2(ctr,3)=U(i,3);
        ctr=ctr+1;
    end
end
end

% Here we load a '.txt' file which has S1-S3 (1st to 3rd Principal
Stress) components of Nodes:
V=load('Box5-Node-S1S3-2.txt');

```

```

% Now we only choose those Rows of V matrix which have the same Node
Number as U2 matrix & we call it V2:
ctr=1;
for i=1:100000
    for j=1:size(V)
        if ctr>size(U2)
            break
        end
        if V(j,1)==U2(ctr,1)
            V2(ctr,:)=V(j,:);
            ctr=ctr+1;
        end
    end
end

% Here we load a '.txt' file which has Sx, Sy & Txy (Normal stress
along X & Y and also XY shear stress) components of Nodes:
W=load('Box5-Node-Sx-Sy-Txy-2.txt');
% Now we only choose those Rows of W matrix which have the same Node
Number as U2 matrix & we call it W2:
ctr=1;
for i=1:100000
    for j=1:size(W)
        if ctr>size(U2)
            break
        end
        if W(j,1)==U2(ctr,1)
            W2(ctr,:)=W(j,:);
            ctr=ctr+1;
        end
    end
end

% (This Node Numbers belong to Ansys)

%-----
% Matrix E has a size of P*8 (Rows*Columns)
% E=[Node No.  X  Y  S1  S3  Sx  Sy  Txy]
E=[U2 V2(:,2) V2(:,4) W2(:,2) W2(:,3) W2(:,5)];

% Matrix E is compared to matrix M and is sorted based on the ascending
% coordinates (x & y). This sorted matrix is now called F, which is
defined here:
ctr=1;
for i=1:1000000
    for j=1:P
        if ctr>P
            break
        end
        if E(j,2)==M(ctr,2) & E(j,3)==M(ctr,3)
            F(ctr,:)=E(j,:);
            ctr=ctr+1;
        end
    end
end
end

```

```
% Now we replace Ansys Node Numbers in F with NEW NODE NUMBERS which  
are well organized:  
F(:,1)=M(:,1);
```

This program (Matlab program #2) is named "NodeSorting-
Real.m".

Matlab program #3:

```

% Here we draw Stress Trajectories based on the information from the
'.m file' named "NodeSorting-Real":
I=(round(n/2)-1)*m+1;
% if n is an Even Number give a warning:
if round((n-1)/2)==n/2
    fprintf('***! WARNING ! **: Choose DY so that n becomes an ODD
number and stress trajectories would be on Neutral Axis\n')
end
N_ST=input('How many Stress Trajectories do you want to draw, N_ST=');
Q=XL/N_ST;
O=round(Q/DX);
counterD=1;
counterD2=N_ST+1;

for J=I:O:I+m-2

    % . . . . . Initial Condition . . . . .
    . . .
    Nom=2*F(J,8);           % F(J,8) is Txy
    DNom=F(J,6)-F(J,7);    % F(J,6) is Sx & F(J,7)=Sy
                           % So Nom/DNom=tg(2Teta_P)

    if Nom>0 & DNom>0
        Teta_P_0=0.5*atan(Nom/DNom); %Teta_P_0 is the initial
condition for Teta_P at Jth Node (Radian)
    else if Nom>0 & DNom<0
        Teta_P_0=pi+0.5*atan(Nom/DNom);
    else if Nom<0 & DNom>0
        Teta_P_0=2*pi+0.5*atan(Nom/DNom);
    else if Nom<0 & DNom<0
        Teta_P_0=pi+0.5*atan(Nom/DNom);
    end
    end
    end

    % Here we define that 0< Teta_P_0<90    OR    180< Teta_P_0 <270
degree
    % 90< Teta_P_Prime_0 <180 OR    270< Teta_P_Prime_0 < 360    degree:
    if (Teta_P_0>=pi/2 & Teta_P_0<=pi) | (Teta_P_0>=(3*pi/2) &
Teta_P_0<=2*pi)
        Teta_P_Prime_0=Teta_P_0;
        Teta_P_0=Teta_P_Prime_0-pi/2;
    else % (Teta_P_0>=0 & Teta_P_0<=pi/2) | (Teta_P_0>=pi &
Teta_P_0<=3*pi/2)
        Teta_P_Prime_0=Teta_P_0+pi/2;
    end
    end
    % . . . . .
    . . .

```

```

% . . . . . General Condition . . . . .
. . .
% S= Step length on trajectory Curve, mm:
S=DY/10; % This S is arbitrary. You can change it.
% Now we define TETA at each Node.
for i=1:size(F)
    Nom=2*F(i,8);
    DNom=F(i,6)-F(i,7);
    if Nom>0 & DNom>0
        TETA(i)=0.5*atan(Nom/DNom);
    else if Nom>0 & DNom<0
        TETA(i)=pi+0.5*atan(Nom/DNom);
    else if Nom<0 & DNom>0
        TETA(i)=2*pi+0.5*atan(Nom/DNom);
    else if Nom<0 & DNom<0
        TETA(i)=pi+0.5*atan(Nom/DNom);
    end
    end
end
end
end
end
TT=transpose(TETA);
% Teta_P_Prime is the angle indicating the direction of S3 (3rd
Principal Stress)
% Here we define if TETA=Teta_P OR TETA=Teta_P_Prime
for i=1:size(TT)
    if (TETA(i)>=0 & TETA(i)<=pi/2) | (TETA(i)>=pi &
TETA(i)<=3*pi/2)
        Teta_P(i)=TETA(i);
        Teta_P_Prime(i)=TETA(i)+pi/2;
    else
        Teta_P_Prime(i)=TETA(i);
        Teta_P(i)=TETA(i)-pi/2;
    end
end
end

F(:,9)=Teta_P;
F(:,10)=Teta_P_Prime;
    XcentrD=F(J,2)+S*cos(Teta_P_Prime_0);
    YcentrD=F(J,3)+S*sin(Teta_P_Prime_0);
    XcentrD2=F(J,2)-S*cos(Teta_P_Prime_0);
    YcentrD2=F(J,3)-S*sin(Teta_P_Prime_0);
    Curv_Points_D(1,1)=F(J,2);
    Curv_Points_D(1,2)=F(J,3);
    Crv_Pnt_D(1,1)=F(J,2);
    Crv_Pnt_D(1,2)=F(J,3);

for k=2:500
    Curv_Points_D(k,1)=XcentrD;
    Curv_Points_D(k,2)=YcentrD;
    Crv_Pnt_D(k,1)=XcentrD2;
    Crv_Pnt_D(k,2)=YcentrD2;

    % First we find the 4 neighboring points:

```

```

for i=1:m
    if XcentrD>F(i,2) & XcentrD<F(i+1,2)
        XnbD(1)=F(i,2);
        XnbD(2)=F(i+1,2);
        XnbD(3)=F(i,2);
        XnbD(4)=F(i+1,2);
    end
end
for i=1:m:P-m;
    if YcentrD>F(i,3) & YcentrD<F(i+m,3)
        YnbD(1)=F(i,3);
        YnbD(2)=F(i,3);
        YnbD(3)=F(i+m,3);
        YnbD(4)=F(i+m,3);
    end
end
for i=1:m
    if XcentrD2>F(i,2) & XcentrD2<F(i+1,2)
        XnbD2(1)=F(i,2);
        XnbD2(2)=F(i+1,2);
        XnbD2(3)=F(i,2);
        XnbD2(4)=F(i+1,2);
    end
end
for i=1:m:P-m;
    if YcentrD2>F(i,3) & YcentrD2<F(i+m,3)
        YnbD2(1)=F(i,3);
        YnbD2(2)=F(i,3);
        YnbD2(3)=F(i+m,3);
        YnbD2(4)=F(i+m,3);
    end
end

if XcentrD<0
    XnbD=[-1 0 0 -1];
    YnbD=[0 0 1 1];
    SM_D=[1 1 1 1;1 1 1 1];
end
if XcentrD2<0
    XnbD2=[-1 0 0 -1];
    YnbD2=[0 0 1 1];
    SM_D2=[1 1 1 1;1 1 1 1];
end
% According to the 4 neighboring points we found, we assign
S3(3rd principal stress) & Teta_P_Prime to each of these 4 points:
ctr=1;
for i=1:size(F)
    if XnbD(ctr)==F(i,2) & YnbD(ctr)==F(i,3)
        SM_D(1,ctr)=abs(F(i,5));
        SM_D(2,ctr)=F(i,10);
        ctr=ctr+1;
    end
    if ctr==5
        ctr=1;
    end
end

```

```

end
ctr=1;
for i=1:size(F)
    if XnbD2(ctr)==F(i,2) & YnbD2(ctr)==F(i,3)
        SM_D2(1,ctr)=F(i,5);
        SM_D2(2,ctr)=F(i,10);
        ctr=ctr+1;
    end
    if ctr==5
        ctr=1;
    end
end

% ***** Now we interpolate: *****

Xc_D=XnbD(1)+DX/2; % Xc belongs to Centroid of element
Yc_D=YnbD(1)+DY/2; % Yc belongs to Centroid of element
Zeta_D=(2/DX)*(XcentrD-Xc_D);
Eta_D=(2/DY)*(YcentrD-Yc_D);

Xc_D2=XnbD2(1)+DX/2; % Xc belongs to Centroid of element
Yc_D2=YnbD2(1)+DY/2; % Yc belongs to Centroid of element
Zeta_D2=(2/DX)*(XcentrD2-Xc_D2);
Eta_D2=(2/DY)*(YcentrD2-Yc_D2);
% According to "Isoparametric formulation of quadrilateral
element" section
% ..... Non-dimensional Shape Functions N are:
N_D(1)=(1/4)*(1-Zeta_D)*(1-Eta_D); N_D2(1)=(1/4)*(1-
Zeta_D2)*(1-Eta_D2);
N_D(2)=(1/4)*(1+Zeta_D)*(1-Eta_D);
N_D2(2)=(1/4)*(1+Zeta_D2)*(1-Eta_D2);
N_D(3)=(1/4)*(1+Zeta_D)*(1+Eta_D);
N_D2(3)=(1/4)*(1+Zeta_D2)*(1+Eta_D2);
N_D(4)=(1/4)*(1-Zeta_D)*(1+Eta_D); N_D2(4)=(1/4)*(1-
Zeta_D2)*(1+Eta_D2);

Vx_D=sum(SM_D(1,:).*cos(SM_D(2,:)).*N_D);
Vy_D=sum(SM_D(1,:).*sin(SM_D(2,:)).*N_D);

Vx_D2=sum(SM_D2(1,:).*cos(SM_D2(2,:)).*N_D2);
Vy_D2=sum(SM_D2(1,:).*sin(SM_D2(2,:)).*N_D2);

if Vx_D>0 & Vy_D>0
    Teta_Centr_D=atan(Vy_D/Vx_D);
end
if Vx_D<0 & Vy_D>0
    Teta_Centr_D=pi+atan(Vy_D/Vx_D);
end
if Vx_D<0 & Vy_D<0
    Teta_Centr_D=pi+atan(Vy_D/Vx_D);
end
if Vx_D>0 & Vy_D<0
    Teta_Centr_D=2*pi+atan(Vy_D/Vx_D);

```

```

end

if Vx_D2>0 & Vy_D2>0
    Teta_Centr_D2=atan(Vy_D2/Vx_D2);
end
if Vx_D2<0 & Vy_D2>0
    Teta_Centr_D2=pi+atan(Vy_D2/Vx_D2);
end
if Vx_D2<0 & Vy_D2<0
    Teta_Centr_D2=pi+atan(Vy_D2/Vx_D2);
end
if Vx_D2>0 & Vy_D2<0
    Teta_Centr_D2=2*pi+atan(Vy_D2/Vx_D2);
end

XcentrD=XcentrD+S*cos(Teta_Centr_D);
YcentrD=YcentrD+S*sin(Teta_Centr_D);
XcentrD2=XcentrD2+S*cos(Teta_Centr_D2);
YcentrD2=YcentrD2+S*sin(Teta_Centr_D2);

if XcentrD<F(1,2) & YcentrD>F(size(F),3) &
XcentrD2>F(size(F),2) & YcentrD2<F(1,3)
    break
end

end

plot(F(J,2),F(J,3),'r^')
hold on
for i=1:size(Curv_Points_D)
    plot(Curv_Points_D(i,1),Curv_Points_D(i,2),'g*')
    hold on
end
hold on
for i=1:size(Crv_Pnt_D)
    plot(Crv_Pnt_D(i,1),Crv_Pnt_D(i,2),'*')
    hold on
end
axis equal
% Saving the required DATA:
Curv_Points_D(1,3)=0;
Crv_Pnt_D(1,3)=0;

F_No_D=int2str(counterD);
F_No_D2=int2str(counterD2);
save(F_No_D,'Curv_Points_D','-ascii','-double')
save(F_No_D2,'Crv_Pnt_D','-ascii','-double')
counterD=counterD+1;
counterD2=counterD2+1;
end

```

This program (Matlab program #3) is named "Ansys-Stress-Trajectories-DOWN-Isoparametric-Interpolation-3.m"

Matlab program #4

```

clc
clear
% According to the Figure (3.24) and 3.25:
% You need to define three parameters Delta_Phi, m, n, length of OM and
ON:

D_Phi=input('Enter Delta_Phi in Degrees, D_Phi= ');
D_Phi=(D_Phi*pi)/180;      % D_Phi in Radian
m=input('Enter the distance OM on Alpha axis, OM =');
n=input('Enter the distance ON on Beta axis, ON =');
N1=input('Enter the desired number of nodes along Alpha axis, m=');
N2=input('Enter the desired number of nodes along Beta axis, n=');

% 1st row on alpha line:
% -----
N_C(1,1)=0;
N_C(1,2)=0;    % N_C = Node_Coordinates Matrix which is in the form of
[x1 y1    x2 y2    ...    xn yn

ctr=3;
for i=3:2:2*N1
    N_C(1,i)=N_C(1,i-2)+m*cos((ctr-3)*D_Phi+D_Phi/2);
    N_C(1,i+1)=N_C(1,i+1-2)-m*sin((ctr-3)*D_Phi+D_Phi/2);
    ctr=ctr+1;
end

% 2nd row above Alpha line:
% -----
% =====
% ==
N_C(2,1)=-n*sin(D_Phi/2);
N_C(2,2)=n*cos(D_Phi/2);
% According to Figure (3.26) for the intersecting point of the 2 lines:
L=50*m;
L_p=50*n;
X1=N_C(2,1);          Y1=N_C(2,2);
X3=N_C(1,3);          Y3=N_C(1,4);

X2=X1+L*cos(D_Phi/2);      Y2=Y1+L*sin(D_Phi/2);
X4=X3+L_p*cos(pi/2-D_Phi/2);  Y4=Y3+L_p*sin(pi/2-D_Phi/2);
Y=((Y1/(Y2-Y1))*(X2-X1)-(Y3/(Y4-Y3))*(X4-X3)+X3-X1)/((X2-X1)/(Y2-Y1)-
(X4-X3)/(Y4-Y3));
X=((Y-Y1)/(Y2-Y1))*(X2-X1)+X1;
% so:
% =====
% ==
N_C(2,3)=X;
N_C(2,4)=Y;

```

```

% = = = = =
= =
ctr=1;
Teta1=D_Phi/2;
Teta2=pi/2-D_Phi/2;
for i=3:2:2*N1-2
    X1=N_C(2,i);      Y1=N_C(2,i+1);
    X3=N_C(1,i+2);    Y3=N_C(1,i+3);

    Teta1=Teta1-D_Phi;
    Teta2=Teta2-D_Phi;
    X2=X1+L*cos(Teta1);
    Y2=Y1+L*sin(Teta1);
    X4=X3+L_p*cos(Teta2);
    Y4=Y3+L_p*sin(Teta2);
    ctr=ctr+1;
    % X & Y are for the intersecting point of the 2 lines:
    Y=( (Y1/(Y2-Y1)) * (X2-X1) - (Y3/(Y4-Y3)) * (X4-X3) + X3 - X1 ) / ( (X2-X1)/(Y2-
Y1) - (X4-X3)/(Y4-Y3) );
    X=( (Y-Y1)/(Y2-Y1) ) * (X2-X1) + X1;
    % so:
    N_C(2,i+2)=X;
    N_C(2,i+3)=Y;
end

% 3rd row and the rest of the rows above Alpha line:
% - - - - -
-
for j=3:N2
    % 1st point of the 3rd (or higher) row(s):
    % = = = = =
= =
    N_C(j,1)=N_C(j-1,1)-n*sin((j-2)*D_Phi+D_Phi/2);
    N_C(j,2)=N_C(j-1,2)+n*cos((j-2)*D_Phi+D_Phi/2);
    % According to Figure (3.26)
    X1=N_C(j,1);      Y1=N_C(j,2);
    X3=N_C(j-1,3);    Y3=N_C(j-1,4);

    Teta1=(j-2)*D_Phi+D_Phi/2;
    Teta2=pi/2+D_Phi/2+(j-3)*D_Phi;
    X2=X1+L*cos(Teta1);      Y2=Y1+L*sin(Teta1);
    X4=X3+L_p*cos(Teta2);    Y4=Y3+L_p*sin(Teta2);
    % X & Y are for the intersecting point of the 2 lines:
    Y=( (Y1/(Y2-Y1)) * (X2-X1) - (Y3/(Y4-Y3)) * (X4-X3) + X3 - X1 ) / ( (X2-X1)/(Y2-
Y1) - (X4-X3)/(Y4-Y3) );
    X=( (Y-Y1)/(Y2-Y1) ) * (X2-X1) + X1;
    % so:
    % 2nd point of the 3rd (or higher) row(s):
    % = = = = =
= =
    N_C(j,3)=X;
    N_C(j,4)=Y;
    % other points on the 2nd row:

```



```
A2NC_points(ctr1,2)=A2_N_C(j,ctr2+1);
ctr1=ctr1+1;
ctr2=ctr2+2;
    end
end
hold on
plot(A2NC_points(:,1),A2NC_points(:,2), 'black-*)
% saving the results:
ANC_points(size(ANC_points),3)=0;
A2NC_points(size(A2NC_points),3)=0;
save('ANC_points.txt','ANC_points','-ascii','-double')
save('A2NC_points.txt','A2NC_points','-ascii','-double')
```

This program (Matlab program #4) is named "Real Michell
4.m"

Appendix B: Confocal Microscopy Images from the Arabidopsis Root Cells

Below are some selected images from confocal microscopy observations. Figure B-1 shows images of the Arabidopsis root when bending moment has been applied to the root. These images have been taken once right after the bending moment has been applied (within half an hour) and then six to seven hours later. The figures demonstrate that the roots are still healthy and growing. As well, they display the root hairs growing around the bend in the curved root.

After 6 to 7 hours

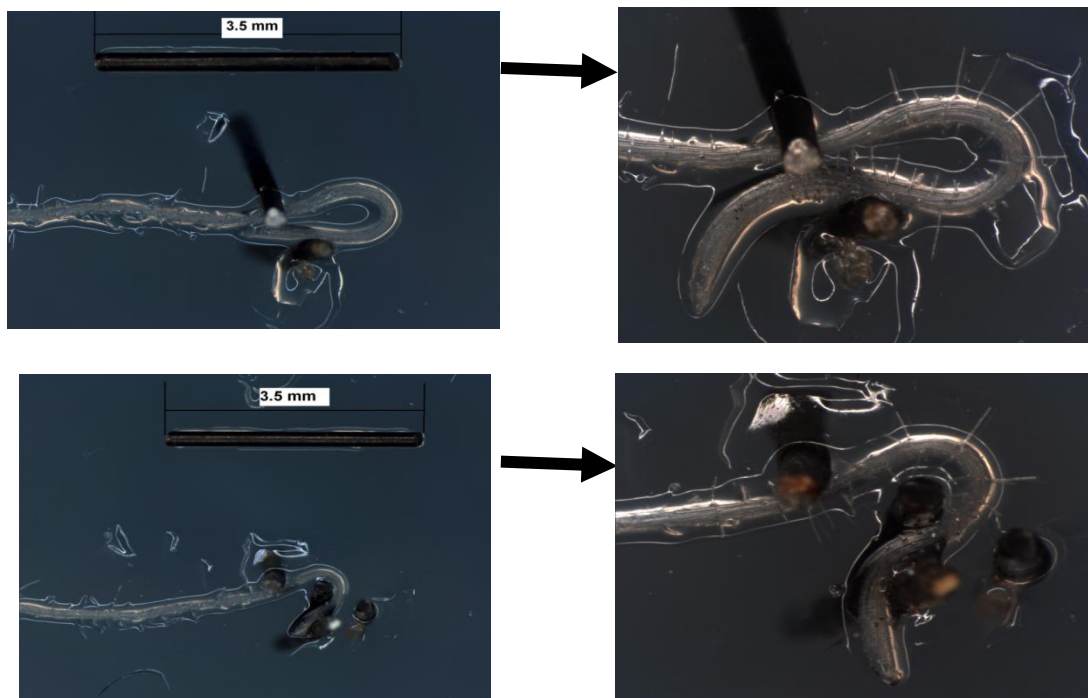


Figure B-1: *Left*- Bending moment just applied to the Arabidopsis root. *Right*- Same root observed 6 to 7 hours after the bending moment was applied.

Figures B-2 to B-6 show the microtubules orientation in a chosen Arabidopsis root cell after the bending load has been applied (one root cell was chosen for each of the

three figures). All these angles have been defined by means of an ImageJ program plugin.

Figure B-2 shows some examples of the microtubule arrangement visualized immediately after the bending load was applied.

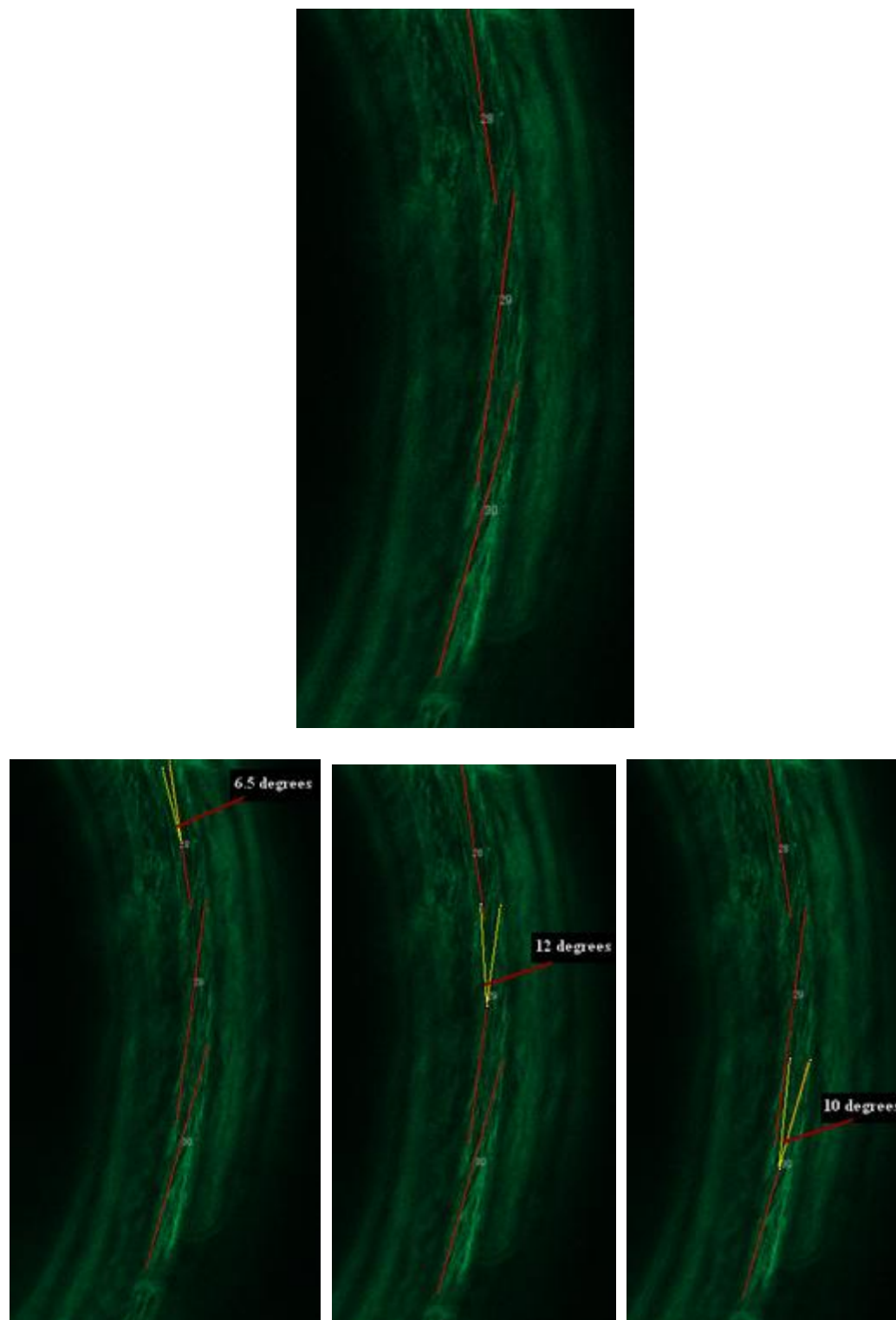


Figure B-2: Microtubules orientation measured immediately after (within minutes) the bending load was first applied.

As shown in the previous figure, microtubule orientations are angled 6.5, 12 and 10 degrees with respect to the main axis of the cell. The same section of the root is visualized under the Confocal microscope immediately after around six to seven hours of continuous bending load exertion. This 6 to 7 hour time frame is how long microtubules need on average to re-orient themselves. Since the Arabidopsis root is continuously growing, one of the main challenges in tracking microtubules orientation is to find exactly the same cell as visualized in previous observations (i.e. observations immediately following when bending load was first applied). There isn't really a practical method to mark or highlight a specific cell to be differentiated from other cells. The only ways to locate the desired cell is by trial and error, and to keep moving the microscope lens along the length of region "A" (from Figure 4-12) until a cell can be found based on its appearance from images taken previously. Another challenge is that sometimes after removing the cover slip, the root might slightly rotate due to the loss of surface tension between the root and cover slip and, the relative alignment will no longer be the same as before. This might cause some difficulty while collecting the data and images; thus this was avoided in order to carry out careful collection of data.

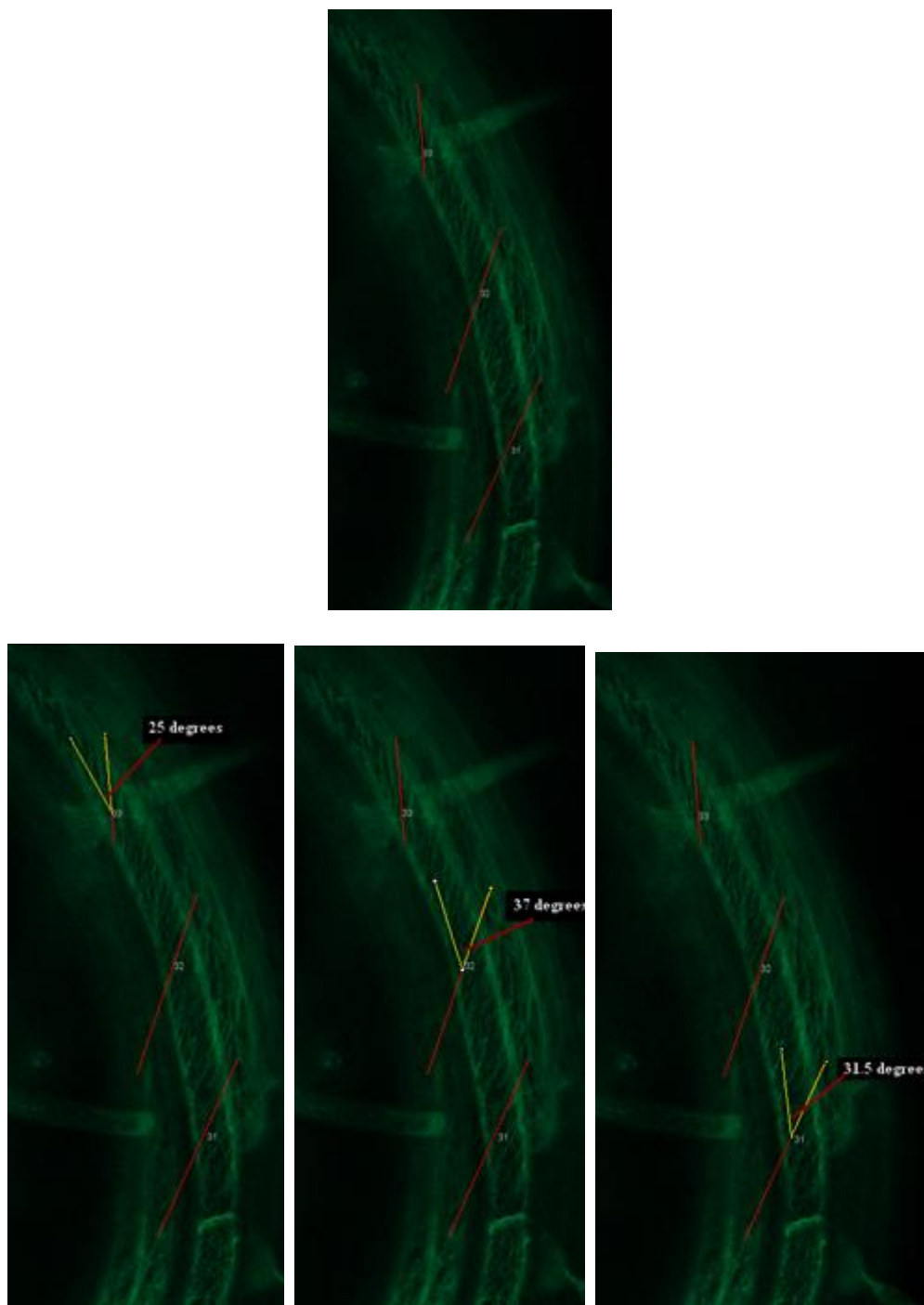


Figure B-3: Microtubules orientation tracked directly after 6 to 7 hours of continuous application of the bending load.

As shown in the previous two figures, microtubules have re-oriented themselves in a different angle with respect to the cell axis. The new angles for the same sections in Figure B-2 are now 25, 37 and 31.5 degrees respectively, as opposed to 6.5, 12 and 10 degrees before load application.

Below is another sample:

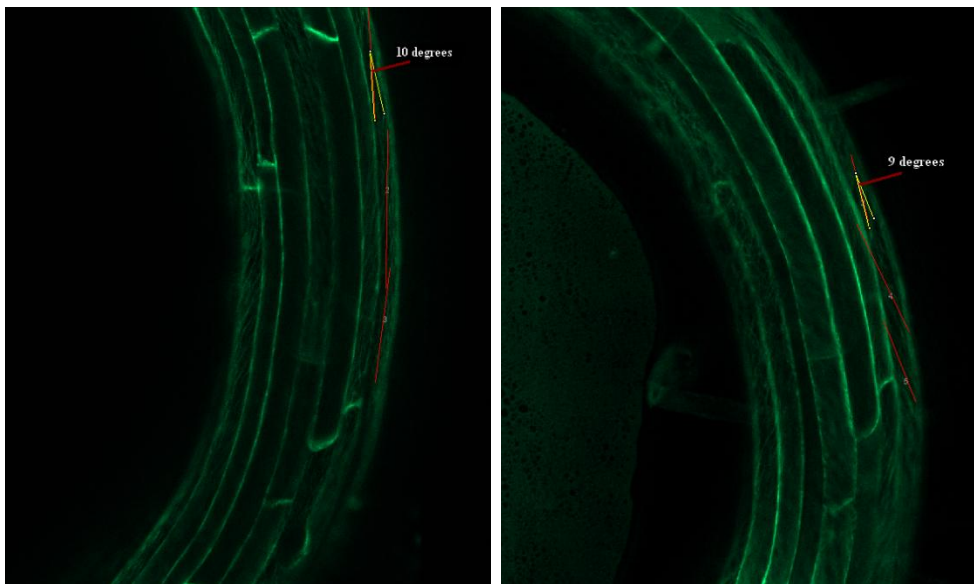


Figure B-4 ((a) - page 1 of 2): Another sample showing microtubules orientation along the root cell visualized immediately (*left*) and 6 to 7 hours (*right*) after the bending moment was applied to the root.

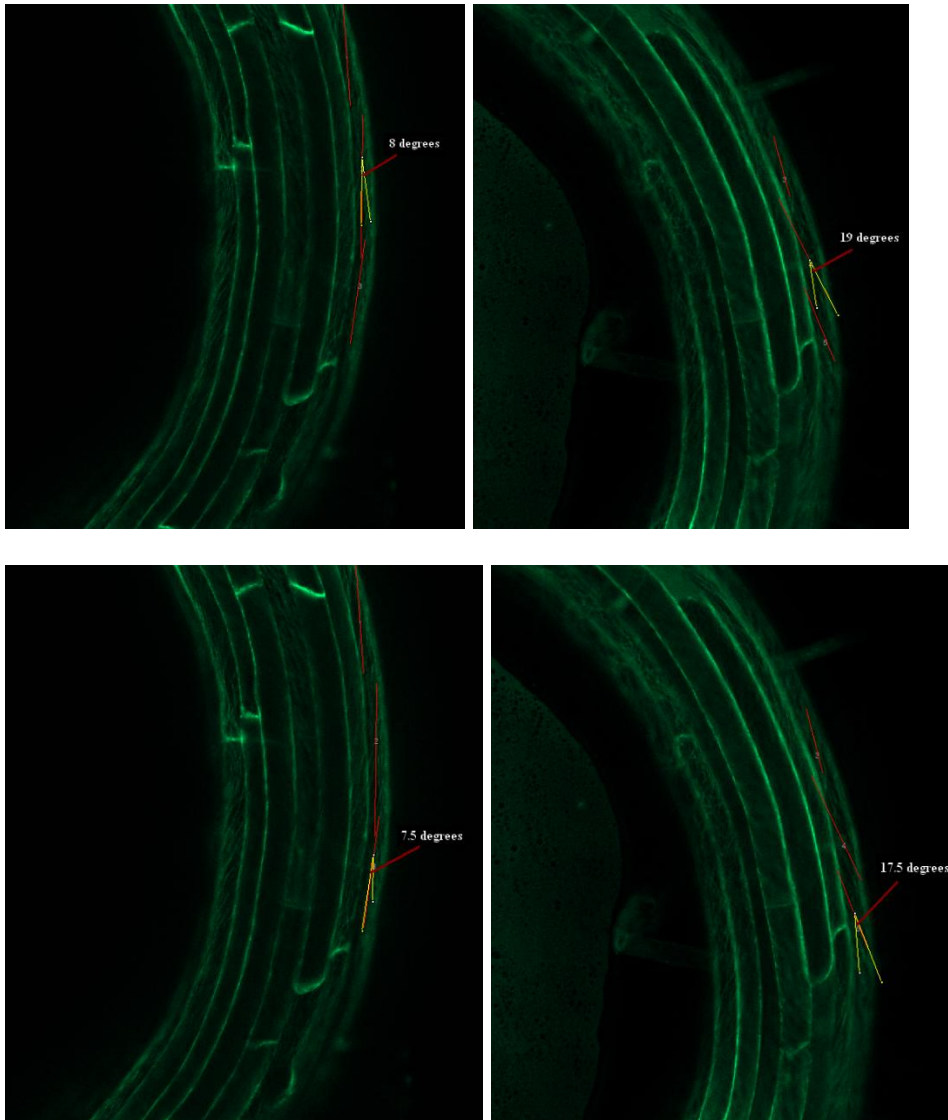


Figure B-4 ((b) - page 2 of 2): Another sample showing microtubules orientation along the root cell visualized immediately (*left*) and 6 to 7 hours (*right*) after the bending moment was applied to the root.

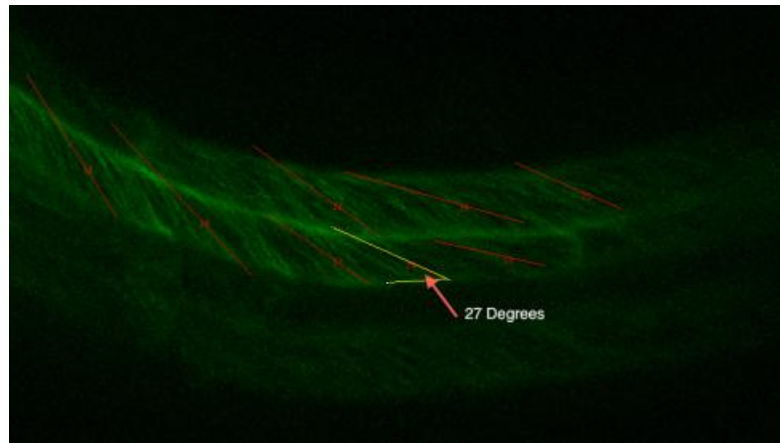
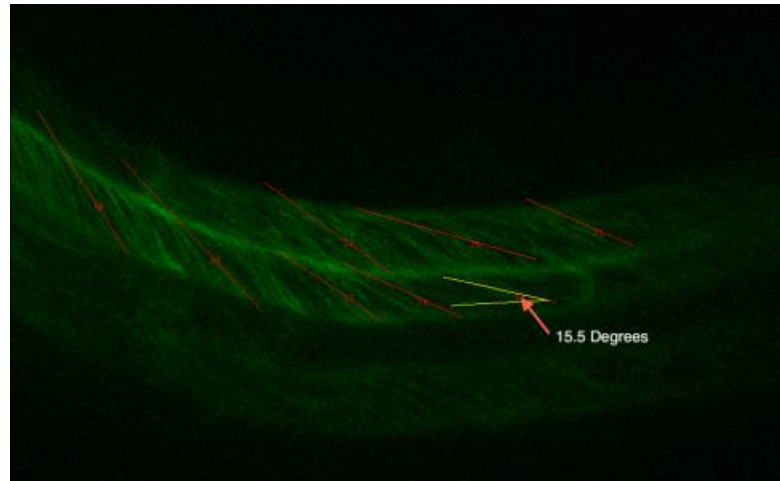


Figure B-5 ((a) – page 1 of 3): Another selected sample showing microtubules orientation along the root cell visualized 6 to 7 hours after the bending moment was applied to the root.

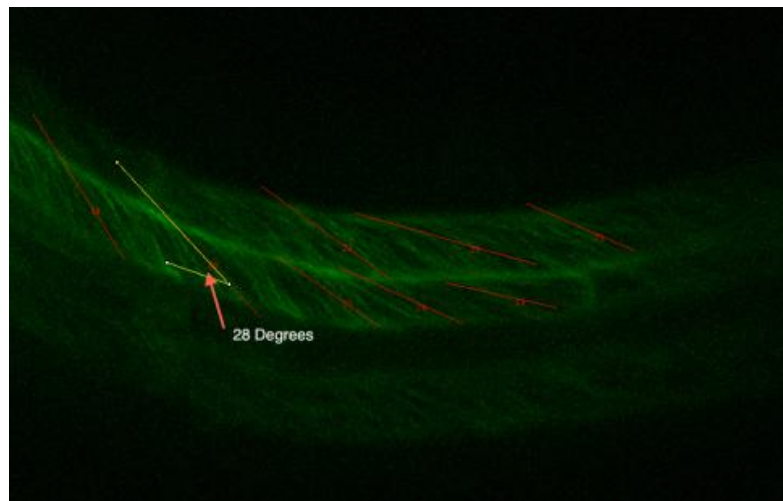
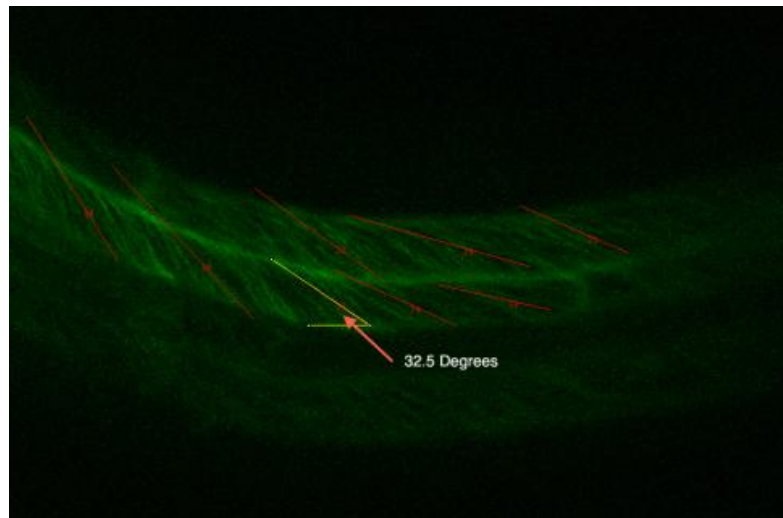


Figure B-5 ((b) – page 2 of 3): Another selected sample showing microtubules orientation along the root cell visualized 6 to 7 hours after the bending moment was applied to the root.

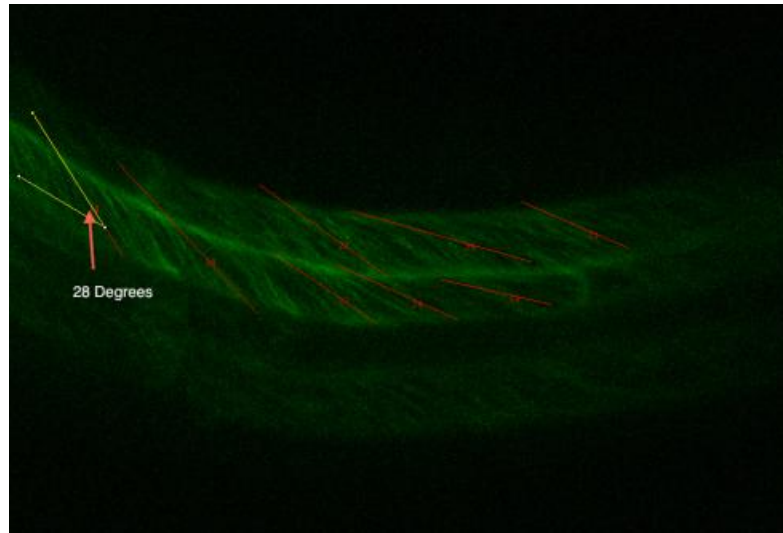


Figure B-5 ((c) – page 3 of 3): Another selected sample showing microtubules orientation along the root cell visualized 6 to 7 hours after the bending moment was applied to the root.

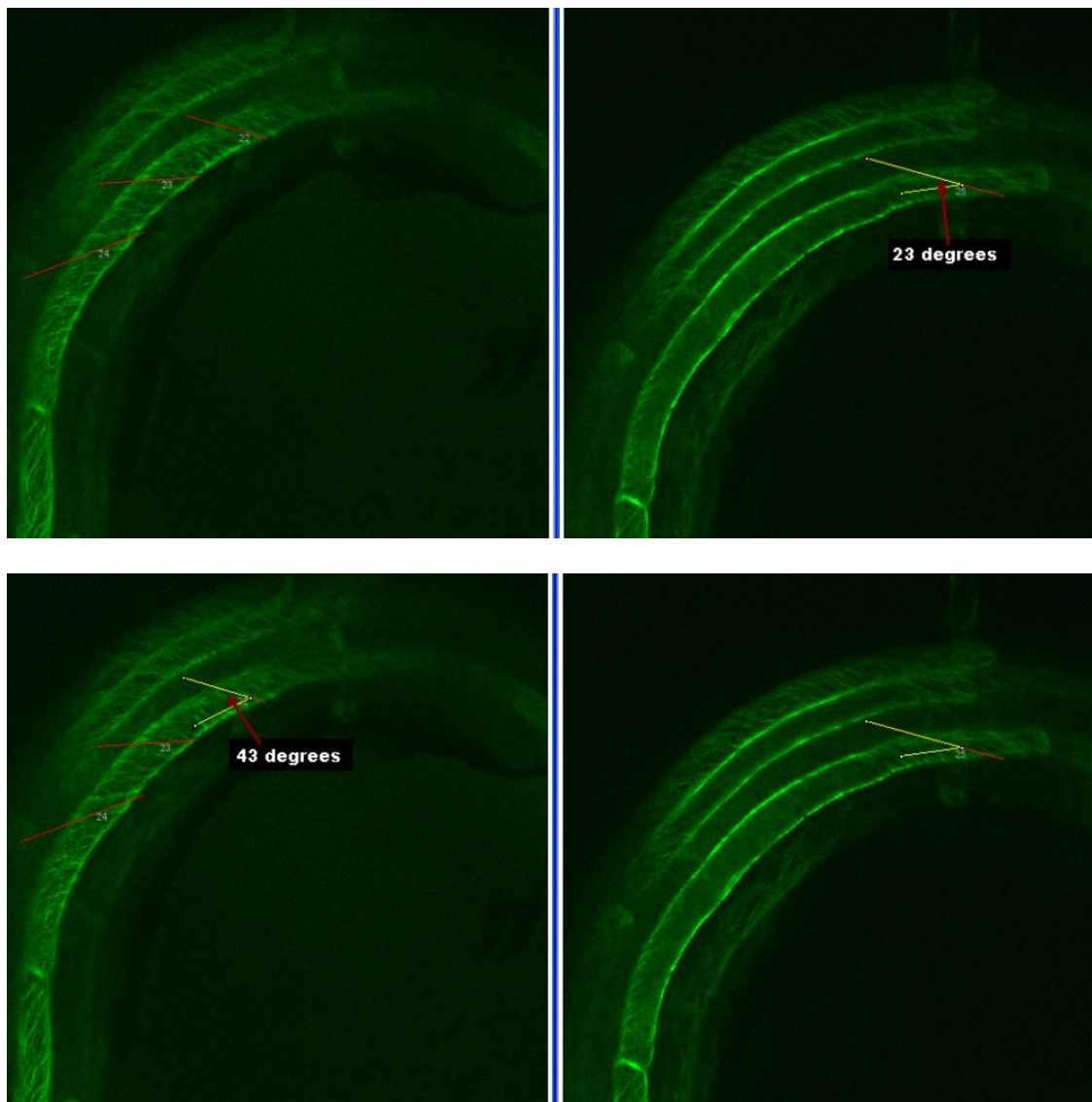


Figure B-6 ((a) – page 1 of 5): Another selected sample showing microtubules orientation along the root cell visualized 6 to 7 hours after the bending moment was applied to the root.

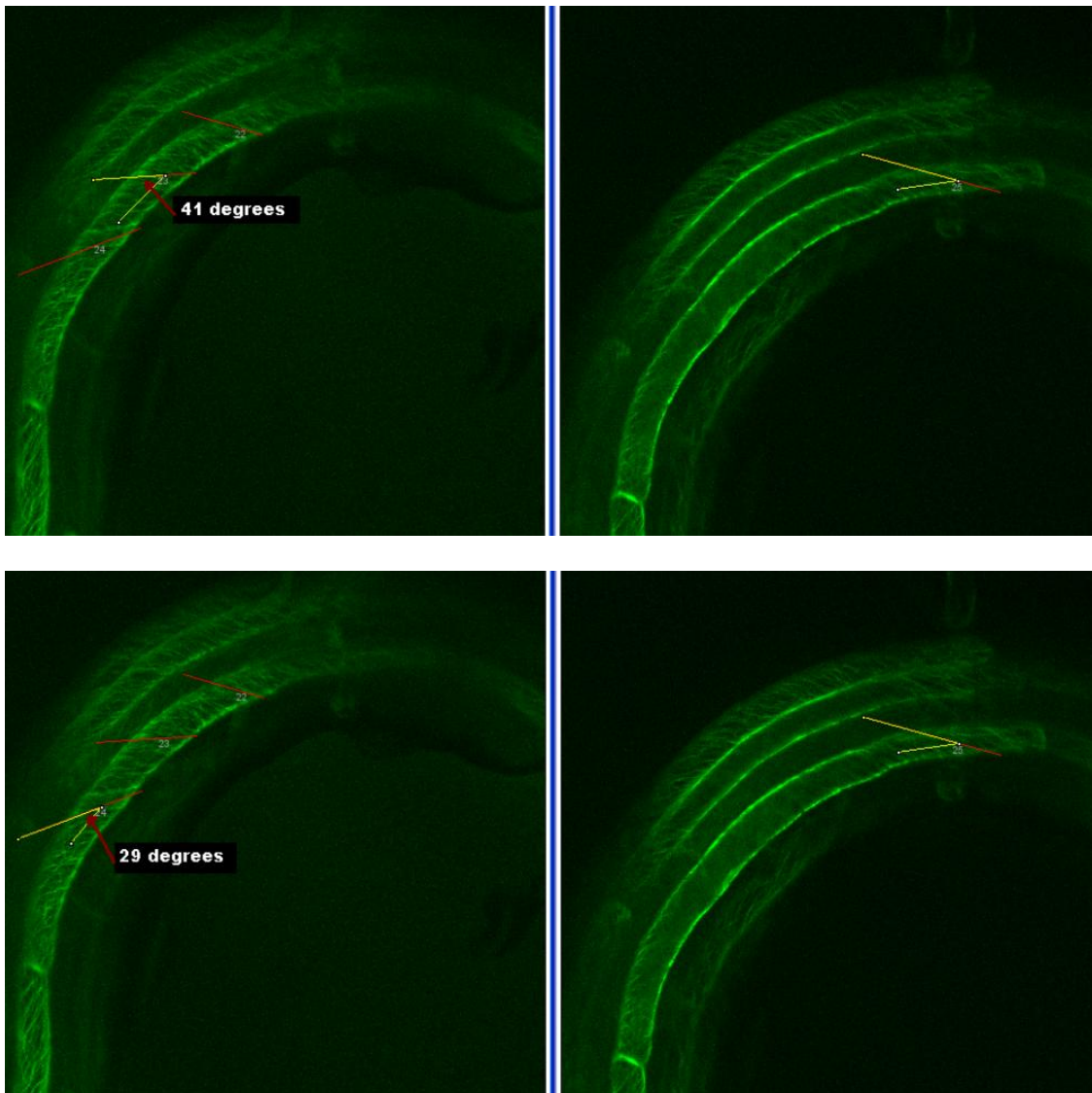


Figure B-6 ((b) – page 2 of 5): Another selected sample showing microtubules orientation along the root cell visualized 6 to 7 hours after the bending moment was applied to the root.

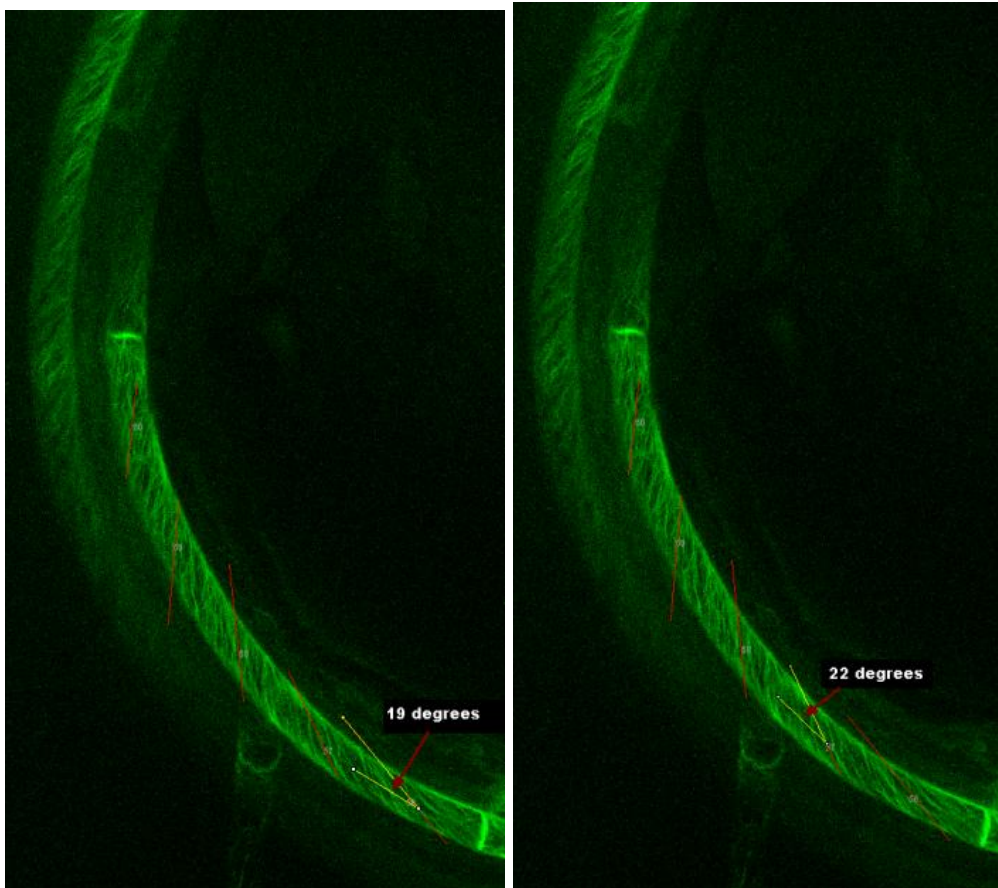


Figure B-6 ((c) – page 3 of 5): Another selected sample showing microtubules orientation along the root cell visualized 6 to 7 hours after the bending moment was applied to the root.

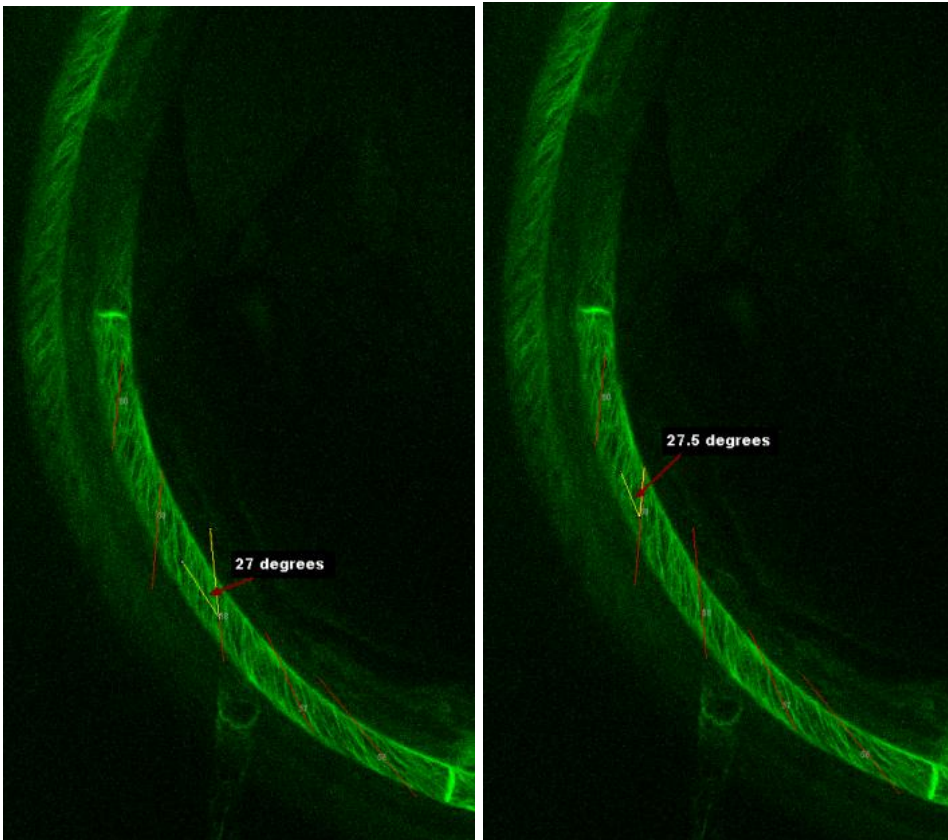


Figure B-6 ((d) – page 4 of 5): Another selected sample showing microtubules orientation along the root cell visualized 6 to 7 hours after the bending moment was applied to the root.

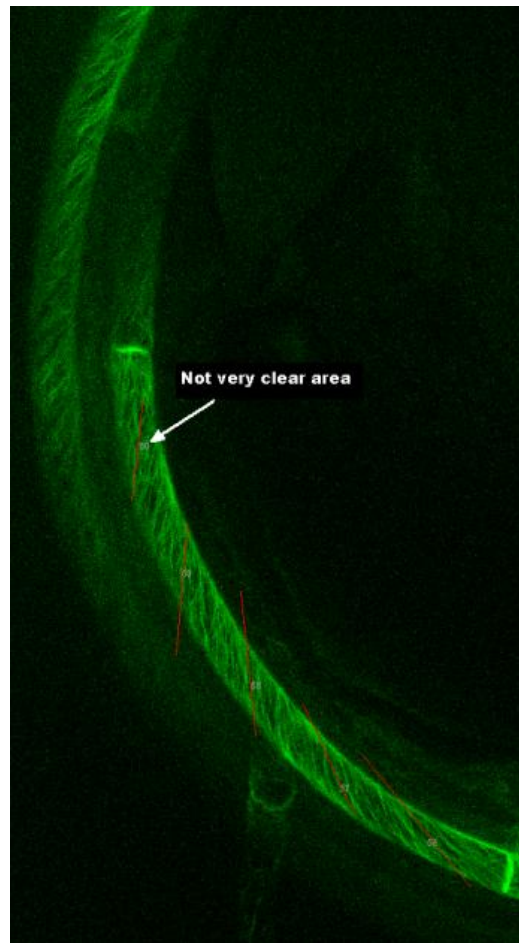


Figure B-6 ((e) – page 5 of 5): Another selected sample showing microtubules orientation along the root cell visualized 6 to 7 hours after the bending moment was applied to the root.

Figure B-7 is an image showing an example of a root cell that had a clear pattern of microtubules orientation once the bending moment was applied (*left*); but it lost the pattern after several hours (*right*). The reason is most likely related to the root hair grown from this cell.

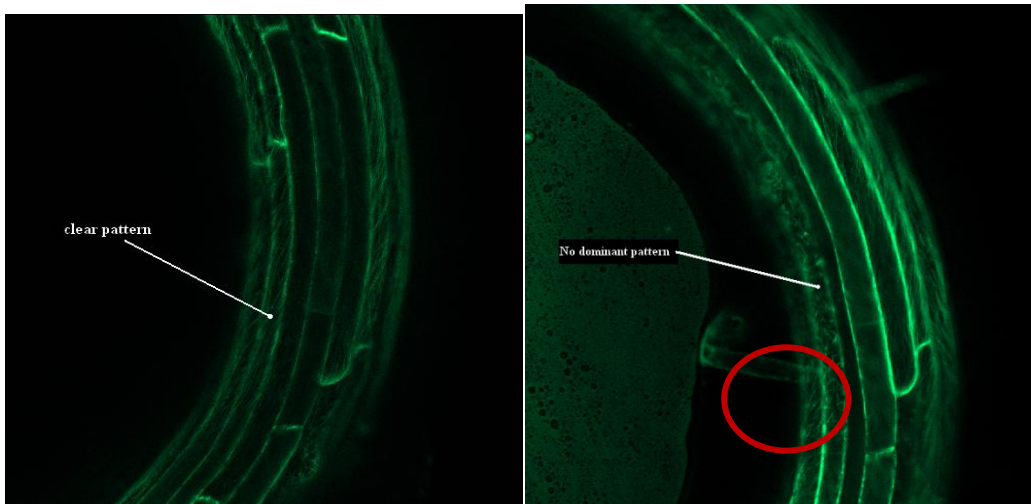


Figure B-7: An example of a root cell losing its microtubules pattern after several hours of being bent with an external bending moment. The reason why the arrangement of microtubules is completely lost is not clear, but most likely it is due to the root hair grown from such cell (circled in red).